CHEMICAL REVIEWS

REVIEW

pubs.acs.org/CR

Spherulites

Alexander G. Shtukenberg,[*,†,‡] Yuri O. Punin,[‡] Erica Gunn,[#] and Bart Kahr[*,†,#]

[†]Department of Chemistry, New York University, 100 Washington Square East, New York City, New York 10010, United States

[‡]Department of Crystallography, Geological Faculty, St. Petersburg State University, Universitetskaya emb., 7/9, St. Petersburg 199034 Russia

[#]Department of Chemistry, University of Washington, Box 351700, Seattle, Washington 98195, United States

CONTENTS

1. INTRODUCTION

If we take a bird's eye view of crystal morphology, the most common habit is not the cube or octahedron, nor the lowly, low-symmetry parallelepiped. It may be the sphere. Almost every

Received: August 1, 2011
Published: November 21, 2011

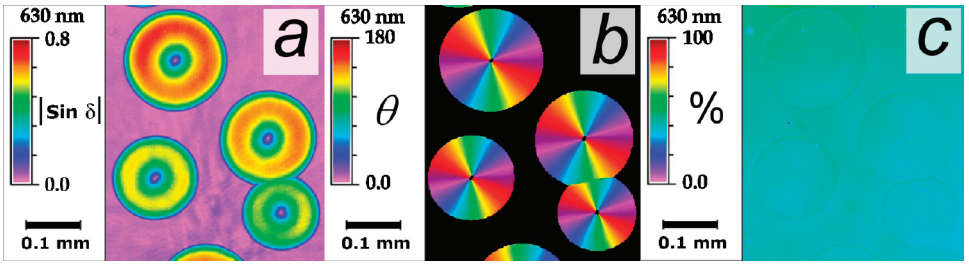

Figure 1. Melt grown sorbitol spherulites. (a) False-color images of $|\sin\delta|$ ($\delta = (2\pi\Delta nL)/\lambda$, where Δn is the linear birefringence, L is the thickness, and λ is the wavelength of incident light). (b) Orientation of the slow vibration direction (θ) in degrees counterclockwise from the horizontal. (c) Transmittance in %. Reprinted with permission from ref 5. Copyright 2008 American Chemical Society.

kind of crystalline substance can, under some conditions, be coaxed into growing with a spherical form including elements, metal alloys, simple salts, minerals, organic molecular crystals, proteins, and biopathological precipitates. Spherical crystals have even been found in outer space.[1]

Of course, the sphere is an idealization. No atomistic substance can possess an infinite order rotational axis, let alone an infinite number of them. Spherical crystalline symmetry is only an approximate result of the association of innumerable crystalline fibrils. Nevertheless, optically, some such ensembles are remarkably spherical. Among the most perfect spherical crystals are those grown from melts of the reduced sugar sorbitol.[2,3] Sorbitol spheres scatter virtually no visible light (Figure 1c) — confectioners use this glassy quality in candies[4] — and thus cannot be distinguished from the surrounding melt without polarizing elements.[5]

The name *spherulite* is given to radially polycrystalline aggregates with an outer spherical envelope, as are the sorbitol crystals in Figure 1. A moment's consideration is enough to realize that such a form can only result from the successive branching of a nucleus. Confined between glasses, spherulites grow as radial disks. Occasionally, these flattened objects are more properly described as *cylindrulites* or *cylindrites*[6] (see section 4.2.1), but we will not fuss here about this pedantic distinction.

Discovering the etiology of branching is the key to understanding spherulitic growth. Crystallography is filled with branched forms. The branching that allows spherulites to fill spherical volumes is called *noncrystallographic branching*. It is distinct from crystallographic branching in snowflakes, for example, where every branch is in single-crystal register with every other branch. It is also distinct from the fractal-like forms of *diffusion-limited aggregates* that have a helter-skelter organization. Of these three kinds of branching modes — crystallographic branching, small-angle branching, and diffusion-limited aggregation — small-angle branching, in which successive branches experience a limited liberation from the directions imposed by crystal structure and symmetry, is probably the least well understood. How, why, and under what conditions spherulites grow through the mechanism of small-angle branching is the subject of this review.

Frequently, coarse aggregates of faceted crystals spike outward from clustered nuclei. The members of the set of radialesque, crystalline aggregates from the smooth, spherical sorbitol to the gross, countable, stellated group of crystals, often carry the same name in the literature: *spherulite*. This is unfortunate because the term is sometimes used pejoratively to describe a failed attempt to prepare well-defined single crystals. In other cases, it is used to indicate the more interesting ability, in our view, of many crystals to mimic objects with crystallographically impossible optical symmetries. Thus, the term spherulite has no satisfactory and consistent definition for the evident reason that knowledge concerning the essential character of the objects to which the term has been applied is inadequate for establishing such a definition. In fact, the immediately preceding sentence was taken, almost verbatim, from an assessment of spherulites by Cross in 1891,[7] but despite having learned a great deal in more than a century, his characterization still rings true. Our goal here is not to list all spherulite-forming substances, but rather to consider the factors controlling spherulitic growth and to develop insights into spherulite formation mechanisms.

One half century ago, the pioneering polymer spherulite researchers Keith and Padden attributed the fragmentary development of spherulite analysis to the preoccupation of scientists with a limited range of spherulite-forming substances thereby "conspiring against a general solution".[8] They argued that whatever the spherulite growth mechanisms might be, "it is clear that they cannot be related too specifically to the molecular characteristics of any one or two species. It should be possible, therefore, to account for mechanisms of spherulitic crystallization on a unified basis, and in terms sufficiently general as to be applicable to spherulite-forming systems of *all* known types."[8] We carry forward their aspirations with the benefit of 50 years of additional experience. The universality of spherulitic growth, impacting metallurgy, ceramics, mineralogy, organic chemistry, biochemistry, pathology, and pharmacy has not been embraced *in toto* to the extent that we aspire to reach herein.

2. HISTORY

In 1837, Talbot observed that the crystallization of borax ($Na_2B_4O_7 \cdot 10H_2O$) from a drop of phosphoric acid produced under the polarized light microscope "minute circular spots, each of which is like a tuft of silk radiating from a centre."[9] The tufts, he said, were "in such close assemblage as to be in optical contact with each other, and to produce the appearance of a single individual."[9] Brewster later called the objects of Talbot's interest[10] *circular crystals*.[11] Today we called them *spherulites*. In 1853, Brewster examined 300 doubly refracting substances and claimed to have observed 70 that formed circular crystals under some conditions.[11] Moreover, he claimed priority, asserting that in 1815, he had observed Talbot-like circular crystals of oil of mace mixed with tallow or rosin during a classification of light polarization-perturbing substances.[12] Oil of mace, rich in a variety of terpenes, deposited "halos" that could never be fully extinguished between crossed polarizers due to the radial orientation of doubly

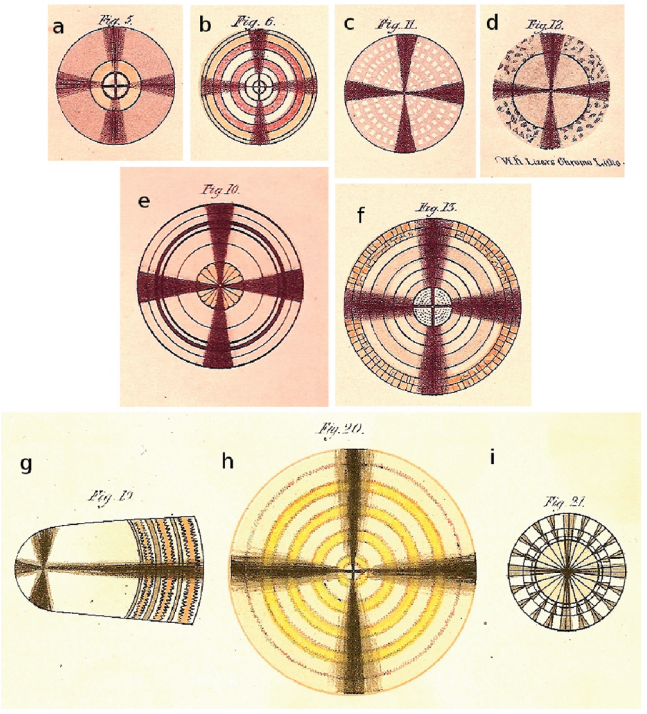

Figure 2. Plates from Brewster[11] showing spherulites. (a−c, e, h) Ammonium oxalurate; (d, f) salicin; (g, i) mannitol.

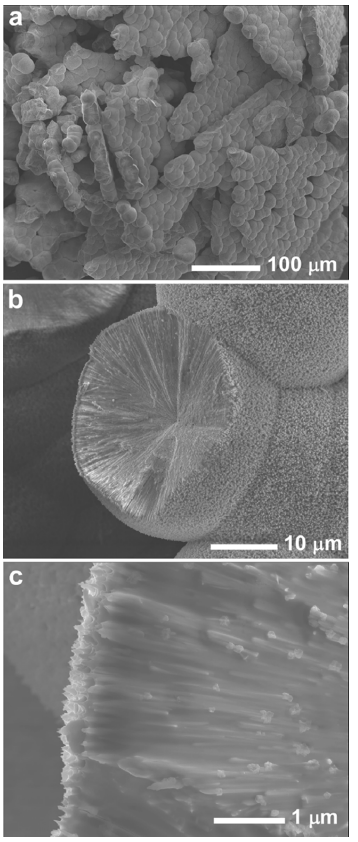

Figure 3. (a−c) Scanning electron micrographs of $Mn(IO_3)_2$ spherulites grown from a gel. Sample prepared by M. Snipes.

refracting bodies. Dallas later recognized the general spherulite promoting effects of resinous additives. With gum arabic he made circular crystals of lead acetate, muriate of morphia, and copper sulfate.[13]

Harting[14] is remembered for his attempts to mimic the complex biocrystalline forms found in radiolaria and coccoliths, by including various biological fluids, aptly characterized as Shakesparean,[15] in crystallizing solutions of calcium carbonate and calcium phosphate. He produced *calcareous* spherulites in this way. Today, legions of researchers have joined the search for some additive among the innumerable synthetic polymers modern chemists have to choose from that may yield the near-magical forms that populate the biological world.[16] At the close of the 19th century, Meyer analyzed spherulites formed by starches isolated from plants.[17]

Lehmann discovered many spherulite forming substances of molecular crystals[18−20] encountered during a career perfecting the hot-stage for the polarization microscope.[21] The biologist Haeckel kept spherulite samples, obtained from Lehmann, in his laboratory in Jena.[22,23] He was under the impression that self-organized crystals were a "missing-link" between animate and inanimate matter. Hundreds of other small molecule organic spherulites were described in the great compendium on thermal micromethods by Kofler and Kofler.[24]

Mineral spherulites begin to show up in the works of the great petrographers in the second half of the 19th century. Zirkel[25] and Vogelsgang[26] thought that spherulites were not really crystalline, but rather on the way to becoming crystalline. This confusion about the nature of spherulites led to a proliferation of qualified spherulites in work of Rosenbusch including *globospherulites*, *granospherulites*, *sphaerocrystals*, *pseudospherulites*, and *felsospherulites*.[27] He promoted a mysterious protosubstance associated with spherulites, *mikrofelsit*, not quite glass but not quite crystal either, that preceded definite mineral compositions and structures. In France, *pétrosiliceux* played a similar role.[28] Other references to spherulitic minerals can be found in the work of Bertrand[29,30] and in the Royal Society's report of consequences of the eruption of Krakatoa, including descriptions of spherulitic minerals in the ejecta.[31] But, it is the American mineralogist Iddings who first began to treat spherulitic minerals as any other crystal with forms determined merely by the special crystallizing conditions of magma.[32,33]

A large subgroup of spherulites show concentric rings of optical contrast between crossed polarizers. The nature and mechanism of concentric optical banding in so-called ring-banded spherulites drove much of the research in the 20th century. However, this work was bimodal. There was active investigation of small, organic, ring-banded spherulites by Wallerant[34−36] and Gaubert[37−50] in Paris prior to 1930. This theme was more or less abandoned following the exhaustive, authoritative monograph *"Gedrillte" Krystalle* by Bernauer in 1929.[51] He described 135 simple molecular crystalline spherulites that formed concentric optical bands. Shortly thereafter, Morse and Donnay[52,53] made a survey of spherulite forming inorganics that may be considered a companion to the organic compendium of Bernauer. We prepared one of the materials that they discussed, $Mn(IO_3)_2$ (Figure 3), so as to characterize its microtexture by electron microscopy. Fractured balls show clearly a radial organization of needles.

Nevertheless, the aforementioned works were not reinvestigated. While giving the impression of a mature subject, they raised more questions than they answered. The 1940s was a nadir in the study of spherulites, but interest returned with the development

of the synthetic polymer industry. Polymers crystallizing from the melt frequently adopt spherulitic forms. In their classic work, Keller, Keith, and Padden summarized key features of spherulitic morphology, growth, and crystal optics.[8,54−60] The most important paper by Keith and Padden[8] proposed a mechanism explaining fibrillation of spherulite crystallites through growth front instability induced by constitutional supercooling. Although this idea turned out to be inconsistent with data, it had a strong impact on the development of the science of spherulitic crystallization. Popoff,[61] Shubkinov,[62,63] and Maleev[64] also considered morphology evolution and geometrical relationships in minerals and small molecule spherulites.

Today, spherulites continue to be intensively studied, especially in the context of polymer crystallization[65,66] and biomineral composite synthesis.[67,68] However, despite a proliferation of modern microstructural electron and scanning probe microscopies that has led to a rich illustration of spherulites, progress in understanding spherulite growth mechanisms has been stymied. The autodeformation concept of Punin developed in 1970−1980s was aimed at a general and universally recognized view of spherulitic growth,[69,70] but most of the related publications were published in Russian and remained unknown to the world scientific community.

3. OVERVIEW OF SPHERULITE FORMING SUBSTANCES AND GROWTH CONDITIONS

A full accounting of all spherulites would contain many thousands of entries and it would undoubtedly be incomplete as the relevant literature is spread over many areas of science. Arguably, any crystalline substance can be made to adopt a spherulitic morphology under some conditions. Here, we will try to summarize the main classes of spherulites in a narrative or annotated list that makes no claim to being comprehensive. Additional examples are scattered throughout the text.

Growth from the Melt

Small Molecule Organic Crystals. Above, we cited the first spherulite from oil of mace mixed with rosin or tallow.[12] Talbot studied ammonium oxalurate, mannitol, palmitic acid, hippuric acid, asparagine, salicin, and santonin, among other substances. Bernauer provided the most extensive list of spherulite forming molecular crystals.[51,71] Most of the 135 substances were grown from the melt, including the following: benzil, benzoic acid, benzamide, naphthalene, anthracene, phenanthrene, phthalic acid, chlorobenzene, as well as several phenols, nitroanilines, ureas, and tartrates, among others (often resins were added to increase viscosities but were not always requisite). Bernauer was focused on ring-banded spherulites. He must have encountered at least an equal number of substances that formed spherulites without rhythmic optical modulation. A contemporary look at some of the compounds described by Bernauer include hippuric acid,[72] tetraphenyl lead,[73] and testosterone propionate.[74] Mannitol[75] and sorbitol[5] are spherulite forming diastereomers. *o*-Terphenyl, salol, and thymol spherulites were studied in the context of the roughening transition.[76] 5-Methyl-2-[(2-nitrophenyl)amino]-3-thiophenecarbonitrile (ROY)[77] is the most prolific polymorph forming molecular crystal; many of its forms crystallize as spherulites from the melt. Long chain carboxylic acids[78] also form spherulites, as do a variety of compounds that form mesophases at elevated temperatures including and cholesteryl esters,[37,38,79] as well as 4-cyano-4′-alkyloxybiphenyls.[80−83]

High-Polymers. Very large *n*-alkanes[84,85] form spherulites, as well as many high polymers including hydrocarbons such polyethylene, polypropylene,[86] polyisobutylene, poly(butene-1),[87] *iso*-poly(4-methylpentene-1),[88] and polystyrene.[60] Polyesters commonly form spherulites such as polyethylene terephthalate,[54] poly(*R*-3-hydroxyvalerate),[89] poly(*R*-3-hydroxybutyrate),[90] polylactic acid,[91] and poly(vinylidene fluoride).[92] Lovinger, among others, studied polyamides.[93] Spherulitic growth has been shown to be important in controlling the conductivity of semiconducting polymers such as poly(3-hexylthiophene).[94] Even natural polymers such as gutta percha form spherulites.[95]

Minerals. Minerals forming spherulites from the melt include silicates that crystallize from magmas,[96] such as alkaline feldspars ($(K,Na)AlSi_3O_8$),[97,98] melilite group minerals ($Ca_2(Mg,Al)((Si,Al)SiO_7)$),[99] plagioclase ($(Na_xCa_{1-x})(Al_{2-x}Si_{2+x}O_8)$),[100,101] and pyroxene ($((Ca,Na)(Mg,Fe,Al)(Si,Al)_2O_6)$).[99,100,102] (We caution that magmas are not true melts; they have complex compositions with volatile components and resemble high-temperature solutions in some characteristics.)

Elements. The three elements that form spherulites from the melt include graphite,[103−106] selenium,[107,108] and sulfur.[109] The latter was first observed by Gaubert.[43]

Inorganic Crystals. Inorganic salts tend to be high melting. Nevertheless, spherulites from the melt have been described for lead fluoride.[110]

Metals. Iron,[111] including some steels,[112] form spherulites as do nickel−titanium alloys.[113]

Growth from Solids

Recrystallization of Amorphous Phases in Thin Films. Distinguishing growth from *bona fide* solids and melts depends upon the precise location of the glass transition temperature of the medium in question. Nevertheless, there are some examples where the medium is probably best described as a solid. These include the following: selenium,[114,115] In_2Se, Sb_2Se_3,[116] α-Fe_2O_3,[115] naphthalene derivates,[117] and the dye 1,7-bis(dimethylamino)-heptamethinium perchlorate.[118]

Recrystallization of Glasses. Bulk glasses heated above the glass transition temperature can transform to spherulites. Some examples include alkaline feldspar in volcanic rocks[96,97] as well as $SrO\cdot 2B_2O_3$,[119] $3PbO\cdot 2SiO_2$,[120] $Li_2O\cdot 2SiO_2$,[121] and $CaSiO_3$ polymorphs.[122] A number of small molecules that form spherulites include those that are susceptible to so-called *glass-crystal* growth, inordinately fast growth near and below the glass transition temperature, including several ROY polymorphs,[77] testosterone propionate,[74] *o*-terphenyl,[123] salol, triphenylethane, and toluene.[124]

Phase Transformation in Crystals. Testosterone propionate produces spherulites in the act of transformation from one polymorph to another.[74]

Growth from Solutions and Gels

Low-Soluble Salts (Solubility < 1 g/L) Grown from Low-Temperature Aqueous Solutions and Gels. Brewster described a number of inorganic spherulite-forming substances including cadmium sulfate, mercury disulfide, and nickel carbonate.[11] Morse and co-workers[125] listed 67 compounds including hydroxides, sulfides, cyanides, carbonates, sulfates, bromates, phosphates, tungstates, chromates, oxalates, and iodates that form spherulites from gels and solutions. Today, biomineral forming substances grown under exotic conditions with unusual additives frequently populate the spherulite literature. Calcite ($CaCO_3$) holds the pride of place.[126−128] Calcium oxalates[129−131] and apatite

($Ca_5(PO_4)_3(OH,F)$)[68,132,133] have also been studied intensively in relation to biomineralization. Other examples of spherulites from solution include several fluorides,[134] rare earth carbonates,[135] hematite (Fe_2O_3),[136,137] β-FeO(OH),[138] rare earth tartrates,[139,140] zinc oxide,[141] several copper iodates,[142] and scheelite ($CaWO_4$).[134,143]

High-Soluble Salts Grown from Low-Temperature Aqueous Solutions and Gels. Brewster likewise observed some highly soluble salts such as *nitrate of uranium* (probably uranyl nitrate), zinc chloride, and strontium chloride.[11] According to our observations, spherulites were observed for sodium citrate,[69] sodium thiosulfate, as well as sodium and ammonium tartrates. Potassium dichromate ($K_2Cr_2O_7$)[144−146] is among the most intensively investigated simple salt forming spherulites.

Ionic and Ionic-Covalent Compounds Grown from Hydrothermal (High-Temperature) Solutions. In the laboratory, spherulites were obtained for zinc oxide,[147] Sb_2Se_3,[148] Bi_2S_3,[149] nickel hydroxide,[150] $Ni_{11}(HPO_3)_8(OH)_6$,[151] $Fe_2(MoO_4)_3$,[152] $PbTiO_3$.[153]

Rapid Solvent Evaporation in Drops. A number of spherulites that appear to crystallize from evaporating fluids likely form fleeting metastable glassy media or viscous films from which spherulites are deposited.[154] These include ascorbic acid,[155,156] palmitic acid,[157] phthalic acid,[154,158,159] hippuric acid,[154] methyl mesitylcarbamate,[160] and potassium dichromate.[73] We also observed this behavior for sodium bromate, $K_4Fe(CN)_6 \cdot 3H_2O$, and potassium dihydrogen phosphate.

Minerals Grown from Solutions (Both Low- and High-Temperature). In nature, the most well-known spherulite forming mineral is chalcedony (fibrous quartz, SiO_2).[51,161−163] Other solution grown minerals that deposit spherulites include malachite ($Cu_2CO_3(OH)_2$), azurite ($Cu_3(CO_3)_2(OH)_2$), and rhodochrosite ($MnCO_3$).[164] Spherulites are known among natural nasturan (UO_2),[165] (Ni,Fe,Co)As_2 solid solutions,[166] tourmaline ($Na_{0.60}Ca_{0.06}(Li_{1.00}Al_{1.98}Fe_{0.02})Al_6(Si_{5.35}B_{0.65})(BO_3)_3O_{18}(OH)_3(OH,F)$),[167] wavellite ($Al_3(PO4)_2(OH,F)_3 \cdot 5H_2O$),[168] celestine ($SrSO_4$),[169] and zeolites such as natrolite ($Ba_2Al_2Si_3O_{10} \cdot 2H_2O$) and stilbite ($(Ca,Na_2,K_2)Al_2Si_7O_{18} \cdot 7H_2O$).[164] Even sodium chloride[164] can be found in the form of spherulites.

Polymers. Some polymer spherulites are deposited from solution including polypropylene,[170] poly-(3-hydroxybutyrate),[171] and poly-(ε-caprolactone).[172]

Proteins. Proteins have long been known to form spherulites from solution. Insulin was studied by Waugh as early as 1946[173] and by Donald and co-workers thereafter.[174−177] Carboxypeptidase was studied by Coleman in 1960.[178] Donald and co-workers have recently made detailed analyses of protein spherulite growth,[179,180] as these processes are related to amyloidosis and associated neurodegeneracies (see next section). They have studied β-lactoglobulin[181−184] and lysozyme[185] as well as the aforementioned insulin. Synthetic peptides have been studied by this group[186] and others as well.[187−192] Hemoglobin S can also form spherulites.[193]

Organic Molecular Crystals. The steroid lithocholic acid[194] resembles protein spherulites in having a large, less ordered core.

Spherulites Formed in Living Systems. Calcium oxalate monohydrate[195,196] and calcium phosphate[197] spherulites are typically found in kidney stones and urinary sediments. Pathologists have long recognized the spherulitic character of amyloid protein deposits associated with a variety of neurodegenerative disorders.[198−200]

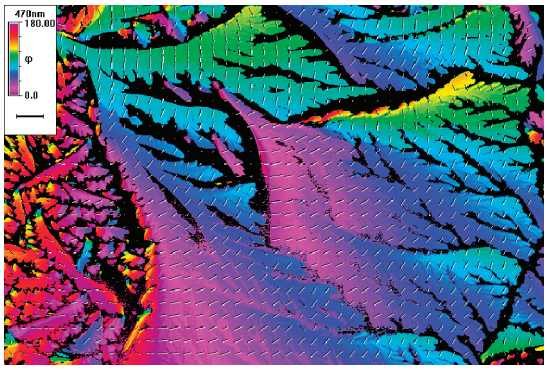

Figure 4. False color extinction map of phthalic acid[154] showing crystallographic and noncrystallographic branching. Angle represents the direction of the larger refractive index plotted counter-clockwise from the horizontal. The size of image is 0.25 mm across. Reproduced with permission from ref 209. Copyright 2010 Royal Society of Chemistry.

4. PROPERTIES OF SPHERULITES AND FACTORS CONTROLLING THEIR FORMATION

4.1. Terminology

Spherulites are polycrystalline aggregates composed by highly anisometric crystallites called *subindividuals* or *subunits*. The prefix sub emphasizes a genetic relationship to the parent crystal from which they split. The original single crystal undergoes *noncrystallographic branching* or splitting and turns into an ensemble of new crystallites or individuals that grow independently of their progenitor. The misorientations typically vary between 0 and 15° and relationships between directions of growth of the primary and secondary crystallites are not crystallographic; in other words, the relative orientations are not fixed by crystal structure or symmetry. Noncrystallographic branching distinguishes spherulites from other branched crystals and polycrystalline aggregates possessing round forms.

For instance, all the branches of *dendritic* or *skeletal* crystals have the same crystallographic orientation and conform to the same single crystal.[164,201] They maintain long-range translational order from branch to branch, are uniformly extinguished between crossed polarizers, and scatter sharp Bragg X-ray peaks. In the physics and metallurgy literature, the term *dendrite* is favored over *skeletal crystal*[202−204] for describing such forms, whereas in mineralogical literature *dendrites* typically refer to crystallographically *mis*oriented branches.[201] *Dendrites* can also refer to polycrystalline aggregates composed of an ensemble of tiny crystals nucleated on one another. This description fits metals grown by electrocrystallization in solutions[205,206] and manganese oxides between layers of rock.[207,208] These forms are often described as *diffusion limited aggregates*. Misorientations in such structures are most often noncrystallographic. In some cases, diffusion limited aggregates form *open spherulites*. Herein, open, crystallographically branched forms (characterized by the same lattice orientation of all crystallites) will be called dendrites. Open morphologies exhibiting noncrystallographic branching will be called open spherulites. Figure 4 is a good illustration of open spherulites with coexistence of crystallographic and noncrystallographic branching in an evaporating drop of phthalic acid.[209] Needless to say, the reader of the primary literature should be mindful that terminology is variable, in large part because classification of polycrystalline forms is fuzzy.

Complex, polysynthetic twin intergrowths sometimes resemble spherulites, but they are characterized by crystallographic twin relationships.[210]

Droplets of liquid crystals sometimes show radial or Maltese cross extinction patterns between crossed polarizers, thus resembling spherulites.[211−215] These droplets do not contain fibers. They are homogeneous down to the level of the molecule. *Bona fide* liquid crystals such as 4-cyano-4′-decyloxybiphenyl[216−218] or 4-cyano-4′-octyloxybiphenyl[219] can crystallize from their mesophases as spherulites composed of compact fibrils. For instance, Figure 5 shows the differential transmission of left and right circularly polarized light through a mixture of cholesteryl acetate-benzoate (80:20) crystallizing from the melt. The spherulites, colorless circles show no circular reflection band characteristic of the cholesteryl esters. The crystals lose all of their liquid crystallinity. References to *spherulites of liquid crystals* sometimes specify radial mesophases made from molecules commonly used as liquid crystals, as well as polycrystalline ensembles. This can be a source of confusion.

Finally, concentric, polycrystalline aggregates formed by means of layered sedimentation are well-known among minerals such as calcite, aragonite, hematite, and pyrite.[164] Others include ferromanganese nodules,[220] and phosphate kidney stones.[221] Sedimentary *framboids* — raspberry-like spheres of spheres — are often called spherulites,[222] Needless to say, sphere-like formations are easily confused with true spherulites,[127,128,196,223] especially if the term *spherulite* is being used descriptively or colloquially. Fascinating sodium chloride crystalline spheres composed of individual hopper type crystals assembling on a bubble were recently described, but they are not spherulites as defined and described herein.[224] There are many ways that crystals can resemble spherical objects.

Be forewarned that Google carries many "false-spherulites". Many liposomes and vesicles are called spherulites. These are used in drug delivery and in dermatological and cosmetic products. The traditional crystallographic use of *spherulite* may be shouted out by commercial uses.

An ideal spherulite consists of one phase. However, there are also *pseudospherulites*[225] composed by subindividuals of two or more phases[96,98] often formed in the course of eutectic crystallization such as quartz and alkaline feldspar,[225] plagioclase and pyroxene,[225] or As, Sb, and AsSb.[226] Sometimes radial growth and concentric sedimentation are concomitant, forming two- and polyphase spherulites with punctuated amounts of a crystalline phase.[155,160] For instance, apatite spherulites grown from gelatin develop from a single nucleus and eventually form spherical aggregates. Impurity adsorption ultimately causes a cessation of growth until new fibers nucleate on the surface leading to core−shell structures.[68,227] All are considered spherulites herein.

An ideal, well-developed spherulite is spherical (vide supra). During its evolution from a single crystal nucleus, it passes through a series of intermediate dumbbell and sheaf-like morphologies (Figure 8). Although, formally, objects with such intermediate morphologies are not spherulites, in that they are not yet spherical, their formation is controlled by the same mechanisms. They are on their way to becoming spherulites, and thus throughout this paper they too will be counted as spherulites.

4.2. Morphology and Anatomy

4.2.1. Habit and Morphology. Individual crystallites that assemble as spherulites in the aggregate are often needle-like but other habits are observed (Figure 6). Plank-like crystallites

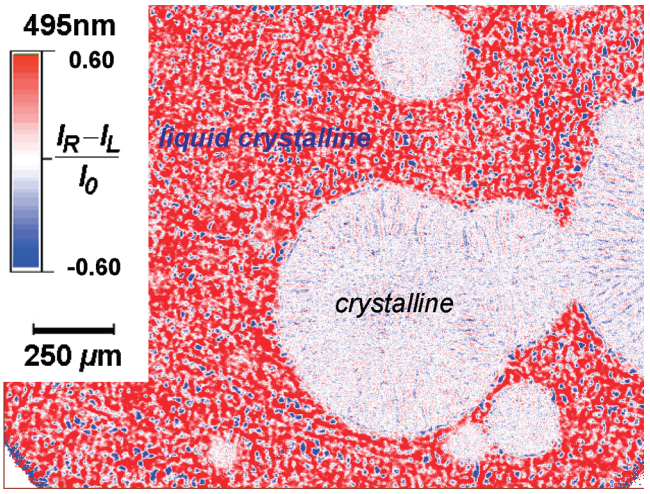

Figure 5. Crystallization of cholesteryl ester spherulites (acetate/benzoate (80:20)) from the liquid crystalline state upon cooling. $(I_R - I_L)/I_0$ is the difference between intensities of transmitted right and left circular polarized light divided by the average transmitted intensity.

(flattened needles) are not infrequent; plate-like crystallites are rare. The predominance of structures with exaggerated aspect ratios is a consequence of the fact that a high crystallographic driving force is a precondition of spherulitic growth. Because of the crystallite shape anisometry (Figure 6b) or because of growth rate anisotropy across the sample free surface and in the interior of the growth medium,[228] spherulites can adopt cylindrical shapes. Shear during crystallization can have the same effect.[229] In this case, *cylindrulite* is better usage than *spherulite*.

The thickness of spherulite fibers, h, varies from 5 to 15 nm for polymers,[230] from 0.05 to 5 μm for archetypal molecular crystals, and from 0.1 to 1 mm for large natural spherulites. The radii (L_s) of spherulites vary from ∼0.1 μm to several centimeters or even meters.[98] If fibers have small cross sections so that it is hard to distinguish individual fibers, the resulting spherulites are *fine* (Figure 7b,d,e); otherwise, they are *coarse*[8] (Figure 7a,f). Melt grown spherulites are characterized by higher ratios $L_s/h = 10^3-10^5$ compared to solution grown spherulites with $L_s/h = 10^2-10^3$, and therefore, they are typically finer.

The needle-like fibers are typically straight (Figure 7a), and plate-, and plank-like crystallites are typically straight and flat (Figure 6b). However, bending, twisting, and scrolling of fibrils and lamellae further confounds spherulite morphology (e.g., twisting: chalcedony,[161,162] hippuric acid[73] Figure 7b,c; bending: potassium dichromate;[144] scrolling: poly(vinylidene fluoride)[231]). Bernauer claimed that one in four molecular crystal grown from the melt[51] formed twisted fibers around their axis of elongation with periods ranging from <0.2 μm to infinity[231] (Figure 7d,e). Tightly packed crystallites of plank-like morphologies (most polymers, selenium) cannot grow independently of each other and form bunches of lamellae[66,87,108,232−236] (Figure 7g). If lamellae are additionally twisted, they can show complicated curved morphologies[66,231,237] (Figure 7h). The optical textures of melt-grown spherulites are often richer than solution grown spherulites for two main reasons: (1) Plasticity is high at elevated temperatures, and (2) bigger L_s/h ratios provide more space for crystallite deformations.

Spherulites can also be classified by their fiber density. *Compact*, *massive*, or *closed* spherulites do not contain free space between

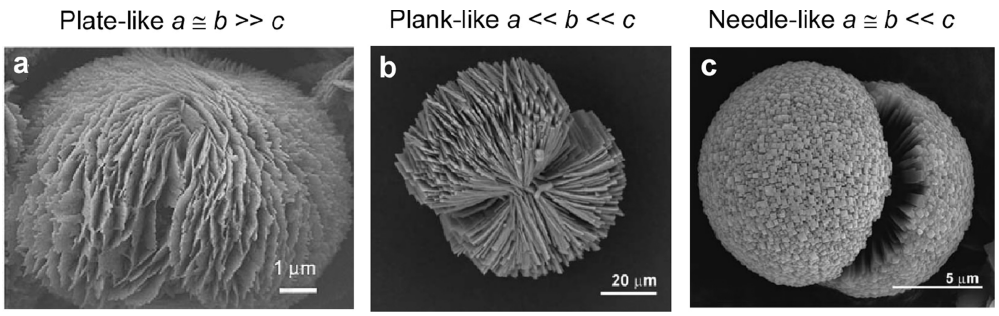

Figure 6. Varied habits of crystallites composing spherulites. Scanning electron microscope images. (a) β-$Fe_2(MoO_4)_3$. Reprinted with permission from ref 152. Copyright 2007 Wiley VCH. (b) Calcium oxalate monohydrate. From ref 130 with permission by A. Thomas. (c) Calcium oxalate dihydrate. From ref 130 with permission by A. Thomas.

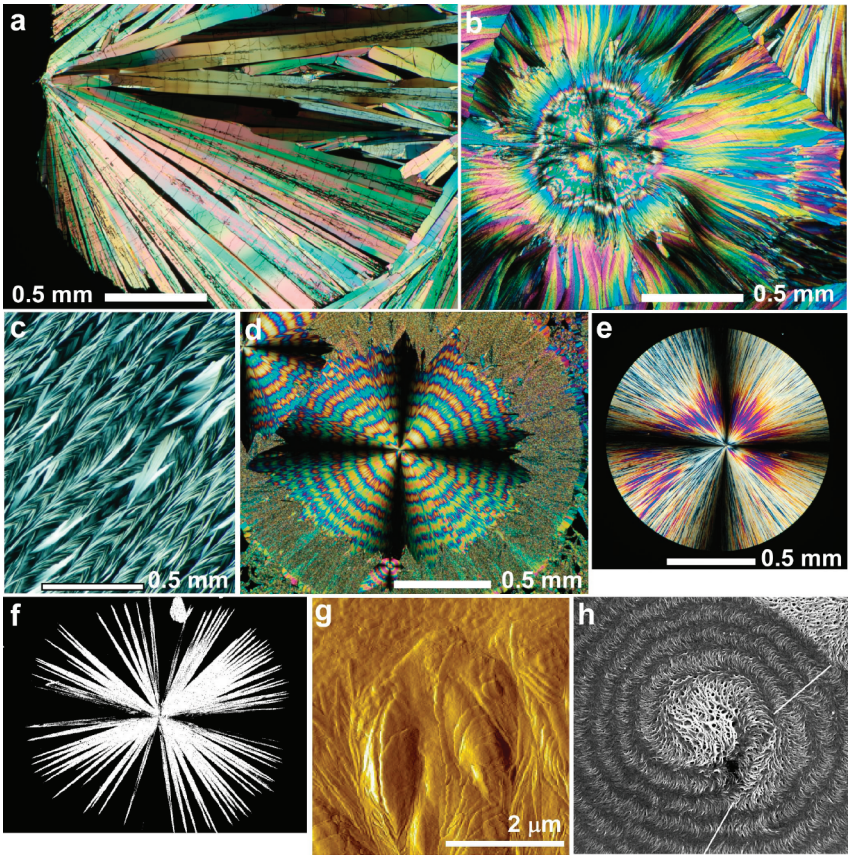

Figure 7. Morphologies of spherulites grown from the melt in thin films and observed with a polarized light microscope (a–f), AFM (g), and SEM (h). (a, d–f) Straight fibers. (b, c) Bent fibers. (d, e) Twisted fibers with large and small band spacings, respectively. (b–e) Compact spherulites. (f) Open spherulite. (a) Coarse spherulite. (b–e) Fine spherulites. Materials: (a–d) Hippuric acid grown at 170, 80, 90, and 75–85 °C, respectively. (e) Resorcinol containing 10 wt % tartaric acid grown at 21 °C. (f) Malonamide containing 10 wt % D-tartaric acid. Reprinted with permission from ref 8. Copyright 1963 American Institute of Physics. (g) Poly(butane-1) at 91.5°C. Reprinted with permission from ref 87. Copyright 2008 Elsevier. (h) Polyethylene. Reprinted with permission from ref 231. Copyright 2005 Elsevier.

individual fibers or crystallites (Figure 7b,d,e), in contrast to *open* or *spiky*[8] spherulites (Figure 7f). Outer surfaces of compact spherulites are often smooth (Figures 6c, 7e, and 8); coarse spherulites typically form rough interfaces.[238,239]

Fibrous, compact spherulites have the highest radial growth rates. Tight fiber packing forces crystallites to maintain growth along the same direction. It is often stated that a given set of conditions will establish the fastest radial growth rate.[196] However, for melt-grown hippuric acid (Figure 9d), tetraphenyl lead,[73] and testosterone propionate[74] different spherulites or different parts of the same spherulite formed under the same growth conditions can be composed of differently oriented fibers. In other words, the radial growth direction, by necessity the fastest direction in a spherulite, is not necessarily the fastest growth direction for an isolated crystallite growing under the same conditions. Spherulites of cubic sodium chloride[164] illustrate this fact.

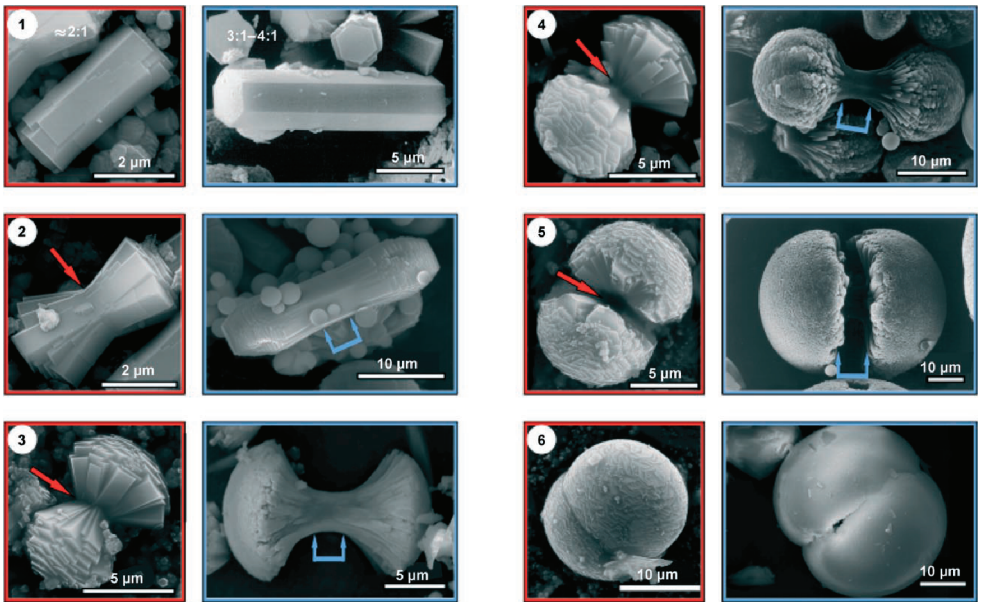

Figure 8. Scanning electron micrographs illustrating subsequent stages (1−6) of fluorapatite $Ca_5(PO_4)_3F$ spherulite formation from gelatin by means of a double diffusion technique (red picture frames correspond to the calcium side in the gel column; blue ones correspond to the phosphate side). Numbers indicated for stage 1 correspond to the length to width crystal aspect ratios. Arrows highlight the central parts of the aggregates. Reprinted with permission from ref 280. Copyright 2006 Wiley-VCH.

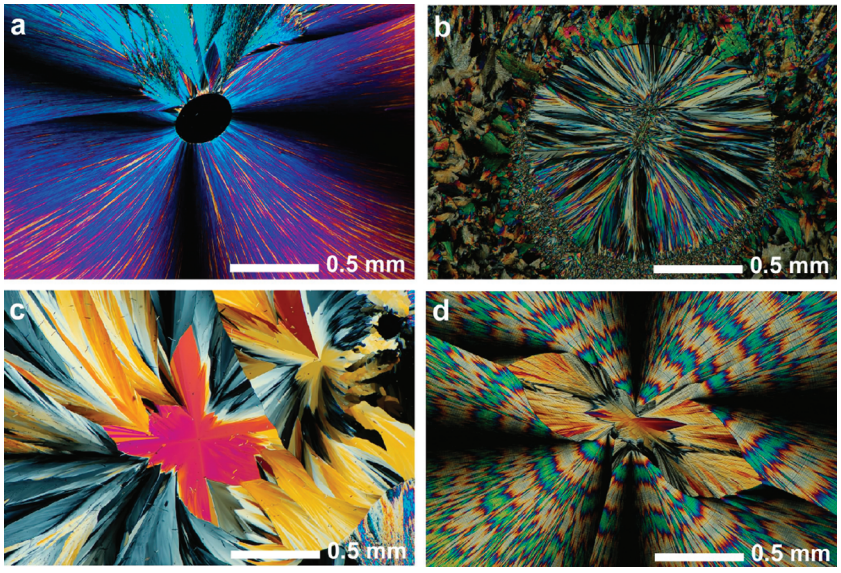

Figure 9. Melt grown spherulites, whose cores do not show double leaves. (a) Hollow core; resorcinol with 10 wt % tartaric acid grown at 35 °C. (b) Nucleation of fibers at elongated nucleus crystal; testosterone propionate.[74] (c) Gradual branching in all directions of single resorcinol crystal with 1.1 wt % D-tartaric acid grown at ∼30 °C. (d) Change of growth direction from [100] to [001] during development of a hippuric acid spherulite grown at 80 °C.

Mutual transformations between elongation directions probably occur via nucleation events on the surface as has been observed for polymorphic transformations.[240]

Typically, noncrystallographically misoriented spherulite crystallites are single crystals, but they can also twin with interfaces parallel to the elongation direction. Such twinned spherulites include $NaHCO_3$,[241] $CaSO_4 \cdot 2H_2O$ (gypsum), $CuCl_2 \cdot 2H_2O$,[69] and were also observed by us for natural malachite.

Toroidal spherulites, in additional to spherical forms, can be formed from high amylose cornstarch.[242] It appears that the etiology of this morphology is unknown.

4.2.2. Crystal Optics. If spherulite fibers are elongated along a principal axis of the optical indicatrix, a so-called *Maltese extinction cross* appears between crossed polarizers (Figure 7b,d,e). The arms of the cross are parallel to the polarizer/analyzer orientation of the microscope and independent of the stage orientation. Spherulites are defined as optically *positive* if the larger refractive index is radial and *negative* if it is tangential. If the fibers are not aligned with a principal axis of the optical indicatrix, the cross will be askew with respect to the polarizer/analyzer orientation.

The transmittance of a flat spherulite between crossed polarizers can be expressed in terms of two parameters, the azimuthal

orientation of the crystallite, θ, and its retardance, δ:[243] $I/I_o = (\sin^2 2\theta)\sin^2(\delta/2)$, where $\delta = 2\pi\Delta nz/\lambda$, Δn is the linear birefringence, z is the thickness, and λ is the wavelength of light.

The apparent optical properties are frequently averages of many imperfectly oriented fibrils,[52,53] and contributions to the optical properties from light scattering are often pronounced.[244,245] Transparent spherulites can often display *pseudopleochroism*, apparent anisotropic absorption by fibrous crystalline substances that arise from the anisotropy of linear light scattering.[39]

Spherulites of twisted fibers are characterized by more or less concentric bands. Band spacings typically correspond to 180° rotations of the indicatrix along the fiber axis with regular minima and maxima in the retardance, δ (Figure 7d). This sort of banding does not obviate the Maltese cross extinction pattern if one principal index of the optical indicatrix is radial; otherwise, the extinction arms zigzag.[54,246] Analyses of the crystal optics of banded spherulites with twisted fibers have been developed previously.[55,57,58,247,248] Banded spherulites will be taken up in greater depth in the next section.

4.2.3. Banded Spherulites. Many spherulites are characterized by concentric bands of optical contrast. Besides the aforementioned *twisting*, *rhythmic deposition* can lead to modulated optical properties.[73,231] Many examples are cited by Dippy[249] along with data provided for 3,5-dichloro-4-methyldiphenyl, piperonal, and salol. Hedges reviewed periodic spherulitic crystallization in a monograph in 1932 with illustrations of benzoic acid and potassium sodium tartrate among other materials.[250]

Rhythmic precipitation usually occurs because of a competition between nonlinear interface kinetics and supply of material by diffusion and/or advection.[251,252] The simplest scenario assumes that in thin films constrained between two flat surfaces, noncrystallizing components are extruded by the growing spherulite and accumulate near the growth front. This slows crystallization and leads to the formation of a crystal-poor band. Then, the high concentration of the main component is restored, resulting in formation of the crystal-rich band. This mechanism probably works for tetraphenyl lead and tetraphenyl tin with polyvinylpyrrolidone[73] and ethylene carbonate with polyacrylonitrile.[253,254]

For crystallization of thin films with free upper surfaces, additional contributions can result from capillary forces that deliver nutrients to the top of growing crystals and enhance nonlinearity in mass transfer. Rhythmic growth with a free upper surface has been observed for ascorbic acid,[155,156,255−257] phthalic acid,[158,159] hippuric acid,[154] potassium dichromate,[73,258] methyl mesitylcarbamate,[160] tribenzylamine,[259] and poly(ε-caprolactone)[172] as well as melt grown crystals such as triphenylamine,[260] isotactic polystyrene,[261] poly(aryl ether ketone)s and blends thereof,[262] poly(3-hydroxybutyrate) and copolymers blends,[263,264] poly(ε-caprolactone), poly(styrene-co-acrylonitrile) blends,[265] and poly(ethylene succinate).[266] Poly(butylene adipate) spherulites are composed of alternating bands of distinct polymorphs.[267]

Radial twisting of fibers (section 4.2.1) as the etiology of concentric optical bands is both common and poorly understood. Mechanisms of fiber twisting have been the subject of vigorous debates.[69,72,231,253,268] There are four main competing twisting mechanisms: (1) Twisting is due to elastic fields generated by screw dislocations (*Eshelby twisting*);[269−271] (2) thermal, concentration, and/or mechanical *fields* that form around growing crystals force reorientation during growth;[232,233,268] (3) anisotropic *surface stresses* deform the crystal;[90,231] (4) *Autodeformation*, the assumption that compositional inhomogeneities within the subindividuals induce mismatch or *heterometry stress* creating a twist moment. The twist is preserved in the crystal volume in the course of plastic stress relaxation.[69,72]

Discussion of these mechanisms is beyond the scope of this paper. The first three mechanisms were weighed by Lotz and Cheng.[231] Here, we provide only several comments. We believe that the fields are unlikely sources of twisting because they cannot explain the observation that similarly twisted structures that occur concomitantly for a variety of different growth conditions. Moreover, they cannot explain the strong effect of minor impurities on twisting.[72,231] Screw dislocations were shown to be insufficient for creating twisted crystals with small pitches.[231,264] On the other hand, dislocations can play an important role in twisting to relax stress. The surface stress hypothesis is plausible, but it is applicable only to very fine (several nm) fibers with larger surface area to volume ratios such as polymer lamellae. However, twisted fibers can be found for most any type of spherulite. The autodeformation mechanism considers all kinds of crystal inhomogeneities (including inhomogeneities leading to surface stress) and, in our opinion, is the most reasonable explanation for twisting of fibers as well as of their noncrystallographic branching. The latter mechanism will be discussed at length in section 5.5.

Continuous periodic change of crystal structure orientation along the fiber growth direction can be realized not only by means of twisting (rotation around fiber elongation) but also by means of lattice rotation around the tangent axes. The crystallites "roll" forward. This phenomenon was observed for Se, Fe_2O_3, and V_2O_3 spherulites growing in thin (<100 nm) amorphous films.[115,272−275]

Because of growth rate anisotropy, fiber twisting can promote rhythmic precipitation so that two etiologies for optical modulation coexist, co-operate, and compete with one another.[73] This is especially pronounced in polymers such as polyethylene,[276] poly(vinylidene flouride) and poly(vinylacetate) blends,[277] poly(epichlorohydrin),[278] and poly(nonamethylene terephthalate).[279]

4.2.4. Morphology Evolution. *Spherulite* is a misnomer. The center of a radially growing sphere is a singularity, a geometric point of symmetry K ($\infty/\infty m$). A real crystalline nucleus must transform into an object that grows radially (section 6.3, Figure 8).

Two major categories of spherulites have been proposed[281,282] depending on the relative size of the *core* and the radial *corona* or *periphery*. Category 1 spherulites have undetected cores with an apparent point nucleus — even though this is crystallographically impossible — and innumerable fibers radiating from this point (Figure 7e). Category 2 spherulites have distinct cores that result from branching of a nucleus that evolves into a *double-leaf* morphology (Figure 8). Poly(bisphenol A octane ether) offers a clear illustration of the Category 1/2 dichotomy.[238,283] However, this is most likely a false dichotomy; it is unnecessary. Category 1 spherulites are likely Category 2 spherulites with submicroscopic nuclei.

Fibers also can nucleate on an amorphous particle[121,139] or an amorphous precursor to a crystalline phase,[284] a void (Figure 9a), or a small crystal (Figure 9b). A single crystal can start branching along its outer surface resulting in gradual transition to a spherulite without a double-leaf (Figure 9c). Alternatively, one spherulite might give way to the nucleation of another, faster growing direction (Figure 9d) or polymorph[240] on its surface.

Double-leaf core morphologies have been studied in detail (see section 6.3)[51,53,56,61] Their evolution is comparable for polymers[66,239,285] and molecular crystals[51,130,218] grown from the melt, as well as for solution grown crystals.[68,149,152] The only

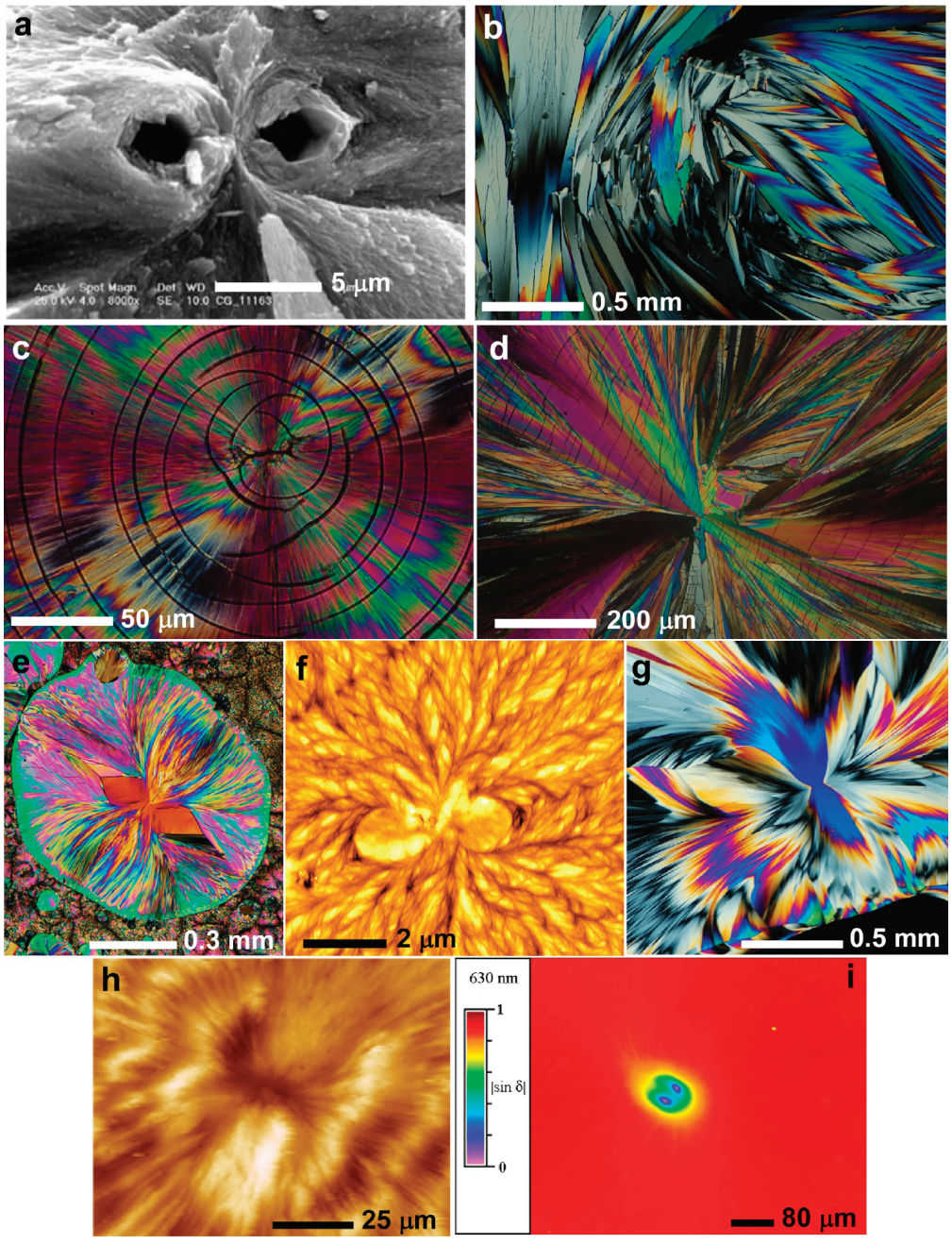

Figure 10. Double-leaf morphologies in gel (a) and melt (b−j) grown spherulites. (a) Fluorapatite spherulite with voids formed in the "eyes". Reprinted with permission from ref 68. Copyright 2007 Springer. (b) Testosterone propionate spherulite grown at 60 °C[74] showing random fiber orientations in the eyes. (c) Hippuric acid grown at 80 °C with [001] elongated fibers showing gradual change of fiber orientations in the core. (d) Hippuric acid with [100] elongated fibers showing unorganized growth and random fiber orientations in the eyes. (e) *N*-(2-Thienylcarbonyl)glycine spherulite with the eyes filled by a single crystal. (f) Poly(*R*-3-hydroxybutyrate) with 8 wt % 3-hydroxyhexanoate spherulite showing one flat-on lamella in each eye (used with permission of H.-M. Ye). (g) Resorcinol containing 7 wt % D-tartaric acid grown at 43 °C showing different fiber elongation directions in the core. (h) Poly(butylene succinate) grown at 80 °C with a gradual change of lamellae orientations in the eyes (used with permission of Y.-X. Xu). (i) Linear retardance (|sin δ|) micrograph of the nucleus of a sorbitol spherulite. Image made by Aden K. Kahr and reproduced with his permission.

difference relates to the contents of the so-called *eyes* (Figure 10) that flank the initial nuclear needle. Because of a lack of material supply in solution-grown spherulites the eyes can be voids (Figure 10a).[68,130,132,148] Spherulites from the melt may contain filled eyes composed of ordered fibers with gradually changing orientations (Figure 10c,h), chaotically misoriented fibers (Figure 10b,d), one single crystal (Figure 10e), or even one flat leaf covering the whole region (Figure 10f). Fiber growth directions in the eyes and the rest of spherulite may be different (Figure 10g).[266] Figure 10i makes the eyes of a sorbitol spherulite come to life, albeit alien life. Deans has referred to the ill-defined cores in siderite ($FeCO_3$) spherulites as *cryptocrystalline*.[286]

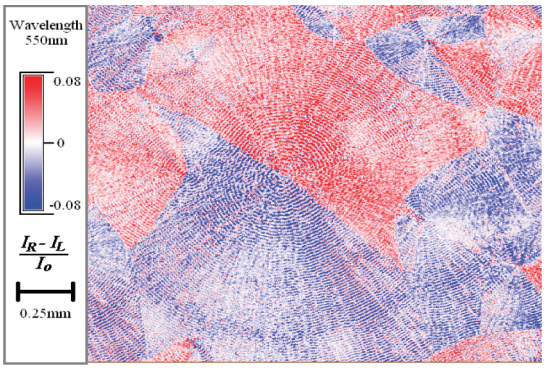

Figure 11. Circular extinction micrograph of a phthalic acid spherulite grown by rapidly evaporating ethanol solution. Reprinted with permission from ref 158. Copyright 2006 American Chemical Society.

Zhong and Chu have shown, for instance, that calcite spherulite growth mediated by polysaccharides leaves behind a metastable phase of amorphous calcium carbonate.[287]

The bifurcation of double-leaves into halves can be manifest as chiral semicircles. Toda and co-workers showed that poly(vinylidene fluoride) spherulites had enantiomorphous textures in halves defined by the bisector of the narrow neck in the early sheaf-of-wheat.[271,288] Gunn et al. showed this likewise in phthalic acid, further supported by differences in the transmission of left and right circularly polarized light (Figure 11).[158]

Other spherulites have large cores but give no evidence of double-leaf development. Among these are amyloid plaque spherulites that form in the brains of those burdened with a variety of neurodegeneracies. Micrographs from orientation-independent linear birefringence imaging systems showed less anisotropy in the cores;[200,289] by conventional polarized light microscopy, a disordered core will be masked by the Maltese extinction cross. The development of bovine insulin spherulites observed with an orientation-independent polarized light imaging system are shown in Figure 12.[290,291]

4.3. Growth

Spherulites form in distinct environments. As crystallization conditions intimately control spherulite growth, melts, solid phases, and solutions have their own idiosyncrasies. These are discussed herein.

4.3.1. Melts. *Temperature and Supercooling.* Typically, as supercooling ($\Delta T = T_m - T$, where T_m is the melting point) increases, and the growth temperature, T, decreases, the following series of morphologies are observed: single crystals → crystals with exaggerated aspect ratios → open spherulites → compact spherulites.[51,65] Illustrations of this sequence for hippuric acid and tetraphenyl lead spherulites were provided recently.[73] In multicomponent melts, skeletal crystals can precede open spherulites.[100,111,216,217,292,293]

Because of the continuous transformation from the onset of noncrystallographic branching to the development of compact spherulites, the threshold supercooling for spherulite formation, ΔT_{sph}, is ambiguous. Values provided in Table 1 correspond to the ranges where such transformations occur. ΔT_{sph} varies from several degrees for mannitol to 70−400 °C for plagioclase,[100,292,293] but, roughly, ΔT_{sph} is slightly smaller than ΔT_{max}, the supercooling for which growth rate approaches a maximum (Table 1, Figure 13). Well-developed, compact

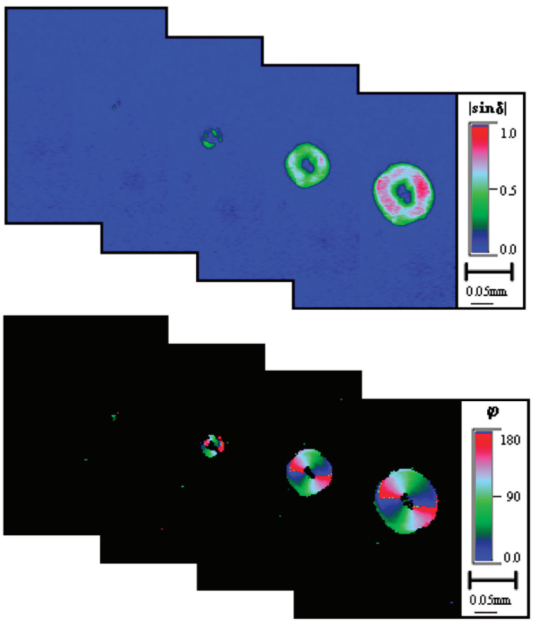

Figure 12. Growth of bovine insulin captured with real-time birefringence imaging system. Top: Tetrad of images separated in time by 900 s displaying the amplitude of the linear retardance. Bottom: The corresponding images showing the extinction angle. The direction of the larger refractive index plotted counterclockwise from the horizontal. Reprinted with permission from ref 291. Copyright 2006 Elsevier.

spherulites with fine fibers often form only when supercooling exceeds ΔT_{max}. The lower limit of the spherulitic growth mode is defined by extremely slow growth near or below the glass transition temperature, T_g (the only exception is fast growth from the glass in the case of the glass-crystal growth mode; see section 4.3.2). This leads to the conclusion that for spherulites grown at a high driving force for crystallization $\Delta\mu/RT \approx \Lambda\Delta T/RTT_m$, where R is the universal gas constant and Λ is a heat of fusion. The conditions summarized in Table 1 suggest that spherulitic growth from the melt is favored by high driving force and comparatively small kinetic coefficients (slow diffusion at large supercoolings).

Spherulites can grow near the melting point far from the glass transition temperature. This means that decoupling of the translational and rotational diffusion near the glass transition temperature[294−296] is not a precondition of spherulitic growth as it is sometimes stated in the literature.[282,297−300] For polystyrene spherulites,[234] decoupling of diffusion with viscosity was not detected.[301] Thus, viscous growth media are not required for spherulite formation, despite statements to the contrary.[281] Additives that increase viscosity encourage spherulitic growth, but this is not a viscosity effect per se.

Fiber thickness, h, decreases as supercooling increases.[8,76,108,122,230] This relationship is supported, indirectly, by the decrease of the band spacing in spherulites with twisted fibers;[72,92,108,230,232,233,246,264,306−309] pitch increases as fibers become finer. Selenium[107,108] crystallite thickness decreases exponentially as supercooling increases (Figure 14b) as does testosterone propionate[74] (Figure 14c) and salol[76] (Figure 14d). For high polymers the thickness of lamellae is very small (5−20 nm) and only increases slightly with temperature.[230] In these cases, h seems to be more strongly controlled by the material properties and thermodynamic conditions[235] with $h \sim (\Delta T)^{-1}$. In the course of branching,

dx.doi.org/10.1021/cr200297f |*Chem. Rev.* 2012, 112, 1805–1838

Table 1. Conditions for Spherulitic Growth from the Melt

compound	ΔT_{sph} °C[a]	$\Delta\mu/RT$[b]	ΔT_{max} °C[c]	T_m, °C[d]	T_g, °C[e]	ref
selenium	<20	<0.07	20	221	30	107, 108
hippuric acid	10−28	0.19−0.53	30	188		73
testosterone propionate	10−20	0.17−0.33	25	120	−1	74
δ-mannitol (with 15% polyvinylpyrrolidone)	5−10	0.18−0.36	38	155	13	present study
1,3,5-tri-α-naphthybenzene	14−19	0.33−0.44	25	199	69	65, 302
poly(butylenesuccinate-co-14 mol % ethylene succinate)	<38	<0.46	63	118	−44	303
polyethylene oxide	10−18	0.07−0.13	27	59	−77	304
poly(trimethylene terephthalate)	10−15	0.14−0.21	73	230	45	305
n-alkane $C_{246}H_{494}$	<3.5	<0.24	6.5	131.5		85
plagioclase ($(Ca_xNa_{1-x})Al_{1+x}Si_{3-x}O_8$, x = 0.3 melt, 2 kbar H_2O)	200	1.41	200	1100	770	293

[a] Minimal supercooling for spherulitic growth. [b] Driving force for crystallization. [c] Supercooling, for which growth rate attains a maximum. [d] Melting point. [e] Glass transition temperature.

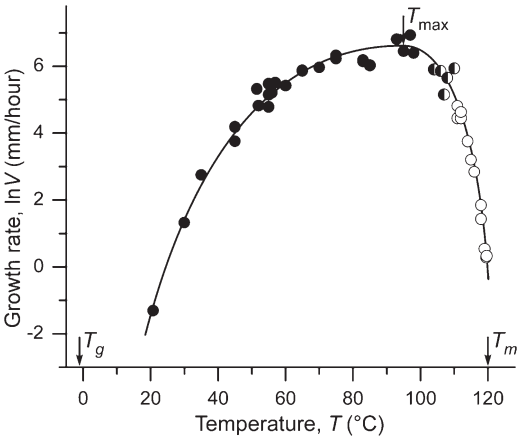

Figure 13. Growth rate and morphology of melt grown testosterone propionate crystals.[74] Solid circles = compact spherulites; open circles = branched single crystals; solid/open circles = crossover from single crystals to compact spherulites.

lamellae split into parts of equal thickness, and branching can be characterized by the width of plank-like lamellae, H, that decreases steeply as supercooling increases, according to an exponential or power-like function (Figure 14a).[87,92,232−234]

Growth Regime. Though diffusion control is not necessary for spherulitic *growth*, the relative importance of diffusion (of heat or nutrient) and interface kinetics determines spherulitic *form*. Near the melting point, morphological instabilities due to restricted diffusion can depend on the speed with which the heat of crystallization can diffuse away from the interface.[202,217] In highly cooled thin films, heat transfer is less important than interface kinetics in controlling crystallization. The interface controlled growth mode has been confirmed for many polymers,[8,264,283,306,307,310] diopside ($CaMgSi_2O_6$),[99] and some small molecular crystals such as maleic anhydride,[306] hippuric acid, and testosterone propionate[74] by the constancy of growth rate, V, with spherulite radius, r, and time, t.

Complications can arise for multicomponent melts. Some components may be extruded by the growing crystal and accumulate ahead of the growth front forming a diffusion boundary layer, shifting growth into the diffusion-controlled regime. Growth rates slow down as spherulites become bigger as for polyethylene and polyethylene oxide polymers[311] as well as for resorcinol crystals growing in the presence of tartaric acid. Moderate, progressive growth rate decreases do not necessarily destabilize the interface. But, eventually, depletion of nutrient will destabilize the smooth, spherical interface allowing fast growth only at the fiber tips, where material supply is still sufficient and branching can occur.[69,70] Fiber sides get too little material and do not split. As a result, compact spherulites turn into open ones. Increasing lack of the material supply further suppresses regular growth leading to dendrites and skeletal morphologies; noncrystallographic branching ceases and spherulites do not form.

Diffusion controlled crystal growth occurs when the rate determining step requires long-range transport. Growth kinetics can be modeled as a diffusion problem with a parabolic time dependence ($r \sim t^{1/2}$). Diffusion limited growth at $\Delta T < \Delta T_{max}$ is evident in the typical growth rate profile in Figure 13. The diffusion coefficient drops as the temperature decreases $D \sim \exp(-U/RT)$, where U is diffusion activation energy. At small supercoolings, the growth rate is small, D is big, and impurities can diffuse away from the crystal/melt interface. At higher ΔT, growth rate V increases rapidly but D continues to fall, increasing the time required for the equilibration of the impurity gradient. Higher V/D ratios favor diffusion controlled growth. After the growth rate passes the maximum, D decreases with increasing ΔT. Interface control of growth can resume if V decreases faster than D. Interface control does not rely on long-range transport but on rearrangements of particles at the propagating interface. These trends do not by themselves explain why spherulitic growth emerges when $\Delta T < \Delta T_{max}$.[292,293] Thinner fibers forming at higher supercoolings (see above) probably accommodate impurities in interstices, reducing the role of long-range diffusive mass transport.

Impurities. Most spherulite-forming melts are impure. The purest spherulites include sulfur (99.999%)[109] and selenium (99.999%).[107,108] However, these elements polymerize in the melt and are polydisperse. Also, because S and Se form molecular crystals, molecules in minor orientations/conformations could act as impurities in the process of forming disordered crystals.[312]

Many pure organic compounds decompose in part prior to melting. Decomposition is critical to the growth of hippuric acid spherulites from the melt. Moreover, resins and polymers have historically been used as additives to encourage spherulitic growth.[8,51] While impurities may have specific stereochemical roles in the spherulite growth process, at 5−30 wt %, they do not

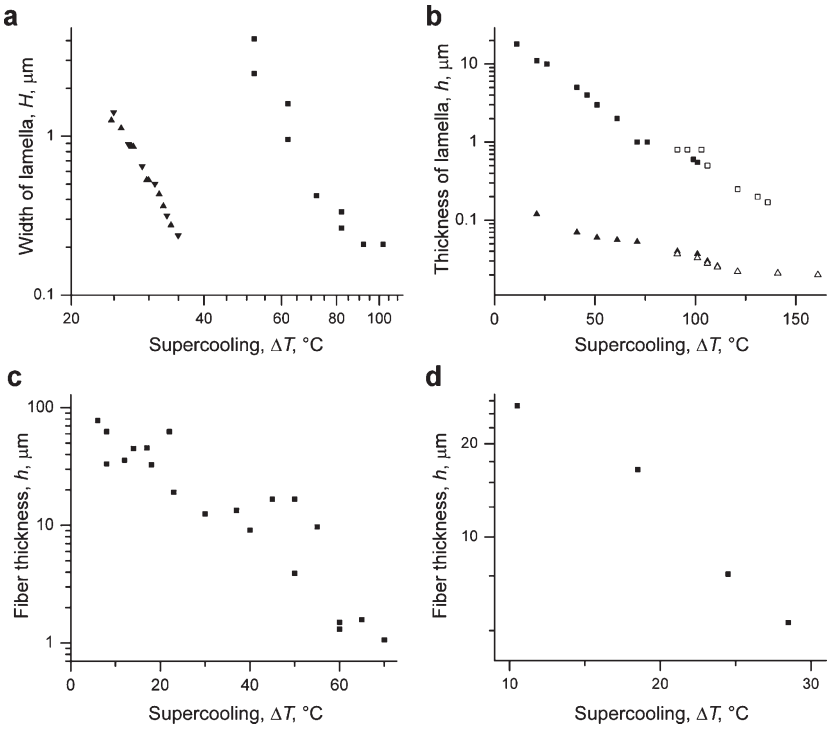

Figure 14. Effect of supercooling on fiber thickness or lamellae width in the melt grown crystals. (a) Polymers. Up and down triangles correspond to polyethylene fractions 32 kDa and 120 kDa, respectively. Recalculated from ref 233. Copyright 2008 American Chemical Society. Squares: polystyrene. Recalculated from ref 234. Copyright 2010 American Chemical Society. (b) Selenium. Triangles denote thickness of individual lamellae, squares denote stacks of lamellae. Adapted from ref 108. Copyright 1991 Elsevier. (c) Testosterone propionate.[74] (d) Salol. Recalculated from ref 76. The power law only fits better than the exponential function for polystyrene.

grossly affect ΔT_{sph}. As shown for various molecular crystals such as mannitol, urea, and tetraphenyl lead impurities function to decrease growth rates, attain higher supercoolings without nucleation, and facilitate growth along uncommon crystallographic directions. For example, tetraphenyl lead without additives forms spherulites at $\Delta T_{sph} > 7°$, while with 22 wt % polyvinylpyrrolidone (PVP) $\Delta T_{sph} > 15°$.[73]

4.3.2. Solid State. There is no sharp division between crystallization from glasses and from highly supercooled, viscous melts. Large deviations from equilibrium and interface control of growth are expected. In some cases, especially if the solid contains foreign components, growth can be shifted into the diffusion-controlled regime.[122] For example, recrystallization of an amorphous rubrene film is characterized by both diffusion and interfacial effects that compete with one another resulting in exponents in the power law $r \sim t^n$ that lie somewhere between 1 and 1/2.[313]

In some cases, growth near T_g can be accompanied by the fast glass-crystal growth mode, a mysterious rate acceleration.[74,77,123,124] This phenomenon is often associated with spherulitic morphologies. However, the dependence of one upon the other cannot be articulated at this time.

4.3.3. Solutions. *Supersaturation.* The driving force for crystallization from solution, supersaturation, is expressed as $\Delta\mu/RT = \ln(IAP/K_{sp})$, where IAP is the ionic activity product and K_{sp} is the solubility product. For stoichiometric solutions of ions, this expression can be roughly approximated by $\Delta\mu/RT \approx \nu\ln(c/c_{eq})$, where c is the salt concentration in the solution, c_{eq} is the saturation concentration, and ν is the number of ions in the neutral complex.

Section 3 shows that it is easy to get spherulites by crystallization of slightly soluble salts from highly supersaturated solution by precipitation or by growth in a gel. In both cases, thermodynamic supersaturation divided by the number of ions in a neutral complex, $\Delta\mu/RT\nu$, is extremely high exceeding 2.3 for calcium carbonate polymorphs,[127] 2.5 for calcium oxalate dihydrate,[130] or 9 for scheelite, $CaWO_4$.[143] Highly soluble salts that grow at low supersaturations ($\Delta\mu/RT\nu < 0.3$) rarely form spherulites. The morphology of $NaHCO_3$ was studied for supersaturations $(c - c_{eq})/c_{eq}$ varying from 0 to 1.15 with spherulites only appearing at values greater than 0.8, corresponding to $\Delta\mu/RT\nu > \sim 0.6$.[241] Thus, high crystallization driving force is a necessary condition for spherulites, in accordance with judgments drawn above for melt growth.

Growth Regime. Electron micrographs[68,130,314−316] show that crystallites in spherulites are polygonal with flat faces. This observation, along with the constancy of growth rate,[185,317,318] argues for interface controlled growth, at least in part. Others attribute the formation of spherulites to diffusion control,[128,164] or simply combine spherulites with dendrites as dense branching morphologies.[145,319] This distinction merits further discussion.

The relationship between diffusion and interface control can be estimated by the ratio $\xi = \Delta c_s/\Delta c$ (Figure 15), where $\Delta c_s = c_s - c_{eq}$ is supersaturation at the growth front, $\Delta c = c - c_{eq}$ is the supersaturation in the growth medium, c_s is the salt concentrations in the solution at the growth front. If $\xi = 1$, local mass transfer within the diffusion boundary layer is much faster than the rate of the incorporation of new growth units. When ξ nears zero, diffusion is rate limiting. Accurate evaluation of ξ requires knowledge of interface kinetics. The growth

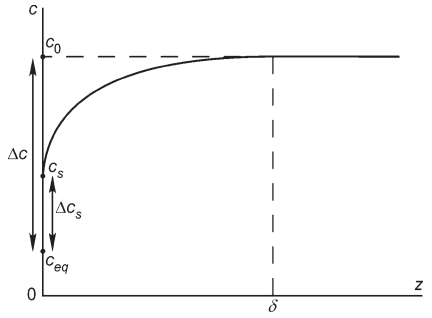

Figure 15. Diffusion boundary layer formed by a crystal growing from solution. The planar crystal/solution interface is normal to the space coordinate, z, which is positive for solution and negative for the crystal.

rate is $V = \beta(\Delta c_s)^m \approx D(\Delta c - \Delta c_s)/\delta_D$, where β, D, δ_D, and m are the kinetic coefficient, diffusion coefficient, thickness of diffusion boundary layer, and order of interface reaction, respectively. The growth regime is primarily defined by the product $\delta_D\beta/D$. In the simplest case of linear interface kinetics $m = 1$ and $\xi = 1/(1 + \delta_D\beta/D)$. In reality, the surface kinetics is nonlinear; $m > 1$ (often $1 < m \leq 2$). For quadratic interface kinetics ($m = 2$), $\xi = ((4\Delta c\delta_D\beta/D + 1)^{1/2} - 1)/(2\Delta c\delta_D\beta/D)$. The diffusion coefficient in a low-temperature aqueous solution or gel is typically 10^{-5} cm^2/s. The thickness of the diffusion boundary layer can be estimated as the growing crystal radius[203] and is equal to 1−30 μm. For slightly soluble salts, the kinetic coefficient is much smaller than 10^{-6} cm/s indicating interface limited growth. For calcium oxalate dihydrate, $\beta = 2 \times 10^{-8}$ cm/s[320] yielding $\delta_D\beta/D = (0.2-5) \times 10^{-6}$ and $\xi \approx 1$. A similar calculation supports interface control for protein crystallization.[321] Impurities usually reduce β resulting in stronger interface control. Even in a gel where the double-diffusion technique is used to set up diffusion gradients along a column, any crystal forming within this column establishes its own diffusion boundary layer, and mass transfer within this layer primarily depends on the $\delta_D\beta/D$ value.[322]

Diffusion coefficients in solution vary slightly. Kinetic coefficients, on the other hand, can vary by many orders of magnitude. When the kinetic coefficient is large for highly soluble salts, diffusion becomes more important. In these cases, spherulites are rare. Solution-grown spherulites typically occur for compounds with small kinetic coefficients. Here, diffusion is less important, and the growth is controlled by the dynamics at the interface.

Impurities. Impurities are often found to be responsible for spherulitic morphologies. Apatite spherulites are promoted by addition of citrate ions,[133] calcite spherulites by Mn^{2+} and Co^{2+},[315] and aragonite spherulites by Mg^{2+}, Ni^{2+}, Sr^{2+}, and Ba^{2+}.[134] Calcium oxalate polymorphs grow as spherulites in the presence of acid-rich polymeric additives such as poly-L-aspartate, poly-L-glutamate, and polyacrylate.[129,130] Carboxymethyl cellulose promotes barium carbonate spherulites.[323] Hydroxypropylmethyl cellulose induces strong noncrystallographic branching of copper oxalate crystals.[324] According to our observations and the literature,[325,326] spherulites are common for the intermediate members of the isomorphous series $(K,NH_4)H_2PO_4$ but absent for the pure potassium and ammonium salts. We have observed that some substances crystallized from drops of solution on a glass slide form spherulites only in the presence specific of additivies. These combinations include $NaBrO_3$ with $K_3Fe(CN)_6$, $K_4Fe(CN)_6 \cdot 3H_2O$ with $NaBrO_3$, and $NH_4H_2PO_4$ with agar−agar.

Some spherulites, for instance, hen egg-white lysozyme, grow from solutions that have undergone liquid−liquid phase separation. Here, the kinetics is further complicated by the fact that the growth solution, once depleted, can be refreshed by the dissolution of other high-concentration droplets.[318]

Temperature. There is no systematic study on the role of temperature control of spherulitic growth from solutions.

4.3.4. Summary. The general features of spherulite crystal growth, formulated previously,[69,70] are here expanded and enumerated:

1. Spherulites are formed via *noncrystallographic branching*, distinguishing them from dendrites and diffusion-limited aggregates.[8,217,327]
2. Spherulites are more commonly grown from the melt where they display compact morphologies. Solution-grown spherulites are rare and usually exhibit open morphologies. On the other hand, there is no fundamental difference between multicomponent melts and solutions; all spherulites, whatever the growth environment, seem to be triggered by comparable processes.
3. Spherulitic growth requires a high crystallization driving forces (typical values of supersaturation or supercooling expressed as differences of chemical potential are $\Delta\mu/RT > 0.5$) with interface control of growth. This is the most important prerequisite for spherulitic growth.
4. Spherulitic growth is comparatively slow. For high supercooling and/or supersaturation at the growth front, slow growth necessitates a comparatively small kinetic coefficient, β. This is consistent with low melt crystallization temperature. For solution grown crystals, small βs are consistent with higher probabilities of spherulites among slightly soluble compounds.
5. A viscous medium is not a prerequisite for spherulitic growth. Melt growth tends to give more well-formed spherulites grown at lower temperatures (higher melt viscosity), but spherulites can be formed near the melting point of nonviscous liquids. For solution grown crystals, experiments are often conducted in a viscous gels since such conditions often facilitate the monitoring of crystallization. Gels double as impurities.[68] On the other hand, in many cases, spherulites of the same compounds can be obtained from freely flowing solutions.[125] Apatite spherulites, for example, can be grown from gelatin[68] *or* by precipitation from solution.[132]
6. Impurities encourage spherulite formation.
7. For melt grown crystals, the thickness of spherulite fibers decreases as supercooling increases (temperature decreases). We lack corresponding quantitative data for solution grown spherulites, but qualitatively it appears that higher supersaturation results in thinner fibers. According to our observations, in natural agates from cavities in effusive rocks, increasing chalcedony fiber thickness and subsequent transformation of chalcedony into quartz corresponds to decreasing supersaturation in the growth chamber.

In 1963, Keith and Padden[8] concluded that spherulite formation required growth of crystals with a fibrous habit and noncrystallographic small-angle branching. The fibrous habit, while common, is not requisite, but noncrystallographic branching lies at the heart of the spherulite growth mechanism.

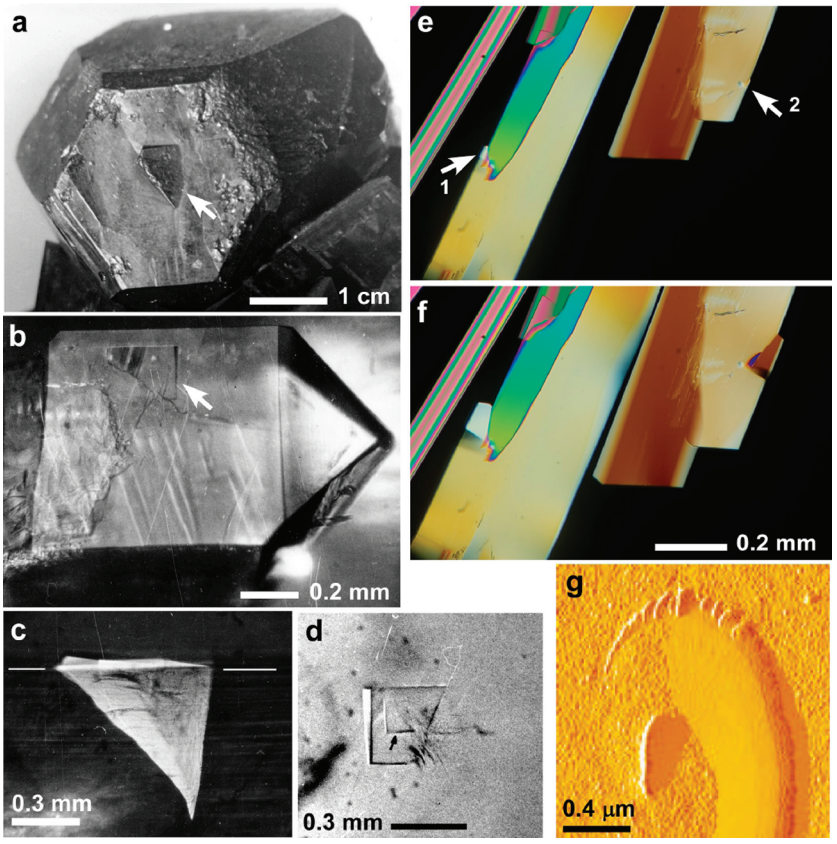

Figure 16. Initial stages of noncrystallographic branching. Some subindividuals are marked by arrows. (a) Natural crystal of galena (PbS) from hydrothermal deposits. From ref 69. (b–d) Potassium dihydrogen phosphate crystals grown from low-temperature aqueous solution. From ref 69. (c) Subindividual block, side view, observation with polarized light microscope (parent crystal is extinct). The crystal surface is marked by white lines. (d) Subindividual on the crystal face with a smaller secondary subindividual atop. (e, f) Subsequent polarized optical images of testosterone propionate needle-like crystals grown from the melt at 116 °C.[74] (g) AFM amplitude image of a polyethylene single crystal grown from the melt. The growth front was split into small twisted branches to form the spiral terraces of the same sense. Reprinted with permission from ref 233. Copyright 2008 American Chemical Society.

5. NON-CRYSTALLOGRAPHIC BRANCHING

5.1. General Characteristics

Spherulitic growth is dictated by noncrystallographic branching, a process informed by the study of imperfect crystals.[66,69,70,78,88,108,239,283,328,329] Branches often arise on a crystal face with apparent spontaneity (Figure 16). Closer examination reveals associations with imperfections such as outcrops of dislocation bundles (Figure 17),[69,330,331] sector zoning boundaries, inclusions, and scratches.[332] It is well-known that the frequency of branching in solution grown crystals (alum, potassium sulfate, potassium dihydrogen phosphate) is enhanced in the presence of nonisomorphous impurities (dyes, colloidal particles, mechanical impurities).[69,333,334] Isomorphous impurities can work likewise. According to our observations mixing of the following isomorphous salt pairs promotes noncrystallographic branching: $(K,NH_4)_2SO_4$, $(K,NH_4)H_2PO_4$, and $Na(ClO_3,BrO_3)$. New branches nucleate more easily near existing branches (Figure 18), points of collision with other crystals (subindividual crystal marked 1 in Figure 16e), and any other region characterized by a stress source.

Dislocations play a significant role in noncrystallographic branching as was shown for spherulites crystallizing from amorphous films[335] including Sb_2S_3[116,336] and Se.[107,335] The correlation between impurities, dislocation density, and noncrystallographic

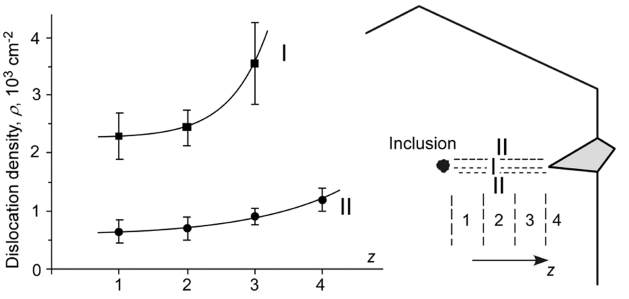

Figure 17. Formation and evolution of dislocation bundle for potassium hydrogen phthalate grown from low-temperature aqueous solution. From ref 69. The bundle nucleates at the liquid inclusion, and the dislocation density increases as a crystal grows and eventually results in formation of subindividuals.

branching was established for variety of crystals including solution grown pentaerythritol,[337] hydrothermally grown zinc oxide,[338,339] flux grown high-temperature superconductor $YBa_2Cu_3O_x$,[340] and natural quartz.[69] Stress in amorphous films affects the development of spherulitic fibrils as in the case of Te_3Se_4 and Te_3Se_4I.[341] In other words, crystal inhomogeneity, dislocations, and stress underlie noncrystallographic branching.

The morphology of subindividuals is generally similar to the morphology of the parent crystal. Blocks beget blocks (Figures 16e,f and 18a,b); needles beget needles (Figure 18c). Thin polymer lamellae branch to give equally thin descendants (5−20 nm), a dimension dictated by material properties and growth conditions.[235] Noncrystallographic branching may result in rupture of a lamella and displacement of its edges with formation of two new overlapping misoriented lamellae of the same thickness.[271,288]

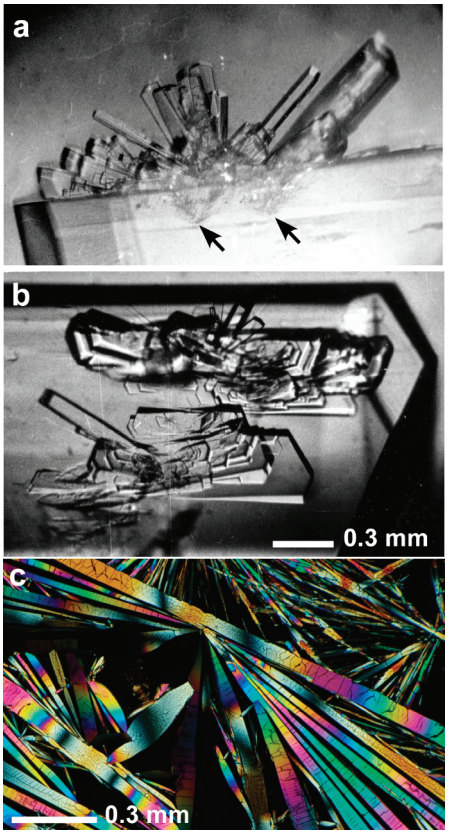

Figure 18. (a, b) Subindividuals on the (100) face of a sodium citrate crystal. Growth from low-temperature aqueous solution. From ref 69. (a) Side view. Two black arrows mark nucleation sites of two primary subindividuals. (b) Top view. (c) Branching of hippuric acid crystals grown from the melt. Branching points are often accompanied by formation of numerous subindividuals.

Subindividuals are misoriented with respect to the parent crystal with misorientation angles, γ, in the range of 0−15°. Distributions are characteristic of particular substances (Figure 19) and γ tend to grow with driving force, $\Delta\mu$.[69] In *n*-alkanes crystallized from the melt, the center of the misorientation or splay angle distributions increase from 10 to 18° as supercooling increases from 2 to 10 °C.[66,78] For melt grown poly(butane-1), the misorientation angle averages grew from 9 to 13° between T = 80−102 °C.[87]

The frequency of noncrystallographic branching is described by an induction period, the time necessary for the generation of a new subindividual, t_I, or by the branching rate, number of subindividuals, N, derived from one parent crystal per unit time, $R_b = dN/dt = 1/t_I$. These parameters are temperature dependent. The most important variable is the driving force, $\Delta\mu$. An empirical relationship, $t_I \sim (1/\Delta\mu)^n$, was established for solution grown crystals of tartaric acid, gypsum, potassium hydrogen phthalate, and pentaerythritol. The exponent n is equal to 3.3−4.7, 3.0, 1.4−1.8, and 1.7−2.0, respectively[69] (Figure 20a). For melt grown crystals, the intensity of branching increases with ΔT at small supercoolings but can reveal more complicated behavior with a maximum or plateau at higher ΔT (Figure 20b−d).

Noncrystallographic branching is more common for interface-controlled growth. It never accompanies extreme skeletal growth that is strongly diffusion controlled. For crystals growing in the intermediate or mixed regime, variations in the degree of diffusion/interface control can strongly affect branching intensity. $CuSO_4 \cdot 5H_2O$ crystals grown from solution undergo stronger branching if the solution is stirred. Interface control becomes stronger as the diffusion boundary layer, δ_D, thins.[69] The effect of

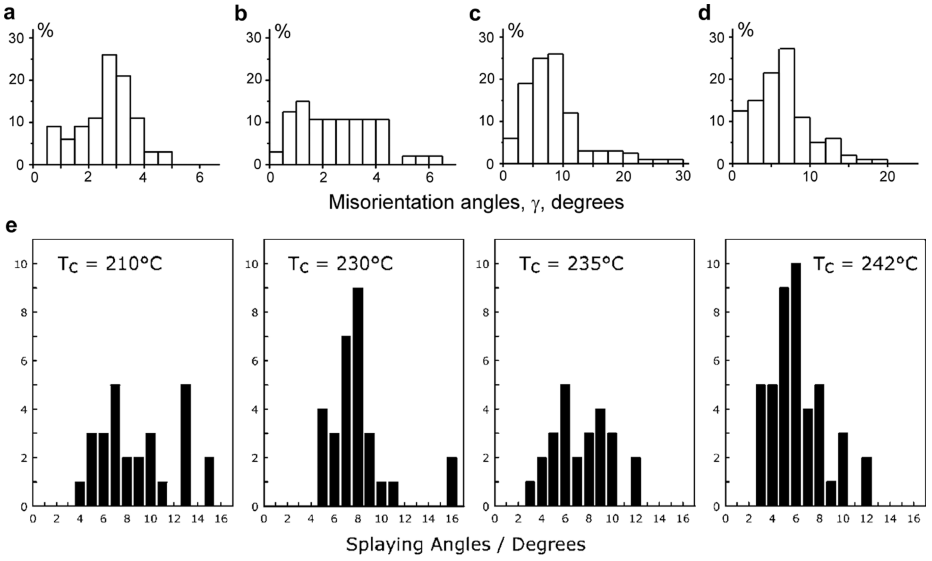

Figure 19. Histograms of the frequency of misorientation angles in a series of solution grown crystals (a−d). From ref 69. (a) Sodium citrate. (b) Potassium dihydrogen phosphate. (c) Potassium hydrogen phthalate. (d) Tartaric acid. (e) Histograms of the frequency of the angle of divergence of adjacent dominant lamellae in *i*-poly(4-methylpentene-1) spherulites grown, respectively, at (a) 210 °C, (b) 230 °C, (c) 235 °C, and (d) 242 °C. T_m = 272 °C. Reprinted with permission from ref 88. Copyright 1994 Highwire Press.

dx.doi.org/10.1021/cr200297f |*Chem. Rev.* 2012, 112, 1805–1838

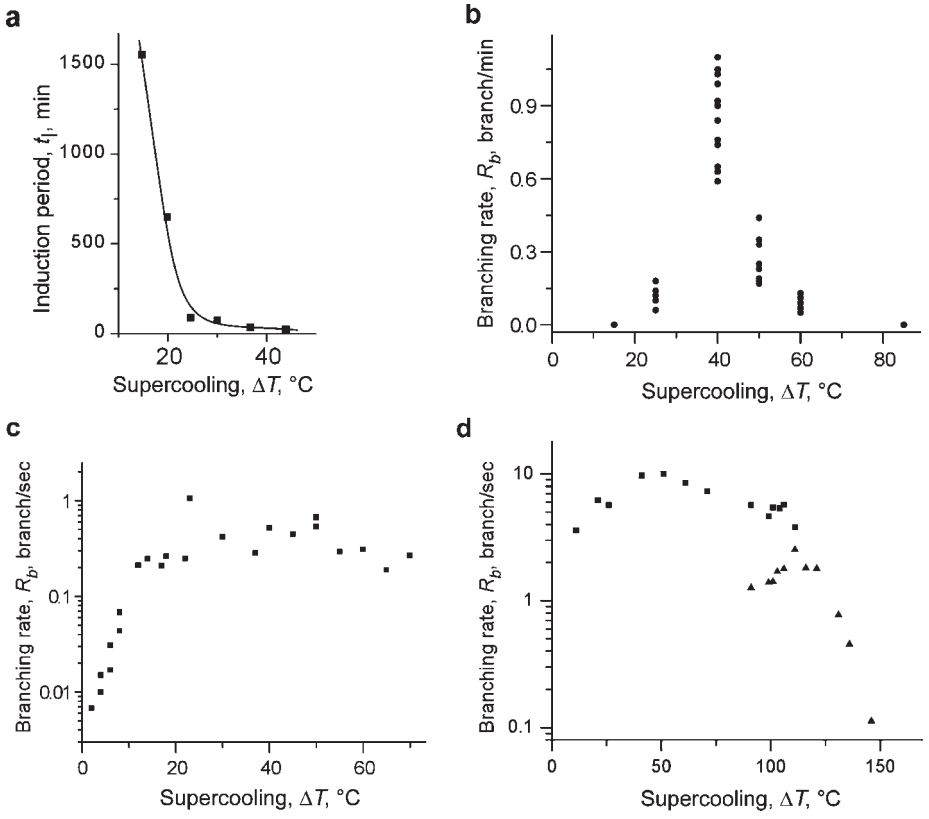

Figure 20. Effect of supercooling on the branching induction period, t_i, or branching rate, R_b. (a) Tartatic acid crystals grown from low-temperature aqueous solution at 20 °C. From ref 69. See also ref 328. (b) Poly(bisphenol A-co-decane) spherulites grown from the melt. Adapted from ref 342. Copyright 2003 American Chemical Society; see also ref 283. (c) Testosterone propionate spherulites grown from the melt.[74] (d) Selenium grown from the melt. Recalculated from refs 107 and 108. Squares and triangles correspond to different types of spherulites.

other growth conditions is equivocal. In solution-grown crystals temperature can promote[343] or hinder[343,344] branching whereas in melt grown crystals its action is coupled to supercooling or $\Delta\mu$. Impurities, in general, promote branching but can have the opposite effect.[69,70]

5.2. Constitutional Supercooling and Mullins-Sekerka Instability

Constitutional supercooling[203,204] was first suggested as a branching mechanism by Keith and Padden[8] who argued that impurities can be rejected by the growth front and form a sharp gradient in the surrounding region of a slowly diffusing melt. Increased impurity concentrations lower melting points and create undercooled regions where any protuberance will grow. This interface instability establishes a cellular growth front. Troughs between outgrowths concentrate impurities turning protuberances into fibers whose diameter can be estimated as $d = D/V$. Cellular structures are known for many industrial melt grown crystals such as germanium,[345] paratellurite (TeO_2),[346] and lead molybdate.[347]

Goldenfeld[348] generalized the constitutional supercooling model in terms of the Mullins-Sekerka instability[202,204,349] that considers perturbation of a growth front whose advancement is controlled by some heat transfer or diffusion. He showed that the size of fibrils has to be proportional to $d \sim (D/V)^{1/2}$ not D/V. The Mullins-Sekerka instability model was further modified to account for density differences between the growing crystal and surrounding liquid.[254,350,351] The stress (pressure) resulting from this difference induces fluid flow. In a viscous medium this process takes time, forming a pressure gradient along the crystal surface that can destabilize the growth front. The characteristic size of this instability scaled as $d \sim \eta^{-1/2}V^{-2}$.[254,350]

The idea of a diffusion driven, Mullins-Sekerka-like planar growth front instability has also been applied — without verification as far as we can tell — to the formation of thin chalcedony fibers in solution grown agates,[162] branching of fibers in selenium spherulites grown from the melt,[108] and in $CaCO_3$ spherulites grown in thin films from solution.[317] Bassett and co-workers[66,236,352−354] showed that the constitutional supercooling model was inconsistent with experiments on polyethylenes for which d barely changed over a wide range of growth conditions (D/V ratios). They also showed that the cellulation observed for polyethylene was independent of noncrystallographic branching;[355] fingering and small-angle branching are not one and the same.

Recently, the concept of Mullins−Sekerka instabilities was applied by Toda and co-workers[87,92,232−234] to explain branching and twisting of lamellae in a series of polymers. They showed that the $d \sim (D/V)^{1/2} \sim (\eta V)^{-1/2}$ expectation of lamellae width conformed to data from polyethylene, poly(vinylidene fluoride), poly(butane-1), and isotactic polystyrene. Unfortunately, the expected behavior was only captured in narrow temperature ranges: 6−10, 7, 22, and 50 °C for the four aforementioned polymers, respectively. For isotactic polystyrene, with the widest temperature range, the correlation is imperfect.[234] This data is insufficient to establish the mechanism of hydrodynamic instabilities.

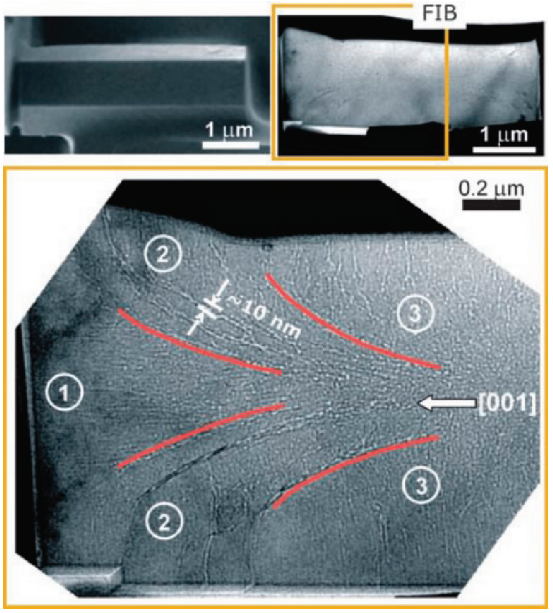

Figure 21. Top left: Scanning ion image of a fluorapatite crystal before focused ion beam (FIB) thinning. Top right: TEM overview image of a longitudinal FIB thin cut. Bottom: enlarged section as visualized by TEM, which reveals a microfibril pattern. Red lines indicate the borders between the distinct areas 1−3. Reprinted with permission from ref 366. Copyright 2008 Wiley-VCH.

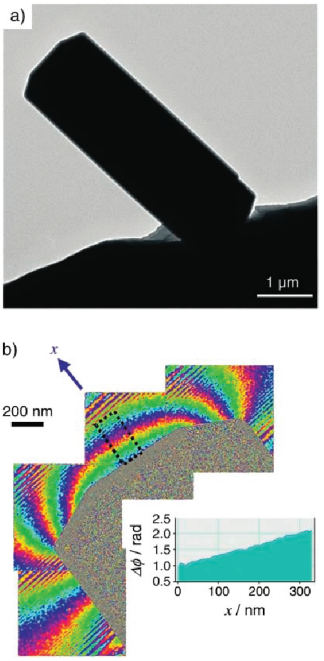

Figure 22. Fluorapatite crystal. (a) Conventional TEM image. (b) Retrieved phase image of an electron hologram (amplified eight-times, composed of four single images) shows the electric potential distribution around a crystal. Color code denotes a phase shift of 2π from green to green. Fresnel fringes of the interferograms appear as striation patterns at the corners of the phase images. The observed projected potential corresponds to a mesoscopic dipole. Inset: The phase profile (depicted for the rectangle with dotted border in the main picture at the basal plane) reveals a phase increase of about 1 rad per 300 nm. Reprinted with permission from ref 358. Copyright 2006 Wiley-VCH.

Although the Mullins−Sekerka instability remains the most popular explanation of branching in spherulites,[168] this hypothesis lacks experimental evidence. Moreover, this concept, in principle, is unable to explain noncrystallographic branching phenomenon because

1. The Mullins-Sekerka instability does not provide an explanation for small-angle branch misorientations, the distinguishing characteristic of spherulites. Indeed, growth front instabilities can create fingering, but there is no necessity of accompanying branch reorientations. At the same time, fibrillation can promote noncrystallographic misorientations since introduction of dislocations and other defects into thin fibers requires much smaller forces.
2. The Mullins−Sekerka instability is only limited to the normal growth mechanism for which attachment of molecules and ions occurs with equal probability on crystal surfaces of any orientation. The anisotropy of surface kinetics should strongly stabilize planar growth fronts.[203] In fact, *all* spherulite-building crystals are formed below the thermodynamic roughening temperature, are shaped by faces, and show growth rate anisotropy. One can expect kinetic roughening of fiber faces at high supercoolings. However, simulations[356] for a (100) Kossel surface show that the roughening transition requires high supercooling (ΔT > 300 °C at T_m = 200 °C), whereas most spherulites form at lower supercoolings. The apparent roughening transition observed by Miller[76] at low ΔT corresponds to the formation of a smooth growth front, when fibers become thin but not to the true roughening transition.
3. Most considerations of the Mullins−Sekerka instability make sense only for diffusion-limited growth. However, as shown in section 4, spherulite formation is controlled by interface kinetics. Under diffusion control spherulites do not form.

5.3. Intrinsic Electrical Field

In the past few years, Kniep with co-workers[68,227,280,357−360] developed an electric field induced growth mechanism for apatite spherulites grown from gelatin. The model was also applied to hydrothermally grown fluorapatite[133] as well as to calcite,[361] barium carbonate,[362,363] Sb_2S_3, Sb_2Se_3,[148] and zinc oxide.[141,147]

Apatite spherulites were grown in a gel column by means of double-diffusion. Although each Liesegang band[364] contained spherulites, the morphologies differ for bands located near the calcium and phosphate sources (Figure 8). Orientation of apatite crystals nucleated in gelatin was strongly controlled by the collagen triple-helix.[280,365] As a result, the [0001] apatite axis was directed parallel to the long axis of collagen macromolecules. After aggregation and reorganization, a well-shaped apatite-gelatin nanocomposite crystal (several μm in size) was formed containing ~2 wt % gelatin, whose molecules have a specific orientational distribution throughout the crystalline ensemble (Figure 21). Co-parallel, polar collagen molecules generate macroscopic electric fields around the crystal that have been observed by electron holography (Figure 22)[358,359] and simulated theoretically.[360]

The evolution of the spherulite morphology depends strongly on the chemical environment. In Liesegang bands enriched in phosphate, collagen molecules remain flexible, whereas in calcium enriched bands they become rigid. In the first case, collagen

molecules stick out of the crystal surface following the directions of electric field lines. These lines are parallel to the [0001] axis in region 1, slightly inclined in region 2, and perpendicular in region 3 (Figure 22). Since crystals primarily grow by {0001} faces, and collagen fibrils play an important role in apatite-gelatin nanocomposites, formation of oblique fibril orientations force new blocks to deviate from their original orientation and follow the directions of the field lines. This mechanism leads to small-angle branching. The subsequent generations of blocks also tend to follow electric field lines resulting in spherulites with smooth changes of branch orientations (Figure 8). Electric field effects on morphologies was confirmed by apatite crystallization under strong (5 kV/1.4 cm) external electrical fields[68,227] that intensified branch disorder and reduced growth rates.

In calcium enriched Liesegang bands, collagen molecules become rigid. They cannot follow the directions of electrical field lines and branching ceases. Morphologically, spherulites of this type are rough (Figure 8), and thus their formation must not be controlled by the macromolecules.

Application of the macromolecular-electric field model is restricted to the systems containing flexible polar additives that are capable of creating macroscopic electric fields. Even for apatite spherulites, its contribution is questionable because the intrinsic electric field mechanism alone is insufficient to explain all observed morphologies and the fact that similar apatite spherulites can be grown by precipitation in gelatin-free solution.[132]

5.4. Induced Nucleation in Polymers

It was proposed that polymer-spherulite branching can result from the imperfect process of lamellar formation by folding of polymer chains.[236,239,283,367−369] The dangling "ends" and "loops" remain hanging off the side surfaces of the lamellae and can work as nuclei for subindividuals. New lamellae can nucleate *near* parent lamellae as in poly(bisphenol A octane ether)[283,367] and *trans*-1,4-polyisoprene.[370] This mechanism of induced nucleation can be further generalized assuming that growing lamellae work as a stress source in a viscous medium accelerating nucleation even in the absence of dangling chain fragments (in original papers this process was considered a separate mechanism).[283,367] In other words, instead of branching on the surface of existing lamellae, new lamellae nucleate in the liquid. This mechanism has a limited application since branching *on the crystal surface* usually predominates and this occurs only for very viscous media.

5.5. Autodeformation Mechanism

The concept of *autodeformation* defects was articulated in the 1970s and 1980s to explain the formation of various crystal processes such as bulk martensitic transformations, crystal bending and twisting during growth, noncrystallographic branching, and growth twinning, among other deviations from single crystal ideality. It was applied to, and verified for, a variety of crystals, primarily grown from solutions. With the exception of two brief reviews in English,[328,371] most of the experimental and theoretical works[329,337,372−381] including one book[69] and one review[70] were published in Russian and remain unknown to a significant part of the international scientific community. For this reason, we give a detailed description of the concept as applied to noncrystallographic branching. In the 1990s, Chernov applied a variation of the same basic idea to explain the imperfections in protein crystals.[321,333]

The concept of autodeformation defects in general, and crystal branching in particular, was primarily developed for highly soluble organic and inorganic compounds (tartaric acid,[328,374] sodium citrate,[70,329] potassium dihydrogen phosphate,[329,375] pentaerythritol,[337] potassium hydrogen phthalate,[69] and potassium sulfate,[69] among others grown from low-temperature aqueous solutions). This group of compounds can be grown under a wide range of controlled conditions and manifests various branched morphologies. However, the autodeformation mechanism is based on general principles of defect formation and can be more widely applied.

Autodeformation stresses the key point of the theory: defects formed during crystal growth induce greater catastrophes. Defects achieve this cascade of woe through internal stress that accompanies crystal growth and relaxes via formation and motion of dislocations. Dislocations, driven by stress fields, organize themselves into ordered ensembles that eventually become manifest as macroscopic defects. In many cases, such defects form new, even stronger stress fields leading to autocatalytic processes of defect generation. The role of dislocations in noncrystallographic branching has been repeatedly emphasized for polymers[88,369] and for selenium,[107] but the mechanism of their generation and self-organization remained unclear.

The driving force for autodeformation is elastic stress. In well-studied, industrially grown crystals from the melt, temperature inhomogeneities are the greatest stress source.[203] Nonlinear temperature changes cause thermoelastic stress and strain. How much? Accurate stress calculations are demanding,[382,383] requiring knowledge of the heat distribution, crystal morphology, elastic constants, and thermal expansion coefficients, but in many cases approximate solutions are applicable.[384] Thermoelastic stress in ionic-covalent crystals typically ranges from 1−1000 MPa, and, for example, it can attain 40 MPa ($\approx 10^{-3}G$, where G is the shear modulus) for lead molybdate[385] and 100 MPa ($\approx 10^{-3}G$) for lithium niobate.[386]

In crystals growing from glasses and viscous liquids stress can be induced by the change of specific volume during crystallization.[6,335] For example, in selenium this stress can attain 0.3 GPa ($\approx 0.1G$).[351,387] Additionally, in crystals grown in the form of very thin (5−20 nm) lamellae (most polymers, selenium), the surface stress can be significant (0.15−0.25 GPa or $0.08G-0.13G$).[90,308]

For solution grown crystals and some melt grown crystals, compositional heterometry is the leading cause of stress.[69,371,384] Crystals grown from impure media may have a variety of spatial inhomogeneities such as concentric zoning, growth sector, and subsector zoning.[388,389] Different regions of the same crystal may have slightly different lattice constants. Requisite adjustments of cell size create elastic stress and strain. Calculation of heterometry stress is even more complicated than of thermoelastic stress. Nevertheless, the stress values can be estimated from simplified expressions[69,384] or simply from Hooke's law $\sigma = E\Delta a/a$, where $E \approx 2G$ is Young's modulus and Δa denotes the difference in lattice constants a between different crystal volumes. The strain ($\varepsilon = \Delta a/a$) in modestly enriched molecular crystals $\varepsilon = \Delta a/a$ can attain 0.008.[371]

Stress can be very high due to the discontinuities at growth sectors boundaries. For instance, σ can achieve values of 1.9 and 0.4 GPa ($\approx 1.3 \times 10^{-2}G$ and $\approx 2.7 \times 10^{-3}G$) in natural tourmalines[372] and garnets,[389] respectively. Figure 23 shows X-ray diffraction topographs of transparent crystals of potassium-ammonium aluminum alum, $(K_{0.5}(NH_4)_{0.5})Al(SO_4)_2 \cdot 12H_2O$, grown from solution at low temperature. One can see that dark areas of stress concentration accompany zoning, sector zoning, subsector zoning boundaries, and dislocation lines. The value of sector zoning stress calculated from anomalous birefringence equals 1−3 MPa or $\approx (1-3) \times 10^{-4}G$.[388]

Internal stress can also be generated by inclusions of foreign phases, dislocations, stacking faults, or twin boundaries,[203,391,392]

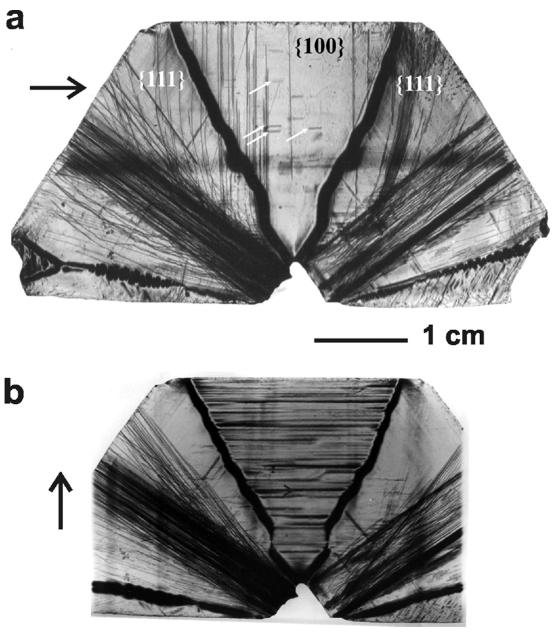

Figure 23. X-ray diffraction topographs of (110) section of an alum crystal $(K_{0.5}(NH_4)_{0.5}Al(SO_4)_2 \cdot 12H_2O$. Large arrows show the orientations of the diffraction vector: (a) reflection 220; (b) reflection 004. From ref 390. Reproduced with kind permission of the Mineralogical Society.

mechanical collisions,[393] gravity, viscous flow,[351] and crystallization pressure.[394] Stress concentrators include kinks associated with zoning and sector zoning boundaries as well as inclusions.[203,395]

Stress Relaxation. Elastic stress increases crystal free energy. Crystals mitigate stress by brittle relaxation or, more commonly, by plastic relaxation. The latter can be realized through slip as well as mechanical twinning and martensitic transformation.

Dislocations move so as to redistribute and reduce stress that has reached a critical value τ_c, the critical shear stress. τ_c drops exponentially with temperature ($\tau_c < 10^{-6}G$ at $T/T_m > 0.85$); therefore, it is easily reached in melts.[396] Near the melting point, any stress is quickly dissipated by dislocation formation resulting in very high dislocation densities up to $\rho = 10^{10-15}$ cm^{-2}.[203,397]

The τ_c drops below $10^{-4}G$ when $T/T_m \sim 0.6$.[396] This is especially true for the majority of crystals growing from the melt/solid phase including molecular crystals (for a relatively high melting point $T_m = 200$ °C, $T/T_m > 0.6$ if $T > 10$ °C, a value that is often lower than the attainable growth temperature), silicates, and other inorganic crystals.[100,119,120] Many solution grown crystals also obey this condition.

Far from the melting point ($T/T_m < 0.5$) critical shear stress remains low ($\tau_c = 10^{-4}-10^{-5}G$) only for metals[398] and other plastic materials.[399,400] For example, in ZnO crystals grown from hydrothermal solutions at ~350 °C ($T/T_m = 0.3$), τ_c is lower than $10^{-4}G$.[338] On the contrary, for brittle materials (various inorganic salts, molecular crystals, or some silicates) $\tau_c = 10^{-3}-10^{-2}G$[396,400] becomes comparable with tensile strength $\sigma_c = 10^{-3}E$,[401] suggesting destruction of the brittle material.[69,402] Plastic deformation in the crystal volume cannot be the main reason for stress relaxation, but it is still possible in the subsurface (several nanometers) crystal layer with smaller nucleation barriers and greater dislocation mobility.[272,403,404]

Nucleation of Primary Subindividuals. In materials with low plasticity, significant dislocation mobility is only possible in the thin subsurface layer. Crystals with high plasticity relax more rapidly and do so throughout the bulk.[203,338] Stress relaxation typically begins in regions with high dislocation densities such as a dislocation bundle propagating from a seed (Figures 17 and 23), inclusion, or from zoning and sector zoning boundaries. In subsurface crystal layers, dislocations driven by internal stress start moving and organize themselves into ordered ensembles as in solid state recrystallization processes.[405−407] New dislocations may be produced concomitantly.[396,405] Direct nucleation of dislocation walls is also possible as for selenium crystals forming in thin amorphous films.[335] Formation of dislocation walls and their ordering into networks[399,403−405,408] reduces long-range elastic fields and thereby lowers free energy of the crystal (free energy may rise due to surface energies associated with grain boundaries, but this is likely to be a small effect when dislocation density is high). The size of network cells grows and eventually exceeds the size of the critical crystal nucleus, r_c. At this point, a block can begin to grow independently. Interfaces between the renegade block and the parent crystal emerge on the surface in the absence of noncrystallographic branching.

On the other hand, Figure 17 shows a solution grown potassium hydrogen phthalate crystal with a dislocation bundle nucleated from a liquid inclusion. Dislocation density in the bundle gradually increases with the ultimate formation of subindividuals.

The subindividual is characterized by several important features:

1. It is misoriented with respect to the parent because dislocation walls (also known as disclinations[403,404]) represent low-angle boundaries.
2. The size of the two-dimensional critical nucleus is inversely proportional to $\Delta\mu$. Therefore, the subindividual nucleates with a higher probability at higher driving force for crystallization.
3. The evolution and reorganization of the dislocation ensemble take time. There is an induction period prior to small-angle branching. This frequently explains the fact that small, perfect crystals suddenly branch for no apparent reason (Figure 8).[68,69,358]

Subindividuals grow not only normal to the parent crystal surface but also laterally (Figures 16c and 18). This process of block spreading and individualization is mainly controlled by growth rate anisotropy.[69,373]

Multiplication of Subindividuals. As soon as a block turns into a subindividual, it forms its own facets. Surfaces between subindividual and parent crystals experience pressure and become a source of stress.[394] Increased levels of stress around subindividuals were detected by means of stress birefringence, formation of cracks, and direct measurements of the surface deflection (Figure 24).[69,70]

In summary, subindividuals form in response to internal stress, and the reduction of this stress becomes a source of stress elsewhere, forming positive feedback and establishing an autocatalytic loop that controls multiplication of subindividuals. Autocatalytic multiplication is indeed observed for both solution and melt grown crystals. Primary subindividuals are accompanied by nearby secondary subindividuals (Figure 18).[69,409]

In general, the number of subindividual crystals in an ensemble, N_Σ, is given by a standard equation describing the rate of chain reactions:

$$\frac{dN_\Sigma}{dt} = R_n A + (R_b - R_d)N_\Sigma \quad (1)$$

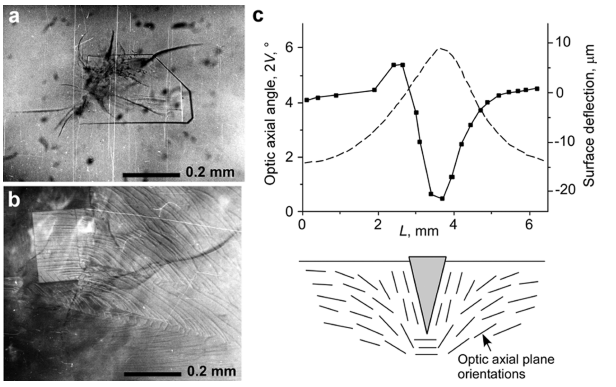

Figure 24. Stress and strain around subindividuals. (a, b) Cracks and, respectively, dislocation step sources in potassium dihydrogen phosphate crystals. (c) Anomalous biaxiality (dashed line; maximum shear stress is proportional to the squared optic axial angle, $\tau_{max} \sim (2\,V)^2$) and surface deflection (squares connected by solid line) in a pentaerythritol crystal. From ref 69.

where R_n, R_b, and R_d are rates of nucleation, multiplication (branching), and death of subindividuals, respectively, and A is the free area of an original crystal not covered by subindividuals.

Below we consider the effect of growth conditions on noncrystallographic branching and evaluate the applicability of the autodeformation mechanism to the formation of spherulites.

1. The driving force for crystallization $\Delta\mu$ is the most important parameter controlling noncrystallographic branching. If a subindividual block increases its size with a constant rate, V_B, depending only on the stress and material plasticity (temperature), it needs some induction period $t_I = d_c/V_B \sim \Delta\mu^{-1}$ to attain the critical size $d_c \sim r_c$, where the radius of critical nucleus $r_c \sim \Delta\mu^{-1}$. Additionally, in accordance with data on recrystallization,[410] the value of V_B drops as the block size increases requiring a stronger dependence of induction time on driving force: $t_I \sim \Delta\mu^{-2}$. Finally, V_B increases as stress τ grows; τ and $\Delta\mu$ are directly proportional[69,337,339] (inverse proportionality is known[402] but infrequent) making the $t_I(\Delta\mu)$ dependence even steeper. In general, the proportionality $t_I \sim \Delta\mu^{-n}$ is expected with $n > 1$. In accordance with this prediction, data for solution grown crystals show strong power-like effects of $\Delta\mu$ on branching with $n = 1.4-4.7$ (see section 5.1; Figure 20a).
   Melt growth is more complicated because increased driving force $\Delta\mu = \Lambda\Delta T/T_m$ is inversely related to material plasticity. Both dislocation velocity and dislocation multiplication rate reveal Arrhenius-like temperature dependencies.[408,411−413] Near the melting point, plasticity decreases slowly but driving force rises rapidly leading to increased branching with supercooling (Figure 20b−d). However, at higher supercooling, plasticity decreases are not compensated by the increased driving force and branching is diminished. Branching typically reaches a maximum rate $R_b = t_I^{-1}$ (Figure 20b−d).[74,107,108,342]
2. The growth regime establishes the relationship between crystallization driving force in the medium and on the crystal surface. Since frequent branching requires high driving force at the growth front, interface controlled growth is a necessary condition for strong branching (section 5.1) and spherulite formation (section 4.3).
3. The effects of growth rate, V, and driving force are hard to separate because these parameters are coupled (at low driving force $V \sim \Delta\mu$; at higher driving force $V(\Delta\mu)$ dependence is even steeper[203]). That is why, even though slower growth provides more time for dislocation ensemble rearrangement, and thus should promote branching, the opposite is observed.
   A more reliable way to evaluate growth rate is to compare kinetic coefficients, β. Lower kinetic coefficients should intensify branching. For instance, in solution grown crystals slightly soluble salts (lower β) form spherulites much more often than highly soluble salts (higher β) (section 3), and slower growing faces show more branching compared to the fast growing faces of the same crystal[69,130,132] (Figures 6 and 8).
4. Growth at elevated temperatures should promote branching via enhanced plasticity. For this reason, spherulites are generally more pronounced in melts than in solutions (section 3). However, varied temperature dependencies may be found in solution because all variables ($\Delta\mu$, V, growth regime, incorporation of impurities) are temperature dependent and some may be oppositional. For example, higher temperatures promote branching in solution-grown tartaric acid,[374] sodium citrate,[329] and gypsum[414] but inhibit it in potassium dihydrogen phosphate,[375] pentaerythritol,[337] potassium dichromate,[69] and in nasturan.[165] Even in melts, the crystallization temperature, T, cannot be detached from supercooling, $\Delta T = T_m - T$, which has the opposite effect on the spherulite formation (see above).
5. Impurities can affect branching in different ways. Simply considered, higher impurity concentrations create stronger internal stress.[69,384] A direct relationship between impurity concentration, internal stress, and degree of branching has been established for quartz,[376] pentaerythritol,[337] sodium citrate, and potassium dihydrogen phosphate.[329] On the other hand, impurities usually decrease plasticity of crystals,[405] inhibiting branching. The opposite effect is, however, also known as *hydrolytic weakening* of quartz[399,415] and other silicate minerals that can intensify branching. Finally, impurities promote or inhibit branching by changing the growth regime, driving force for crystallization, or growth rate anisotropy.[69] Data show that impurities promote branching more often than they inhibit it.

The autodeformation mechanism can explain, at least qualitatively, all features of noncrystallographic branching for different types of materials in different growth media. Among all the hypotheses heretofore considered, the autodeformation mechanism seems to have wide applicability to spherulite phenomenology, without denying the contributions of other mechanisms in specific cases. On the other hand, the autodeformation mechanism requires further development, since there is a dearth of information on the emergence of subindividuals from dislocation ensembles under internal stress fields in bulk crystals.

Requisite now are well-crafted high-resolution experiments that show the growth process of dislocation self-organization with formation of low-angle boundaries and, eventually, subindividuals in ionic and molecular crystals under action of internal stress. Little is known about the actual stresses in growing crystals and possible effects of such stresses on defect formation. In particular, it would be incisive to compare growth defects forming in

internally stressed crystals and those of the same substance that are not stressed.

6. MORPHOLOGY EVOLUTION

6.1. Geometrical Selection

Vigorous, noncrystallographic branching is requisite for spherulite growth. However, the development of spherical morphologies is controlled by growth rate anisotropy as well as geometrical selection processes[164,201,416−418] that are also known as *competitive* or *trans-crystalline growth*. In the latter process, succinctly stated, the survival of individual crystals within an aggregate is determined by crystal orientation with respect to the substrate surface and their growth rates. Faster growing crystals oriented normal to the aggregate interface or the spherulite envelope will have a better chance of survival (Figure 26). As fibrils grow longer, the more constricting becomes the perpendicular growth condition. This is true for flat and convex surfaces. In terms of spherulites, this means that only radial directions can provide uninterrupted growth. In a real spherulite, through the process of noncrystallographic branching, new subindividuals continually emerge (Figure 25) that may satisfy the normal growth constraint.

In spherulite cores, as the radial morphology is being established, constraints are few and fiber orientations change drastically (Figures 8−10). The periphery is where fibers maintain their orientations established in the course of geometric selection (Figure 7d,e). The formation and structure of these regions, the core and the periphery or corona, will be considered separately.

6.2. Spherulite Periphery

Compact, two-dimensional, well-developed spherulites with thin fibers are easiest to analyze. Growth of plank- or plate-like lamellae in three dimensions, however, are not qualitatively different. In the case of polymers, plank-like lamellae possess constant thicknesses, h, and branching affects only the width of lamellae, H. The approach developed below should work for H instead of h. Open spherulite formation is distinct and will be discussed separately.

In compact spherulites, subindividual crystals are packed tightly, permitting fiber multiplication only near the growth front. Reentrant angles, $\varphi = 2\pi/N_\Sigma$, emerge. Crystals in non-normal orientations will collide with others and stop growing. As shown in section 4.1 (Figure 19) misorientation angles are more or less uniformly distributed over the range from 0 to $2\gamma_{av}$, where γ_{av} is the average misorientation angle. When subindividuals form acute angles less than φ to the normal, further growth is possible. A crystallite at the supplementary, obtuse angle can not grow far. As a result, the probability of splinter survival is $P = \varphi/(4\gamma_{av})$.

The number of subindividual crystals, N_Σ, defined by eq 1, takes the following form:

$$\frac{dN_\Sigma}{dt} = (R_b - R_d)N_\Sigma = PR_bN_\Sigma \quad (2)$$

where the first term in eq 1 is dropped for well-developed spherulites, in which the free surface (A) of the nucleus is zero. The probability of crystallite survival, $P = 1 - R_d/R_b$, is controlled by geometrical selection whereas branching or multiplication rate, R_b, is determined by internal stress and material plasticity.

Combining eq 2 with expressions for P and φ one can eliminate N_Σ:

$$\frac{dN_\Sigma}{dt} = \frac{\pi R_b}{2\gamma_{av}} \quad (3)$$

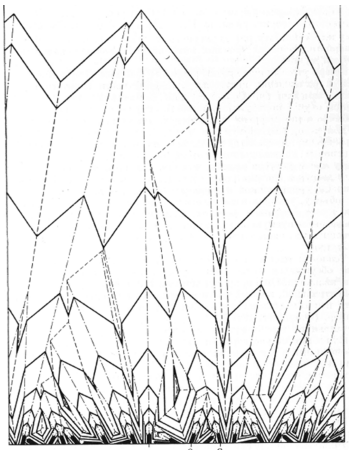

Figure 25. Principle of geometrical selection process.[203] Reproduced with the permission of A. Chernov.

Fiber thickness is then

$$h = 2\pi\frac{dr}{dN_\Sigma} = 2\pi V\frac{dt}{dN_\Sigma} \quad (4)$$

where $V = dr/dt$ is the normal growth rate. Substitution of 3 into 4 gives

$$h = \frac{4\gamma_{av}V}{R_b} = 4\gamma_{av}r_I \quad (5)$$

where $r_I = V/R_b$ is the spacing between two successive branching events. Equation 5 was indirectly confirmed by γ_{av} values calculated from experimentally measured h and r_I for Se spherulites grown from the melt.[108] The calculated average misorientation angles turn out to be approximately constant over a wide temperature range (100−210 °C) and equal to 0.01−0.03° and 0.2−0.9° for a single lamella and stacks of lamellae, respectively. The measured values of γ_{av} presented in the same paper are ≪1° and 5°, respectively. Agreement is good given the approximate character of eq 5.

Equation 5 contains average misorientation angles, growth, and branching rates, but does not contain time or spherulite radius suggesting the constancy of fiber thickness under constant growth conditions as spherulites develop radially. In fact, constancy of fiber thickness is common for spherulites[56] and confirmed for a number of substances. Figure 26 illustrates testosterone propionate. It also follows from constant band spacing along twisted spherulite radii grown under constant conditions.[58,59,74,87,92,108,218,231,419,420] As shown above, this constancy is a trivial consequence of the geometrical selection process. This conclusion was made previously on the basis of a slightly different form of eq 5.[69]

Open spherulites form if the branching rate (R_b) is very low (Figure 7f). Geometrical selection is not of primary importance and fiber thickness is dictated by growth rate anisotropy $\alpha = V_n/V$, where V_n is the growth rate normal to the fiber elongation. A simple geometrical construction shows that at $R_b \rightarrow 0$ open spherulites turn into compact ones if $\gamma_{av} < \alpha$.

6.3. Double-Leaves

Spherulitic cores are remarkable (Figures 9 and 10) and their formation attracted attention of the earliest spherulite researchers.[18,51,53] The evolution of the most common double-leaves (Figure 10) was already described in the 19th century,[421]

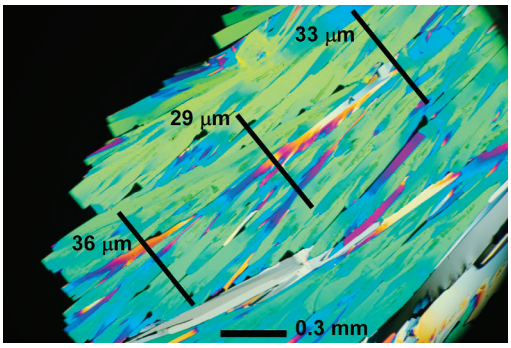

Figure 26. Testosterone propionate spherulite grown from the melt at ΔT = 18 °C.[74] Numbers near diagonal bars indicate average fiber thickness measured along corresponding bars.

and there were several attempts to model them[51,53,61,422] that eventually resulted in a *regular periodic branching model*.[56,64,423] This idea assumes that any subindividual crystal undergoes branching after a certain constant distance, r_I, or, assuming constant growth rate, after an induction period, t_I. The misorientation angles are always constant and equal to γ_{av}. At the outer spherulite boundary, there are no space constraints; therefore, the geometrical selection is obviated and new branches span outward leaving two voids (Figure 27a). The void diameter, L, can then be simply approximated. A 2π turn of fiber orientations around the circular void requires N branching events or $2\pi = N\gamma_{av}$. Since the circumference is equal to $\pi L = Nr_I$, one gets $L = 2r_I/\gamma_{av}$ (Figure 27a). This expression was obtained by Shubnikov[423] and then analyzed by Maleev.[64] It assumes all branching leads to further increases of the total misorientation between the original nucleus and the last generation of subindividual crystals. However, with equal probability new misoriented crystals can start to grow in the opposite direction (Figure 27b). Therefore, the actual core radius will be twice as large:

$$L = \frac{4r_I}{\gamma_{av}} = \frac{4V}{\gamma_{av}R_b} \quad (6)$$

Combining eqs 6 and 5 one can get simple relationships between thickness of the fibers and the core radius in a compact spherulite:

$$L = \frac{h}{\gamma_{av}^2} = \frac{16r_I^2}{h} \quad (7)$$

With measured values of h = 30 nm and γ_{av} = 1.8° for apatite crystals grown from gelatin[68] expression 7 gives L = 30 μm. Observations show that $L \approx 10-15$ μm (Figure 8) demonstrating reasonable agreement with the theory.

Spherulites can exhibit fine or coarse changes of fiber orientations. For example, see hippuric acid (Figure 10c,d). In the first case, the spherulite is fine and it is characterized by more or less smooth changes in fiber orientations; L = 20 μm and h = 0.3 μm (measured with SEM) that gives γ_{av} = 7.0° and r_I = 0.6 μm. In the second case, the spherulite is coarser and it is characterized by greater changes in fiber orientations in the spherulite core; L = 150 μm and h = 5 μm that gives γ_{av} = 10.5° and r_I = 6.8 μm. There are several possible explanations for varied core "smoothness"?:

1. The larger the average value of misorientation angles the broader is the distribution of angles and the more discernible are the branching events. However, for the spherulites in Figure 10c, d, misorientation angles are close to each other and to the typical γ_{av} values (section 5.1).
2. Low growth rate anisotropy, α, accompanying weak branching, at relatively low supercoolings, can coarsen the core. Geometrical selection is not very efficient and requires more time leading to a bigger area of chaotic fiber orientation.
3. Weak branching (bigger r_I) leads to larger straight segments and stronger stress inhomogeneity. Because the branching is not intense, nucleation of new subindividuals preferably occurs near already existing branching points characterized by greater internal stress.

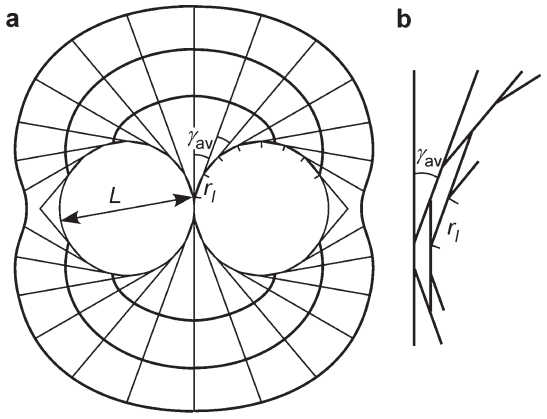

Figure 27. (a) Formation of double-leaf with circular "eyes" under constant growth conditions (r_I = const; γ_{av} = const). (b) Central part of the same construction illustrating branching in two opposite directions forming angles γ_{av} and 180°-γ_{av} with growth direction, respectively.

Ultimately, in the realm of weak branching and small growth rate anisotropy, no spherical void is formed. Instead, new more or less straight branches gradually fill the space around the original nucleus leading to radial fiber distributions (Figures 18 and 28).

This mechanism gives a straightforward explanation of variability of apatite spherulites grown in different Liesegang bands of the same gel column (left and right columns of images in Figure 8). For the right column of images (blue frames), strong branching and high growth rate anisotropy are accompanied by a gradual change of fiber orientation. For the left column of images (red frames) branching intensity and growth rate anisotropy are smaller, resulting in larger crystallites and abrupt changes of fiber orientations in the core (compare Figures 8 and 28). Note that the authors' explanation,[280] based on ion-modified collagen rigidity, differs from ours.

If the misorientation angle or the branching rate changes with time, simple geometrical constructions[64,423] predict spirals and other complicated morphologies instead of the double-leaf.[51,424] In cross section, instead of "eyes", voids become asymmetric leaf-like structures elongated along the crystal radii (Figure 8).[68,130,133,137,280,357] Closing-up of the spherulite takes much more time than is predicted because insufficient material supply inside the voids decreases supersaturation at the growth front and suppresses branching. For solution grown crystals the geometrical construction shown in Figure 27a often predominates over that shown in Figure 27b where material supply is not restricted.

6.4. Simulation

Simple geometrical constructions like those in Figure 27, first illustrated 80 years ago,[51,53,56,64,423] while instructive, are unable to account for diversity factors acting during crystallization. Today,

dx.doi.org/10.1021/cr200297f |*Chem. Rev.* 2012, 112, 1805–1838

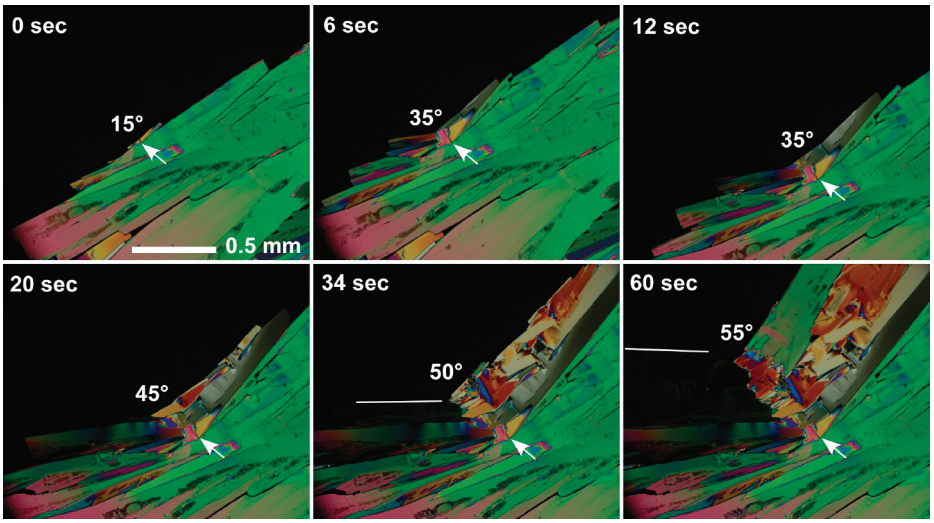

Figure 28. Sequence of images showing initial stages of spherulitic growth in testosterone propionate[74] at low supercooling $\Delta T = 8$ °C. Arrows show spherulite nucleation point. White lines highlight outer edges of extinct subindividuals. Total misorientation angles between outmost branches are written near re-entrant angles.

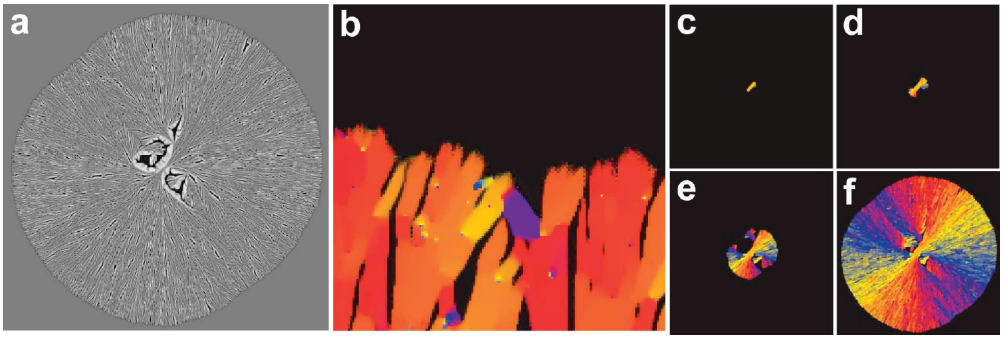

Figure 29. Phase field simulations of two-dimensional polycrystalline morphologies. Formation of a spherulite from a needle crystal via branching with random angle induced by trapped orientational disorder. (a) Composition map. (b) Magnified section of the orientation map of the interface. (c–f) Snapshots of the orientation map taken at 500, 1000, 2500, and 7500 dimensionless time-steps, respectively, on a 2000 × 2000 grid. Reprinted with permission from ref 300. Copyright 2006 Taylor and Francis.

computational simulation has become increasingly important in gaining insight into the complexities of polycrystalline growth.[425]

Simulations of complicated polycrystalline patterns including spherulite morphologies apply local rules of crystal growth behavior to any point of an evolving system. In the simplest case one can use the regular periodic branching model discussed in section 6.3. Time dependent branching rates and misorientation angles, when coupled to probabilities for branching, have been coded to simulate the spherulite morphologies of apatite[227] and lysozyme.[318] Spherulite morphologies of polymers were also modeled using more sophisticated Monte Carlo[426] and cellular automaton[427] methods.

So-called *phase-field* models have been paramount in this work. Phase-field modeling simulates macroscopic morphologies by introducing an order parameter that varies smoothly between the liquid and solid states.[428] The other basic field variables are the chemical composition and orientation of crystallites. In application to spherulites this method was first used for the simulation of concentric rhythmic deposition patterns in spherulites of ascorbic acid[257] as well as of more complicated spiral rhythmic deposition patterns in spherulites of poly(vinylidene fluoride) blends.[252,429]

In phase-field simulations by Gránásy and co-workers, the continuum of crystallographic and noncrystallographic branching is embraced by adjusting the variable parameters in the model.[297−300] The phase-field model showed that noncrystallographic branching and geometrical selection processes are sufficient to describe and simulate spherulitic growth (Figure 29) in a simple Ni−Cu alloy. Later, this approach was generalized to polymer spherulites.[430] There is no denying that the outputs of such simulations, displayed graphically, mimic natural forms with great fidelity.

7. USES OF SPHERULITES

A Yorkshire mineralogist commented in 1934: "Spherulitic ironstones are at present of practically no value as ores. They are often a source of trouble in working of fireclay, for they must be carefully removed."[286] In other words, in the practical world, spherulites were a nuisance. Since then, a variety of useful things in medicine and arts have indeed been derived from spherulites. Approaching the end of this essay, we briefly address for what good spherulites have been considered in recent decades.

7.1. Medical

Amyloid is a pathological proteinaceous material deposited in the extracellular space of various tissues and organs. The progressive accumulation of fine fibrils as spherulitic plaques

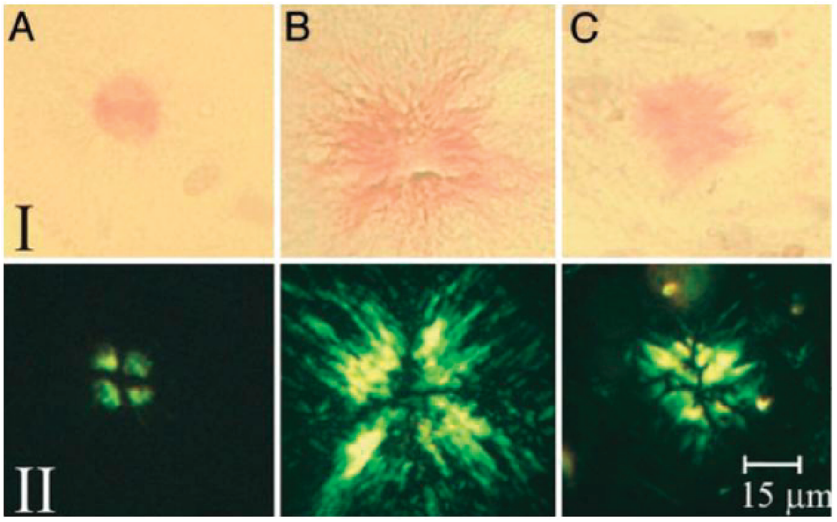

Figure 30. Congo red-stained amyloid plaques characteristic of three diseases: Alzheimer's disease (A), Gerstmann–Sträussler–Scheinker disease, a prion disorder (B), and Down's syndrome (C). I, amyloid in linearly polarized white light; II, amyloid between crossed polarizers. Reprinted with permission from ref 200. Copyright 2003 National Academy of Sciences.

characterize an increasing list of diseases, most notably Alzheimer's disease, Parkinson's disease, and adult-onset diabetes. The characteristic Maltese cross of the radial plaques between crossed polarizers has long been used by pathologists to identify spherulitic, biopathological entities (Figure 30).[198,199] The mechanism of formation of neurodegenerative plaques is still unknown. The disordered core may imply that the crystals are nucleating around a disorganized, catalytic structure.

Crystal-morphological analysis of cerebrospinal fluid was used to diagnose various diseases of the central nervous system. Copper chloride crystallized in the form of $CuCl_2 \cdot 2H_2O$ single crystals and spherulites when added to cerebro-spinal fluid.[431,432] Tumors of the brain and spinal cord were accompanied by single pyramidal crystals, but multiple sclerosis led to formation of open spherulites while inflammatory diseases of the brain and spinal cord resulted in compact spherulites. Ninhydrin (2,2-dihydroxyindane-1, 3-dione) added to the substance extracted from lower extremity veins showed different spherulitic morphologies depending on the degree of varicose disease.[432] Spherulites have likewise been used phenomenologically to identify evaporated alcoholic beverages.[433]

Spherulites of microbial polyhydroxyalkanoates have been considered as drug delivery vehicles due to their favorable biocapatibility.[434] In this context, the drug release from spherulites of polyhydroxbutyrate and copolymers with hydroxyvaterate were studied using a model compound, methyl red dye.[435,436] Likewise, spherulites made from high amylose maize starch form inclusion complexes with a number of fatty acid esters and may be used for the delivery of vitamins and drugs.[437] Spherulites of human interferon have been shown to have improved pharmacokinetics as compared with other formulations.[438]

7.2. Miscellaneous

Optically perfect spherulites, such as sorbitol shown in Figure 1, can be deliberately grown with impurities having spectroscopic signatures. The radial medium thus orients the included analytes that can then be studied in each and every orientation at the same time in non-normal incidence. This technique was used to clarify some concepts in spectroscopy with polarized light.[439]

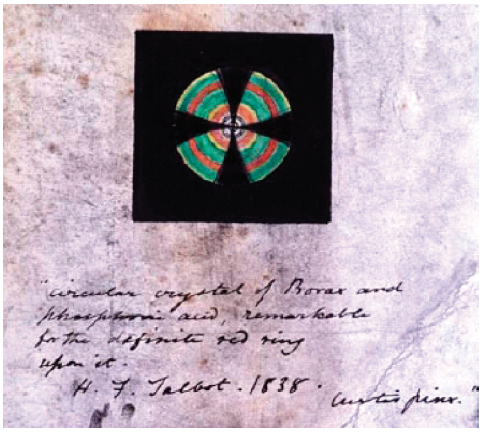

Figure 31. William Henry Fox Talbot and Curtis Pinx, "*Circular Crystal of Borax and Phosphoric Acic, remarkable for the definite red ring upon it*" (1838) Watercolour of Interference Pattern, National Library of Scotland with permission. Obtained courtesy of L. Dowlatshahi, ref 443.

Lloyd et al. used spherulites as photovoltaic cells. An anthradithiophene donor crystal formed spherulitic aggegrates dispersed in a disordered medium containing fullerene acceptors. Substrates with greater than 80% spherulite coverage gave a 1% conversion efficiency.[440] Microengineered interpenetration of spherulites can improve the elasticity of some fibrous materials.[441]

In mineralogy, spherulites can be used as indicators of crystallization conditions,[201] in particular, to analyze thermal history of effusive rocks,[96,98] or to estimate supersaturation and diffusion/interface control of solution grown minerals. For example, goethite (α-FeO(OH)), hematite, and malachite form spherulites only if they crystallize in zones of oxidation of sulfide ore bodies.[442]

7.3. Spherulites in Art

7.3.1. Photography. Brewster, who credited himself with the discovery of the first circular crystal, was a close friend of Talbot who invented — in addition to photography — the polarized light microscope. As discussed in section 2, Talbot prepared

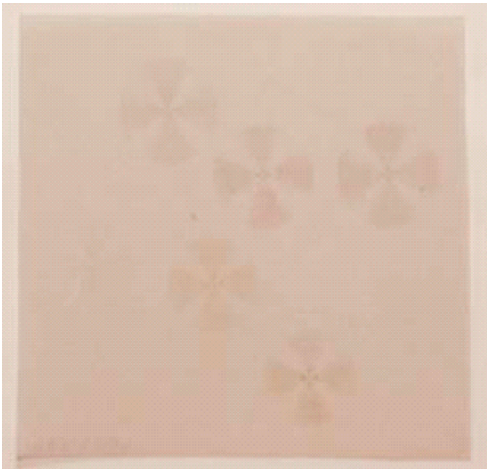

Figure 32. William Henry Fox Talbot, Five circular depictions of polarized light through crystals (ca. 1848). Calotype Negatives, 1937−2509, National Media Museum. Obtained courtesy of L. Dowlatshahi, ref 443.

Figure 33. Willemite (α-Zn_2SiO_4) spherulites in crystalline glaze. Ceramic by John Mankameyer. Photo reproduced with permission of John Mankameyer, Miles City, Montana.

circular crystals himself. His borax spherulites were very small, and he detected them only with the great resolving power of his newly invented microscope. Talbot drew, and then colored, what he saw under the microscope (Figure 31).[443] Later, he succeeded after some trials in impressing images of the spherulites directly onto photosensitive paper through the agency of the microscope, the first bona fide photographs of crystals, to the best of our knowledge (Figure 32).

7.3.2. Ceramics. Spherulites of willemite (α-Zn_2SiO_4)[444] form in ceramic glazes fired to high temperatures.[445] The polycrystalline circles that grow in the thin glaze layer on the curved surfaces of jars and pots (Figure 33) form the decorative elements in a rapidly growing craft. Controlling[446] the number, size, and texture (nucleation, growth, and morphology) of willemite spherulites determines the design of a ceramic piece. The principal components of glazes that yield willemite include SiO_2, K_2O, and ZnO (about 50, 5, and

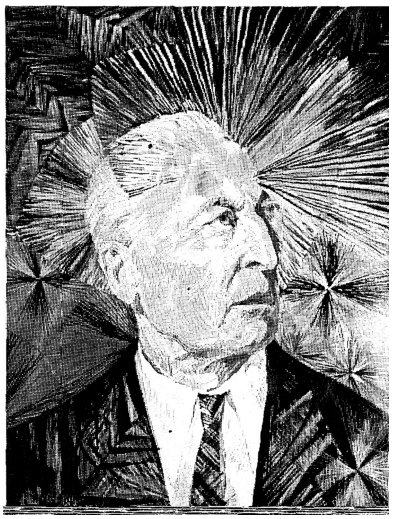

Figure 34. Portrait of crystallographer and spherulite researcher, A. V. Shubnikov, by his daughter, Vera A. Shubnikova. From ref 449.

25%, repectively). Other components are frequently added to control melt viscosity and include Al_2O_3, CaO, Na_2O, among other oxides. Typically glasses are fired at a maximum temperature (∼1250 °C) to ensure spreading of the glass over the ceramic surface. Selective seeding occurs by dropping the temperature to ∼950 °C, followed by growth at ∼1050 °C. This recipe ensures large, isolated spherulites as shown in Figure 33. The chemical dynamic between the ceramic and the glaze is complex. There is evidence of mass transport, and the formation of new compounds in the transition layer between the ceramic and glaze. Willemite crystals can be tinted by including transition metal oxides (e.g., CoO, NiO, CuO, MnO, Cr_2O_3, Fe_2O_3) in the glaze.[447] The microstructure of willemite glazes was clarified by confocal fluorescence and electron microscopy. The crystals grow along the *c* axis (space group $R\bar{3}$).[448] Despite increasing scientific interest in crystalline glazes, willemite spherulite growth remains more an art than a science.

7.3.3. Painting. Figure 34 shows a portrait of the great crystallographer A. V. Shubnikov (1887−1970) by his daughter Vera Shubnikova. She has used the spherulite as a principle of design in her excellent portrait.[449] Here, we see Shubnikov in the process of being consumed by spherulites. They become the fabric of his suit and merge with the fibrils of his hair. Shubnikova has created striking visual metaphor of a parent consumed by his crystallographic investigations.

8. SUMMARY

In 1836, Talbot wrote to the secretary of the French Academy of Sciences, François Arago, to call his attention to the remarkable, newly discovered crystals of borax "composed of an infinity of needles which radiate from a central point".[450] This review aimed to answer the questions of how and why such an "infinity" of needles organized themselves as they do, questions that have lingered for the better part of two centuries. To the best of our knowledge, these questions have not been answered directly and with sufficient attention to all spherulite forming materials and media. Only in this way do we find that is possible to bring the totality of spherulite research

within the focus of a small number of generative mechanisms, while at the same time disposing of prejudices relating to spherulitic growth that have arisen from attention to a limited number of spherulite forming substances.

Today, with the development of microstructural methods of analysis, we can qualify Talbot's "infinity". We know that spherulites are composed of a countable number of needles (a real lot, in many cases) of finite size. We know that they cannot radiate from a point and that their development into radial bodies follows a succession of stages. The conditions that tend to be requisite for this development include impurities, high crystallographic driving forces, and comparatively small kinetic coefficients. Large viscosities, often linked to spherulitic growth, seem to act by limiting kinetic coefficients. There is no intrinsic connection and many spherulites grow from nonviscous media.

Research on spherulites is spread among an "infinity" (>4000) of publications. Here, we have referred to about 10% (a real lot), emphasizing those that contain quantitative data. This proves to be sufficient to cover the great range of spherulites in depth. Ten percent of this 10% was published in Russian. This is unfortunate for our increasingly Anglocentric scientific world. A number of the Russian papers contain concepts seminal to the picture of spherulite growth developed here and are unavailable to much of the crystallographic community.

While we concede that two identical looking objects need not have arisen by the same mechanism — there are many ways that nature achieves radial organization — we do offer one mechanism, above all others, that seems to best account for the noncrystallographic branching that is the earmark of spherulitic kingdom, the autodeformation mechanism. The autodeformation mechanism concedes that impurities — in the form of additives, decomposition products, disordered molecules, or polydisperse polymers — play an undeniable role in spherulite growth. Impurities act principally by creating elastic stresses in imperfect crystals. The relaxation of such stress in plastic materials leads to disclinations and noncrystallographic branching.

AUTHOR INFORMATION

Corresponding Author

*(A.S.) Tel.: +1 (212) 992-9815. Fax: +1 (212) 995-3884. E-mail: shtukenberg@mail.ru. (B.K.) Tel.: +1 (212)992-9579. Fax: +1 (212) 995-3884. E-mail: bart.kahr@nyu.edu.

BIOGRAPHIES

Alexander Shtukenberg was born in Leningrad (now Saint-Petersburg, Russia) in 1971. He got a specialist degree in 1993 at Geological Faculty of Saint-Petersburg State University. Under the supervision of Yuri Punin, he received a Candidate of Science degree (equivalent to Ph.D., 1997) and continued to work at the Geological Faculty first as a researcher and then as a member of the faculty. He spent about three years from 1997 to 2006 at Bonn University and the Paul Drude Institute for Solid State Electronics, Germany. In 2009, he earned the Doctor of Science degree and in 2010 became a professor of the Geological Faculty of Saint-Petersburg State University. Since 2010, he has been working with Bart Kahr at New York University.

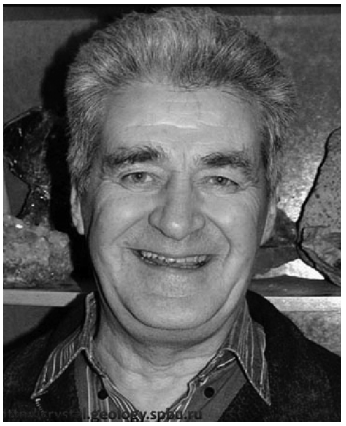

Yuri Punin was born in Leningrad (now Saint-Petersburg, Russia) in 1941. He got a specialist degree (1963) and a Candidate of Science degree (equivalent to Ph.D., 1970) at Geological Faculty of Leningrad State University and worked there as a researcher. He defended the Doctor of Science degree (equivalent of habilitation) in 1994, and the next year was appointed professor of crystallography/mineralogy at the Crystallography Department of the same university.

Erica Gunn was born in Plymouth, Massachusetts. She earned a bachelor degree at Simmons College in Boston and a Ph.D. under the supervision of Bart Kahr at the University of Washington in Seattle in 2009 for a study of *Small Molecule Banded Spherulites*. Erica was a postdoctoral fellow with Lian Yu, in the School of Pharmacy at the University of Wisconsin, Madison, and currently lives in Chicago.

Bart Kahr was born in New York City in 1961. He studied chemistry with I. D. Reingold at Middlebury College, with Kurt Mislow at Princeton University (Ph.D., 1988), and with J. M. McBride at Yale University. He was a faculty member at Purdue University from 1990 to 1996 and at the University of Washington, Seattle from 1997 to 2009. He returned to his hometown where he is currently Professor of Chemistry in the Molecular Design Institute at New York University. His research group studies the growth, structure, and optical properties of single crystals and polycrystalline patterns.

ACKNOWLEDGMENT

B.K. thanks the U.S. National Science Foundation (CHE-08545526) for support of this research. A.S. thanks E. Rosseeva, P. Simon, and R. Kniep who inspired him to initiate work on this review.

SYMBOLS

a	lattice constant
A	free area of original crystal not covered by subindividuals
c	solution concentration
c_{eq}	saturation concentration
c_s	concentration at the growth front
d	size of fibrils
d_c	critical size of subindividual block
D	diffusion coefficient
E	Young's modulus
G	shear modulus
H	crystal lamellae width
h	crystal lamellae thickness or fiber thickness
I/I_o	transmittance
$(I_R - I_L)/I_0$	the difference between intensities of transmitted right and left circular polarized light divided by the averaged transmitted intensity
IAP	ionic activity product
K_{sp}	solubility product
L	void diameter for double leaves
L_s	radius of spherulite
m	order of interface reaction
n	exponent
N	number of subindividuals
N_Σ	total number of subindividuals in ensemble
P	probability of crystallite survival in geometrical selection process
r_c	critical nucleus size
r_I	branch spacing
R	universal gas constant
R_b	$1/t_I$; rate of multiplication of subindividuals, branching rate
R_d	rate of death of subindividuals
R_n	rate of nucleation of subindividuals
t	time
t_I	time needed to generate one subindividual
T	crystal growth temperature
T_g	glass transition temperature
T_m	melting point
U	activation energy for diffusion
ν	number of ions in the salt molecule
V	growth rate
V_n	growth rate normal to the fiber elongation
V_B	growth rate of subindividual block
2 V	optic axial angle
z	crystal thickness; space coordinate
α	V_n/V; growth rate anisotropy
β	kinetic coefficient
γ	misorientation angle
γ_{av}	average misorientation angle
δ	retardance
δ_D	thickness of diffusion boundary layer
Δa	change in lattice constant
Δc	$c - c_{eq}$; absolute supersaturation in volume of solution
Δc_s	$c_s - c_{eq}$; absolute supersaturation at growth front
Δn	linear birefringence
ΔT	supercooling
ΔT_{max}	supercooling at maximum growth rate
ΔT_{sph}	spherulite threshold supercooling
$\Delta\mu$	driving force for crystallization expressed as a difference in chemical potentials
ε	strain
η	viscosity
θ	azimuthal crystal orientation
λ	wavelength of light
Λ	heat of fusion
ξ	$\Delta c_s/\Delta c$
ρ	dislocation density
σ	stress
σ_c	tensile strength
τ	shear stress
τ_c	critical shear stress
τ_{max}	maximum shear stress
φ	re-entrant angle

REFERENCES

(1) Lofgren, G. In *Proceedings of the Lunar Science Conference*; MIT Press: Cambridge, USA, 1971; Vol. 2, p 949.
(2) Yu, L. *Cryst. Growth Des.* **2003**, *3*, 967.
(3) Yu, L. *J. Am. Chem. Soc.* **2003**, *125*, 6380.
(4) Nezzal, A.; Aerts, L.; Verspaille, M.; Henderickx, G.; Redl, A. *J. Cryst. Growth* **2009**, *311*, 3863.
(5) Benedict, J. B.; Freudenthal, J.; Hollis, E.; Kahr, B. *J. Am. Chem. Soc.* **2008**, *130*, 10714.
(6) Blatter, A.; Ortiz, C. *J. Cryst. Growth* **1994**, *139*, 120.
(7) Cross, W. *Bull. Phil. Soc. Washington* **1892**, *11*, 411.
(8) Keith, H. D.; Padden, F. J. *J. Appl. Phys.* **1963**, *34*, 2409.
(9) Talbot, W. H. F. *Phil. Trans. R. Soc. London* **1837**, *127*, 25.
(10) Talbot, W. H. F. *Phil. Trans. R. Soc. London* **1837**, *127*, 29.
(11) Brewster, D. *Trans. R. Soc. Edinburgh* **1853**, 607.

(12) Brewster, D. *Phil. Trans. R. Soc. London* **1815**, *105*, 29.
(13) Dallas, E. W. *Proc. R. Soc. Edinburgh* **1876**, *9*, 129.
(14) Harting, P. *Recherches de Morphologie Synthétique sur la Production Artificielle de Quelques Formations Calcaires Organiques*; Van der Post: Amsterdam, 1872.
(15) Ball, P. *Shapes*; Oxford University Press: Oxford, UK, 2009; p 98.
(16) Meldrum., F. C.; Kim, Y.-Y.; Maillot, F.; Ward, O. *Adv. Mater.* **2010**, *22*, 2082.
(17) Meyer, A. *Untersuchngen über der Stärkekörner*; Verlag von Gustav Fischer: Jena, 1895.
(18) Lehmann, O. *Molecularphysik, Band 1*; Verlag von Wilhelm Engelmann: Leipzig, 1888.
(19) Lehmann, O. *Flüssige Krisalle*; Verlag von Wilhelm Engelmann: Leipzig, 1904.
(20) Lehmann, O. *Die neue Welt der flüssigen Krisalle*; Akademische Verlagsgesellschaft: Leipzig, 1911.
(21) Knoll, P. M.; Kelker, H. *Otto Lehmann, Research of the Liquid Crystals*; Books on Demand GmbH: Norderstedt, 2010.
(22) Breidbach, O. *Visions of Nature: The Art and Science of Ernst Haeckel*; Prestel: Münich, 2006
(23) E-mail: O. Briedbach to B. Kahr, 12 March 2007.
(24) Kofler, L.; Kofler, A. *Thermo-Mikromethoden zur Kennzeichnung Organischer Stoffe und Stoffgemiche*; Verlag Chemie: Weinheim, 1954.
(25) Zirkel, F. *Lehrbuch der Petrographie*; Adolf Marcus: Bonn, 1866; Vol. II.
(26) Vogelsgang, H. *Die Krystalliten*; M. Cohen und Sohn: Bonn, 1875.
(27) Rosenbuch, H. *Mikroskopische Physiographie der Mineralien und Gesteine*, 2nd ed.; Schweitzerbart: Stuttgart, 1887.
(28) Michel-Lévy, A. *Structures et Classification des Roches Eruptives*; Librairie Polytechnique: Paris, 1889.
(29) Bertrand, E. *Bull. Soc. Fr. Mineral.* **1880**, *3*, 58.
(30) Bertrand, E. *Bull. Soc. Fr. Mineral.* **1881**, *4*, 60.
(31) Judd, J. In *The Eruption of Krakatoa Committee of the Royal Society*; Symond, G. J., Ed.; Harrison & Sons: London: 1888; p 1.
(32) Iddings, J. P. *Am. J. Sci.* **1887**, *88*, 46.
(33) Iddings, J. P. *Bull. Phil. Soc. Washington* **1892**, *11*, 445.
(34) Wallerant, F. *C. R. Hebd. Seances Acad. Sci.* **1906**, *143*, 1169.
(35) Wallerant, F. *C. R. Hebd. Seances Acad. Sci.* **1906**, *143*, 555.
(36) Wallerant, F. *Bull. Soc. Fr. Mineral.* **1907**, *30*, 45.
(37) Gaubert, P. *C. R. Hebd. Seances Acad. Sci.* **1908**, *146*, 829.
(38) Gaubert, P. *C. R. Hebd. Seances Acad. Sci.* **1909**, *149*, 456.
(39) Gaubert, P. *Bull. Soc. Fr. Min.* **1911**, *32*, 422.
(40) Gaubert, P. *C. R. Hebd. Seances Acad. Sci.* **1911**, *153*, 683.
(41) Gaubert, P. *Bull. Soc. Fr. Mineral.* **1913**, *36*, 45.
(42) Gaubert, P. *C. R. Hebd. Seances Acad. Sci.* **1913**, *156*, 1161.
(43) Gaubert, P. *Ann. Chim. Phys.* **1916**, *5−6* (series 9), 356.
(44) Gaubert, P. *C. R. Hebd. Seances Acad. Sci.* **1917**, *164*, 355.
(45) Gaubert, P. *Bull. Soc. Fr. Mineral.* **1918**, *41*, 198.
(46) Gaubert, P. *C. R. Hebd. Seances Acad. Sci.* **1918**, *167*, 368.
(47) Gaubert, P. *C. R. Hebd. Seances Acad. Sci.* **1922**, *175*, 973.
(48) Gaubert, P. *C. R. Hebd. Seances Acad. Sci.* **1928**, *187*, 98.
(49) Gaubert, P. *C. R. Hebd. Seances Acad. Sci.* **1931**, *193*, 1576.
(50) Gaubert, P. *C. R. Hebd. Seances Acad. Sci.* **1932**, *195*, 733.
(51) Bernauer, F. *"Gedrillte" Kristalle*; Gebürder Borntraeger: Berlin, 1929.
(52) Morse, H. W.; Donnay, J. D. H. *Am. J. Sci.* **1932**, *223*, 440.
(53) Morse, H. W.; Donnay, J. D. H. *Am. Mineral.* **1936**, *21*, 391.
(54) Keller, A. *J. Polym. Sci.* **1955**, *17*, 291.
(55) Keller, A. *J. Polym. Sci.* **1959**, *34*, 151.
(56) Keller, A.; Waring, R. S. *J. Polym. Sci.* **1955**, *17*, 447.
(57) Keith, H. D.; Padden, F. J. *J. Polym. Sci.* **1959**, *34*, 101.
(58) Keith, H. D.; Padden, F. J. *J. Polym. Sci.* **1959**, *34*, 123.
(59) Keller, A. *Macromol. Chem* **1959**, *34*, 1.
(60) Keith, H. D.; Padden, F. J. *J. Appl. Phys.* **1964**, *35*, 1270.
(61) Popoff, B. *Latv. Farm. Zurn. (Riga)* **1934**, 1.
(62) Shubnikov, A. V. *How the Crystals Grow*; Akad. Nauk SSSR: Moscow-Leningrad, 1935 (in Russian).
(63) Shubnikov, A. V. *The Formation of Crystals*; Akad. Nauk SSSR: Moscow-Leningrad, 1947 (in Russian).
(64) Maleev, M. N. *Tschermak's Min. Petr. Mitt.* **1972**, *18*, 1.
(65) Magill, J. H. *J. Mater. Sci.* **2001**, *36*, 3143.
(66) Bassett, D. C. *J. Macromol. Sci. B* **2003**, *42*, 227.
(67) Cölfen, H.; Antonietti, M. *Mesocrystals and Nonclassical Crystallization*; Wiley: New York, 2008.
(68) Kniep, R.; Simon, P. In *Biomineralization I*; Springer: Heidelberg. *Top. Curr. Chem.* **2007**, *270*, 73.
(69) Punin, Yu. O.; Shtukenberg, A. G. *Autodeformation Defects in Crystals*; St. Petersburg University Press: St. Petersburg, 2008 (in Russian).
(70) Punin, Yu. O. *Zap. Vseross. Mineral. O-va.* **1981**, *110*, 666 (in Russian).
(71) Bernauer, F. *N. Jahrb. Min. Geol. Paleontol.* **1927**, *55*, 92.
(72) Shtukenberg, A. G.; Freudenthal, J.; Kahr, B. *J. Am. Chem. Soc.* **2010**, *132*, 9341.
(73) Shtukenberg, A.; Gunn, E. G.; Gazzano, M.; Freudenthal, J.; Camp, E.; Sours, R.; Rosseeva, E.; Kahr, B. *ChemPhysChem* **2011**, *12*, 1558.
(74) Shtukenberg, A. G.; Gunn, E.; Yu, L.; Kahr, B. *Cryst. Growth Des.* **2011**, *11*, 4458–4462.
(75) Jones, F. T.; Lee, K. S. *Microscope* **1970**, *18*, 279. Yu, L. *J. Am. Chem. Soc.* **2003**, *125*, 6380. Tao, J.; Yu, L. *J. Phys. Chem. B* **2006**, *110*, 7098. Tao, J.; Jones, K. J.; Yu, L. *Cryst. Growth Des.* **2007**, *7*, 2410.
(76) Miller, C. E. *J. Cryst. Growth* **1977**, *42*, 357.
(77) Sun, Y.; Xi, H.; Chen, S.; Ediger, M. D.; Yu, L. *J. Phys. Chem. B* **2008**, *112*, 5594.
(78) Prasad, P. B. V. *Cryst. Res. Technol.* **1984**, *19*, 1549.
(79) Price, F. P.; Fritzsche, A. K. *J. Phys. Chem.* **1973**, *77*, 396. Madhava, M. S.; Krishnamurti, D. *Mol. Cryst. Liq. Cryst.* **1977**, *39*, 87.
(80) Hutter, J. L.; Bechhoefer, J. *Phys. Rev. Lett.* **1997**, *79*, 4022.
(81) Hutter, J. L.; Bechhoefer, J. *Phys. Rev. E.* **1999**, *59*, 4342.
(82) Hutter, J. L.; Bechhoefer, J. *J. Cryst. Growth* **2000**, *217*, 332.
(83) Jain, S. C.; Aginhotry, S. A.; Bhilde, V. G. *Mol. Cryst. Liq. Cryst.* **1982**, *88*, 281.
(84) Hosier, I. L.; Bassett, D. C.; Vaughan, A. S. *Macromolecules* **2000**, *33*, 8781.
(85) Hosier, I. L.; Bassett, D. C. *Polymer* **2000**, *41*, 8801.
(86) Wang, X.; Liu, R.; Wu, M.; Wang, Z.; Huang, Y. *Polymer* **2009**, *50*, 5824.
(87) Kajioka, H.; Hikosaka, M.; Taguchi, K.; Toda, A. *Polymer* **2008**, *49*, 1685.
(88) Patel, D.; Bassett, D. C. *Proc. R. Soc. London A* **1994**, *445*, 577.
(89) Ye, H.-M.; Xu, J.; Guo, B.-H.; Iwata, T. *Macromol* **2009**, *42*, 694.
(90) Ye, H.-M.; Wang, J.-S.; Tang, S.; Xu, J.; Feng, X.-Q.; Guo, B.-H.; Xie, X.-M.; Zhou, J.-J.; Li, L.; Wu, Q.; Chen, G.-Q. *Macromolecules* **2010**, *43*, 5762.
(91) Xua, J.; Guoa, B.-H.; Zhoub, J.-J.; Lib, L.; Wuc, J.; Kowalczuk, M. *Polymer* **2005**, *46*, 9176.
(92) Toda, A.; Taguchi, K.; Hikosaka, M.; Kajioka, H. *Polymer J* **2008**, *40*, 905.
(93) Lovinger, A. J. *J. Appl. Phys.* **1978**, *49*, 5014.
(94) Brinkmann, M. J. *Polymer Sci. Part B: Polym. Phys* **2011**, *49*, 1218.
(95) Schnur, G. *Rubber-Stichting Communication* No. *276*; Rubber-Stichting: Delft, Netherlands, 1955.
(96) Fowler, A. D.; Berger, B.; Shore, M.; Jones, M. I.; Ropchan, J. *Precambr. Res* **2002**, *115*, 311.
(97) Davis, B. K.; McPhie, J. *J. Volcanol. Geotherm. Res.* **1996**, *71*, 1.
(98) Smith, R. K.; Tremallo, R. L.; Lofgren, G. E. *Am. Mineral.* **2001**, *86*, 589.
(99) Kirkpatrick, R. J. *Am. J. Sci.* **1974**, *274*, 215.
(100) Lofgren, G. *Am. J. Sci.* **1974**, *274*, 243.
(101) Fowler, A. D.; Jensen, L. S.; Peloquin, S. A. *Can. Mineral.* **1987**, *25*, 275.
(102) Coish, R. A.; Taylor, L. A. *Earth Planet. Sci. Lett.* **1979**, *42*, 389.
(103) Miao, B.; Wood, D. O. N.; Bian, W.; Fang, K.; Fan, M. H. *J. Mater. Sci.* **1994**, *29*, 255.

(104) Akhmatov, Yu. S.; Taran, Yu. N.; Lisnyak, A. G.; Zaspenko, N. Ya *Sov. Phys.: Crystallogr.* **1977**, *22*, 207.
(105) Minkoff, I.; Nixon, W. C. *J. Appl. Phys.* **1966**, *37*, 4848.
(106) He, K.; Daniels, H. R.; Brown, A.; Brydson, R.; Edmonds, D. V. *Acta Mater.* **2007**, *55*, 2919.
(107) Ryschenkow, G.; Faivre, G. *J. Cryst. Growth* **1988**, *87*, 221.
(108) Bisault, J.; Ryschenkow, G.; Faivre, G. *J. Cryst. Growth* **1991**, *110*, 889.
(109) Bolotov, I. E.; Kleptsova, G. N.; Mel'nikov, P. S. *Sov. Phys.: Crystallogr* **1971**, *16*, 327.
(110) Timofeeva, V. A.; Voskanyan, R. A. *Sov. Phys.: Crystallogr* **1963**, *8*, 227.
(111) Alfintsev, G. A.; Ovsienko, D. E.; Stoichev, N. V.; Maslov, V. V. In *Kinetics and Mechanism of Crystallization*; Nauka i Technika: Minsk, 1973; p 332 (in Russian).
(112) Chalmers, B. *Physical Metallurgy*; Wiley: New York, 1959; p 272.
(113) Geveling, N. N.; Maslenkov, S. B. *Met. Sci. Heat Treat.* **1976**, *18*, 755.
(114) Fitton, B.; Griffiths, C. H. *J. Appl. Phys.* **1968**, *39*, 3663.
(115) Kolosov, V. Yu.; Shvamm, K. L.; Gainutdinov, R. V.; Tolstikhina, A. L. *Bull. Russ. Acad. Sci.: Physics* **2007**, *71*, 1442.
(116) Bolotov, I. E.; Kozhin, A. V.; Fisheleva, S. B. *Sov. Phys.: Crystallogr.* **1970**, *15*, 461.
(117) Bannov, V. S.; Imamov, R. M.; Kovaleva, O. V.; Chayanov, B. A. *Izvest. Akad. Nauk SSSR, Ser. Fiz.* **1977**, *41*, 1024 in Russian.
(118) Tao, J.; Mao, G.; Daehne, L. *J. Am. Chem. Soc.* **1999**, *121*, 3475.
(119) Zaitsev, A. I.; Zamkov, A. V.; Koroleva, N. S.; Molokeev, M. S.; Cherepakhin, A. V. *Crystallogr. Rep.* **2011**, *56*, 44.
(120) Carr, S. M.; Subramanian, K. N. *J. Cryst. Growth* **1982**, *60*, 307.
(121) Hing, P.; McMillan, P. W. *J. Mater. Sci.* **1973**, *8*, 340.
(122) Weston, R. M.; Rogers, P. S. *Mineral. Mag.* **1978**, *42*, 325.
(123) Xi, H.; Sun, Y.; Yu, L. *J. Phys. Chem.* **2009**, *130*, 094508.
(124) Hatase, M.; Hanaya, M.; Oguni, M. *J. Non-Cryst. Solids* **2004**, *333*, 129.
(125) Morse, H. W.; Warren, C. H.; Donnay, J. D. H. *Am. J. Sci.* **1932**, *223*, 421.
(126) Braissant, O.; Cailleau, G.; Dupraz, C.; Verrecchia, E. P. *J. Sedimentary Res* **2003**, *73*, 485.
(127) Beck, R.; Andreassen, J.-P. *J. Cryst. Growth* **2010**, *312*, 2226.
(128) Beck, R.; Andreassen, J.-P. *Cryst. Growth Des.* **2010**, *10*, 2934.
(129) Jung, T.; Kim, W.-S.; Choi, C. K. *J. Cryst. Growth* **2005**, *279*, 154.
(130) Thomas, A. *Biomimetic Growth and Morphology Control of Calcium Oxalates*; Ph.D. Thesis, Dresden, Germany, 2009. Thomas, A.; Rosseeva, E.; Hochrein, O.; Carrillo-Cabrera, W.; Simon, P.; Duchstein, P.; Zahn, D.; Kniep, R. *Chem. Eur. J.* DOI: 10.1002/chem.201102228.
(131) Thomas, A.; Kniep, R.; Hochrein, O. Z. *Anorg. Allg. Chem* **2006**, *632*, 2109.
(132) Prymak, O.; Sokolova, V.; Peitsch, T.; Epple, M. *Cryst. Growth Des.* **2006**, *6*, 498.
(133) Wu, Y.-J.; Tseng, Y.-H.; Chan, J. C. C. *Cryst. Growth Des.* **2010**, *10*, 4240.
(134) McCauley, J. W.; Roy, R. *Am. Mineral.* **1974**, *59*, 947.
(135) Gu, F.; Wang, Z.; Han, D.; Guo, G.; Guo, H. *Cryst. Growth Des.* **2007**, *7*, 1452.
(136) Sasaki, N.; Murakami, Y.; Shindo, D.; Sugimoto, T. *J. Colloid Interface Sci.* **1999**, *213*, 121.
(137) Golden, D. C.; Ming, D. W.; Morris, R. V. 41st Lunar and Planetary Science Conference, March 1−5, 2010, The Woodlands, TX; Lunar and Planetary Institute: Houston, TX, 2010; p 2541.
(138) Hu, Y.; Chen, K. *J. Cryst. Growth* **2007**, *308*, 185.
(139) Kotru, P. N.; Raina, K. K. *J. Cryst. Growth* **1988**, *91*, 221.
(140) Mansotra, V.; Raina, K. K.; Kotru, P. N. *J. Mater. Sci.* **1991**, *26*, 3780.
(141) Li, Z.; Geβner, A.; Richters, J.-P.; Kalden, J.; Voss, T.; Kübel, C.; Taubert, A. *Adv. Mater.* **2008**, *20*, 1279.
(142) Nassau, K.; Cooper, A. S.; Shiever, J. W.; Prescott, B. E. *J. Solid State Chem.* **1973**, *8*, 260.
(143) Pina, C. M.; Fernández-Díaz, L.; Astilleros, J. M. *Cryst. Res. Technol.* **2000**, *35*, 1015.
(144) Imai, H.; Oaki, Y. *Angew. Chem., Int. Ed.* **2004**, *43*, 1363.
(145) Oaki, Y.; Imai, H. *J. Am. Chem. Soc.* **2004**, *126*, 9271.
(146) Imai, H.; Oaki, Y. *CrystEngComm* **2010**, *12*, 1679.
(147) Liu, Z.; Wen, X. D.; Wu, X. L.; Gao, Y. J.; Chen, H. T.; Zhu, J.; Chu, P. K. *J. Am. Chem. Soc.* **2009**, *131*, 9405.
(148) Chen, G.-Y.; Dneg, B.; Cai, G.-B.; Zhang, T.-K.; Dong, W.-F.; Zhang, W.-X.; Xu, A.-W. *J. Phys. Chem.* **2008**, *112*, 672.
(149) Tang, J.; Alivisatos, A. P. *Nano Lett.* **2006**, *6*, 2701.
(150) Buscaglia, M. T.; Buscaglia, V.; Bottino, C.; Viviani, M.; Fournier, R.; Sennour, M.; Presto, S.; Marazza, R.; Nanni, P. *Cryst. Growth. Des.* **2008**, *8*, 3847.
(151) Gu, Z.; Zhai, T.; Gao, B.; Zhang, G.; Ke, D.; Ma, Y.; Yao, J. *Cryst. Growth Des.* **2007**, *7*, 825.
(152) Ding, Y.; Yu, S.-H.; Liu, C.; Zang, Z.-A. *Chem.—Eur. J.* **2007**, *13*, 746.
(153) Wang, G.; Sæterli, R.; Rørvik, P. M.; van Helvoort, A. T. J.; Holmestad, R.; Grande, T.; Einarsrud, M.-A. *Chem. Mater.* **2007**, *19*, 2213.
(154) Gunn, E. *Small Molecule Banded Spherulites*, Ph.D. Dissertation, University of Washington, Seattle, Washington, USA, 2009.
(155) Iwamoto, K.; Mitomo, S.-I.; Seno, M. *J. Colloid Interface Sci.* **1984**, *102*, 477.
(156) Uesaka, H.; Kobayashi, R. *J. Cryst. Growth* **2002**, *132−137*, 237.
(157) Prasad, P. B. V. *Cryst. Res. Technol.* **1985**, *20*, 1015.
(158) Gunn, E.; Sours, R.; Benedict, J. B.; Kaminsky, W.; Kahr, B. *J. Am. Chem. Soc.* **2006**, *128*, 14234.
(159) Freudenthal, J.; Kahr, B. *Chirality* **2008**, *20*, 973.
(160) Iwamoto, K.; Mitomo, S.-I.; Fukide, J.-I.; Shigemoto, T.; Seno, M. *Bull. Chem. Soc. Jpn.* **1982**, *55*, 709.
(161) Frondel, C. *Am. Mineral.* **1978**, *63*, 17.
(162) Heany, P. J.; Davis, A. M. *Science* **1995**, *269*, 1562.
(163) Wang, Y.; Merino, E. *Am. J. Sci.* **1995**, *295*, 49.
(164) Sunagawa, I. *Crystals. Crowth, Morphology, and Perfection*; Cambridge University Press: New York, 2005.
(165) Dymkov, Yu. M. *The Nature of Nasturan*; Atomizdat: Moscow, 1973 (in Russian).
(166) Gritzenko, Yu. D.; Spiridonov, E. M. *Zap. Vseross. Mineral. O-va.* **2005**, *134* (1), 53, in Russian.
(167) Lussier, A. J.; Hawthorne, F. C.; Herwig, S.; Abdu, Y.; Aguiar, P. M.; Michaelis, V. K.; Kroeker, S. *Mineral. Mag.* **2008**, *72*, 999.
(168) Meakin, P.; Jamtveit, B. *Proc. R. Soc. A* **2010**, *466*, 659.
(169) Yushkin, N. P. In: *The Genesis of Mineral Individuals and Aggregates*; Nauka: Moscow, 1966; p 201 (in Russian).
(170) Khoury, F. *J. Res. Natl. Bur. Stand. Sect. A* **1966**, *70*, 29.
(171) Cao, Q. K.; Qiao, X. P.; Wang, H.; Liu, J. P. *Sci. China Ser. B: Chem* **2008**, *51*, 853.
(172) Wang, Z.; Alfonso, G. C.; Hu, Z.; Zhang, J.; He, T. *Macromolecules* **2008**, *41*, 7584.
(173) Waugh, D. F. *J. Am. Chem. Soc.* **1946**, *68*, 247.
(174) Krebs, M. R. H.; MacPhee, C. E.; Miller, A. F.; Dunlop, I.; Dobson, C. M.; Donald, A. M. *Proc. Natl. Acad. Sci. U. S. A.* **2004**, *101*, 14420.
(175) Krebs, M. R. H.; Bromley, E. H. C.; Rogers, S. S.; Donald, A. M. *Biophys. J.* **2005**, *88*, 2013.
(176) Krebs, M. R. H.; Bromley, E. H. C.; Donald, A. M. *J. Struct. Biol.* **2005**, *149*, 30.
(177) Rogers, S. S.; Krebs, M. R. H.; Bromley, E. H. C.; van der Linden, E.; Donald, A. M. *Biophys. J.* **2006**, *90*, 1043.
(178) Coleman, J. E.; Allan, B. J.; Vallee, B. L. *Science* **1960**, *131*, 350.
(179) Krebs, M. R. H.; Domike, K. R.; Donald, A. M. *Biochem. Soc. Trans.* **2009**, *37*, 682.
(180) Krebs, M. R. H.; Domike, K. R.; Cannon, D.; Donald, A. M. *Faraday Discuss.* **2008**, *139*, 265.
(181) Bromley, E. H. C.; Krebs, M. R. H.; Donald, A. M. *Faraday Discuss.* **2005**, *128*, 13.

(182) Domike, K. R.; Donald, A. M. *Biomacromolecules* **2007**, *8*, 3930.
(183) Domike, K. R.; Donald, A. M. *Int. J. Biol. Macromol.* **2009**, *44*, 301.
(184) Domike, K. R.; Hardin, E.; Armstead, D. N.; Donald, A. M. *Eur. Phys. J. E* **2009**, *29*, 173.
(185) Chow, P. S.; Liu, X. Y.; Zhang, J.; Tan, R. B. H. *Appl. Phys. Lett.* **2002**, *81*, 1975.
(186) Martin, R.; Waldmann, L.; Kaplan, D. L. *Biopolymers* **2003**, *70*, 435.
(187) Ban, T.; Morigaki, K.; Yagi, H.; Kawasaki, T.; Kobayashi, A.; Yuba, S.; Naiki, H.; Goto, Y. *J. Biol. Chem.* **2006**, *281*, 33677.
(188) Fezoui, Y.; Hartley, D. M.; Walsh, D. M.; Selkoe, D. J.; Osterhout, J. J.; Teplow, D. B. *Nat. Struct. Biol.* **2000**, *7*, 1095.
(189) Aggeli, A.; Bell, M.; Carric, L. M.; Fishwick, C. W. G.; Harding, R.; Mawer, P. J.; Radford, S. E.; Strong, A. E.; Boden, N. *J. Am. Chem. Soc.* **2003**, *125*, 9619.
(190) Hamodrakas, S. J.; Hoenger, A.; Iconomidou, V. A. *J. Struct. Biol.* **2004**, *145*, 226.
(191) Lockwood, N. A.; van Tenkeren, R.; Mayo, K. H. *Biomacromolecules* **2002**, *3*, 1225.
(192) Westlind-Danielsson, A.; Arneup, G. *Biochemistry* **2001**, *40*, 14736.
(193) Briehl, R. W. *J. Mol. Biol.* **1995**, *245*, 710.
(194) Tamhane, K.; Zhang, X.; Zou, J.; Fang, J. *Soft Matter* **2010**, *6*, 1224.
(195) Catalina, F.; Cifuente, L. *Science* **1970**, *169*, 183. Izatulina, A. R.; Shtukenberg, A. G.; Punin, Yu. O. *Proc. Russ. Mineral. Soc.* **2009**, *N4*, 71, in Russian.
(196) Al-Atar, U.; Bokov, A. A.; Marshall, D.; Teichman, J. M. H.; Gates, B. D.; Ye, Z.-G.; Branda, N. R. *Chem. Mater.* **2010**, *22*, 1318.
(197) Díaz-Espiñeira, M.; Escolar, E.; Bellanato, J.; Rodriguez, M. *Res. Veterin. Sci.* **1996**, *60*, 238–242.
(198) Divry, P.; Florkin, M. *C. R. Soc. Biol.* **1927**, *97*, 1808.
(199) Kelényi, G. *Acta Neuropathol.* **1967**, *7*, 336.
(200) Jin, L. W.; Claborn, K.; Kurimoto, M.; Sohraby, F.; Estrada, M.; Kaminsky, W.; Kahr, B. *Proc. Natl. Acad. Sci. U. S. A.* **2003**, *100*, 15294.
(201) Grigor'ev, D. P. *Ontogeny of Minerals*; Israel Program for Scientific Translations: Jerusalem, 1965.
(202) Langer, J. S. *Rev. Modern Phys.* **1980**, *52*, 1.
(203) Chernov, A. A. *Modern Crystallography III. Crystal Growth*; Springer: Berlin, 1984.
(204) Jackson, K. A. *Kinetic Processes*; Wiley: Weinheim, 2004.
(205) Tajima, S.; Ogata, M. *Electrochim. Acta* **1970**, *15*, 61.
(206) Murashova, I. B.; Korkin, S. L.; Pomosov, A. V.; Nikol'skaya, N. Yu.; Susloparov, D. G. *Powder Metall. Metal Ceram.* **1986**, *25*, 792.
(207) Xu, H.; Chen, T.; Konishi, H. *Am. Mineral.* **2010**, *95*, 556.
(208) Potter, R. M.; Rossman, G. R. *Am. Mineral.* **1979**, *64*, 1219.
(209) Gunn, E.; Wong, L.; Branham, C. W.; Marquardt, B.; Kahr, B. *CrystEngComm* **2011**, *13*, 1123.
(210) Punin, Yu. O.; Shtukenberg, A. G.; Smetannikova, O. G.; Amelin, K. S. *Eur. J. Mineral.* **2010**, *22*, 139.
(211) Rinne, F. *Trans. Faraday Soc.* **1933**, *29*, 1016.
(212) Robinson, C. *Trans. Faraday Soc* **1956**, *52*, 571.
(213) Humar, M.; Mušvič, I. *Opt. Express* **2010**, *18*, 26995.
(214) Jabarin, S. A.; Stein, R. S. *J. Phys. Chem.* **1973**, *77*, 399.
(215) Bouligand, Y.; Livolant, F. *J. Phys. (Paris)* **1984**, *45*, 1899.
(216) Hutter, J. L.; Bechhoefer, J. *Phys. Rev. Lett.* **1997**, *79*, 4022.
(217) Hutter, J. L.; Bechhoefer, J. *Phys. Rev. E.* **1999**, *59*, 4342.
(218) Hutter, J. L.; Bechhoefer, J. *J. Cryst. Growth* **2000**, *217*, 332.
(219) Jain, S. C.; Aginhotry, S. A.; Bhilde, V. G. *Mol. Cryst. Liq. Cryst.* **1982**, *88*, 281.
(220) Han, X.; Jin, X.; Yang, S.; Fietzke, J.; Eisenhauer, A. *Earth Planet. Sci. Lett.* **2003**, *211*, 143.
(221) Pramanik, R.; Asplin, J. R.; Jackson, M. E.; Williams, J. C., Jr. *Urol. Res* **2008**, *36*, 251.
(222) Morse, J. W.; Arvidson, R. S. *Earth Sci. Rev* **2002**, *58*, 51–84.
(223) Guo, X.-H.; Xu, A.-W.; Yu, S.-H. *Cryst. Growth Des.* **2008**, *8*, 1233.
(224) Zhang, J.; Zhang, S.; Wang, Z.; Zhang, Z.; Wang, S.; Wang, S. *Angew. Chem., Int. Ed. Engl.* **2011**, *50*, 6044–6047.
(225) Krasnova, N. I.; Petrov, T. G. *Genesis of Mineral Individuals and Aggregates*; Nevskii Kurier: St. Petersburg, Russia, 1997 (in Russian).
(226) Brodin, B. V. In *The Genesis of Mineral Individuals and Aggregates*; Nauka: Moscow, 1966; p 167 (in Russian).
(227) Busch, S.; Dolhaine, H.; DuChesne, A.; Heinz, S.; Hochrein, O.; Laeri, F.; Podebrad, O.; Vietze, U.; Weiland, T.; Kniep, R. *Eur. J. Inorg. Chem.* **1999**, 1643.
(228) Sun, Y.; Zhu, L.; Kearns, K. L.; Ediger, M. D.; Yu, L. *Proc. Natl. Acad. Sci. U. S. A.* **2011**, *108*, 5990.
(229) Zhou, Q.; Liu, F.; Guo, C.; Fu, Q.; Shen, K.; Zhang, J. *Polymer* **2011**, *52*, 2970.
(230) Barham, P. J.; Keller, A.; Otun, E. L.; Holmes, P. A. *J. Mater. Sci.* **1984**, *19*, 2781.
(231) Lotz, B.; Cheng, S. Z. D. *Polymer* **2005**, *46*, 577.
(232) Toda, A.; Taguchi, K.; Kajioka, H. *Macromolecules* **2008**, *41*, 7505.
(233) Toda, A.; Okamura, M.; Taguchi, K.; Hikosaka, M.; Kajioka, H. *Macromolecules* **2008**, *41*, 2484.
(234) Kajioka, H.; Yoshimoto, S.; Taguchi, K.; Toda, A. *Macromolecules* **2010**, *43*, 3837.
(235) Bassett, D. C. *Principles of Polymer Morphology*; Cambridge University Press: Cambridge, UK, 1981.
(236) Bassett, D. C.; Vaughan, A. S. *Polymer* **1985**, *26*, 717.
(237) Lustiger, A.; Lotz, B.; Duff, T. S. *J. Polym. Sci., Part B* **1989**, *27*, 561.
(238) Lei, Y.-G.; Chan, C.-M.; Wang, Y.; Ng, K.-M.; Jiang, Y.; Lin, L. *Polymer* **2003**, *44*, 4673.
(239) Li, L.; Chan, C.-M.; Yeung, K. L.; Li, J.-X.; Ng, K.-M.; Lei, Y. *Macromolecules* **2001**, *34*, 316.
(240) Yu, L. *J. Am. Chem. Soc.* **2003**, *125*, 6380.
(241) Aslanian, S.; Kostov, I.; Neels, H. *Krist. Tech.* **1968**, *3*, 619.
(242) Fanta, G. F.; Felker, F. C.; Shogren, R. L.; Salch, J. H. *Carbohyd. Polym.* **2008**, *71*, 253.
(243) Born, M.; Wolf, E. *Principles of Optics*; Cambridge University Press: Cambridge, UK, 1997.
(244) Keith, H. D.; Padden, F. J. *J. Polym. Sci.* **1958**, *31*, 415.
(245) Point, J. J. *Polymer* **2006**, *47*, 3186.
(246) Hobbs, J. K.; Binger, D. R.; Keller, A.; Barham, P. J. *J. Polym. Sci., Part B* **2000**, *38*, 1575.
(247) Price, F. P. *J. Polym. Sci.* **1959**, *39*, 139.
(248) Tentori, D.; Ayala-Díaz, C.; Treviño-Martínez, F.; Mendieta-Jiménez, F. J.; Soto-Ortiz, H. *J. Modern Opt.* **2001**, *48*, 1767.
(249) Dippy, J. F. J. *J. Phys. Chem.* **1932**, *36*, 2355.
(250) Hedges, E. S. *Liesegang Rings and Other Periodic Structures*; Chapman & Hall: London, 1932.
(251) Ortoleva, P. *Geochemical Self-Organization*; Oxford University Press: New York, 1994.
(252) Kyu, T.; Chiu, H.-W.; Guenthner, A. J.; Okabe, Y.; Saito, H.; Inoue, T. *Phys. Rev. Lett.* **1999**, *83*, 2749.
(253) Sadlik, B.; Talon, L.; Kawka, S.; Woods, R.; Bechhoefer, J. *Phys. Rev. E* **2005**, *71*, 061602.
(254) Sadlik, B. *The Role of Viscosity in Banded-Spherulitic Growth*; Ph.D. Dissertation, Simon Fraser University, Burnaby, Canada, 2004.
(255) Paranjpe, A. S. *Phys. Rev. Lett.* **2002**, *89*, 075504.
(256) Ito, M.; Yamazaki, Y.; Matsushita, M. *J. Phys. Soc. Jpn.* **2003**, *72*, 1384.
(257) Uesaka, H.; Kobayashi, R. *J. Cryst. Growth* **2002**, *237−239*, 132.
(258) MacMasters, M. M.; Abbott, J. E.; Peters, C. A. *J. Am. Chem. Soc.* **1935**, *57*, 2504.
(259) Shevchuk, I. A.; Borodai, Yu. K. *J. Anal. Chem. USSR* **1978**, *33*, 1893.
(260) Shubnikov, A. V. *Sov. Phys.: Crystallogr.* **1958**, *3*, 500.
(261) Duan, Y.; Jiang, Y.; Jiang, S.; Li, L.; Yan, S.; Schultz, J. M. *Macromolecules* **2004**, *37*, 9283.

(262) Chen, J.; Yang, D. C. *Macromolecules* **2005**, *38*, 3371.
(263) Xu, J.; Guo, B.-H.; Chen, G.-Q.; Zhang, Z.-M. *J. Polym. Sci., Part B* **2003**, *41*, 2128.
(264) Xu, J.; Guo, B.-H.; Zhang, Z.-M.; Zhou, J.-J.; Jiang, Y.; Yan, S.; Li, L.; Wu, Q.; Chen, G.-Q.; Schultz, J. M. *Macromolecules* **2004**, *37*, 4118.
(265) Wang, Z.; An, L.; Jiang, W.; Jiang, B.; Wang, X. *J. Polym. Sci., Part B* **1999**, *37*, 2682.
(266) Kawashima, K.; Kawano, R.; Miyagi, T.; Umemoto, S.; Okui, N. *J. Macromol. Sci* **2003**, *B42*, 889.
(267) Zhao, L.; Wang, X.; Li, L.; Gan, Z. *Polymer* **2007**, *48*, 6152.
(268) Schultz, J. M. *Polymer* **2003**, *44*, 433.
(269) Eshelby, J. D. *J. Appl. Phys.* **1953**, *24*, 176.
(270) Schultz, J. M.; Kinloch, D. R. *Polymer* **1969**, *10*, 271.
(271) Toda, A.; Arita, T.; Hikosaka, M.; Hobbs, J. K.; Miles, M. J. *J. Macromol. Sci* **2003**, *B42*, 753.
(272) Bolotov, I. E.; Kolosov, V. Yu.; Kozhyn, A. V. *Phys. Status Solidi A* **1982**, *72*, 645.
(273) Kolosov, V. Yu.; Thölén, A. R. *Acta Mater.* **2000**, *48*, 1829.
(274) Kolosov, V. Yu.; Schwamm, C. L.; Gainutdinov, R. V.; Tolstikhina, A. L. *J. Phys. Conf. Ser.* **2008**, *100*, 082037.
(275) Bagmut, A. G.; Zhuchkov, V. A.; Kolosov, V. Yu.; Kosevich, V. M.; Melnichenko, D. V. *Crystallogr. Rep.* **2006**, *51*, S150.
(276) Janimak, J. J.; Markey, L.; Stevens, G. C. *Polymer* **2001**, *42*, 4675.
(277) Okabe, Y.; Kyu, T.; Saito, H.; Inoue, T. *Macromolecules* **1998**, *31*, 5823.
(278) Singfield, K. L.; Klass, J. M.; Brown, G. R. *Macromolecules* **1995**, *28*, 8006.
(279) Woo, E. M.; Chen, Y.-F. *Polymer* **2009**, *50*, 4706.
(280) Tlatlik, H.; Simon, P.; Kawska, A.; Zahn, D.; Kniep, R. *Angew. Chem., Int. Ed.* **2006**, *45*, 1905.
(281) Norton, D. R.; Keller, A. *Polymer* **1985**, *26*, 704.
(282) Gránásy, L.; Pusztai, T.; Tegze, G.; Warren, J. A.; Douglas, J. F. *Phys. Rev. E* **2005**, *72*, 011605.
(283) Chan, C.-M.; Li, L. *Adv. Polym. Sci.* **2005**, *188*, 1.
(284) Raz, S.; Weiner, S.; Addadi, L. *Adv. Mater.* **2000**, *12*, 38.
(285) Li, J. X.; Cheung, W. L. *J. Appl. Polym. Sci.* **1999**, *72*, 1529.
(286) Deans, T. *Geol. Mag.* **1934**, *71*, 49.
(287) Zhong, C.; Chu, C. C. *Cryst. Growth Des.* **2010**, *10*, 5043.
(288) Toda, A.; Arita, T.; Hikosaka, M. *Polymer* **2001**, *42*, 2223.
(289) Kurimoto, M.; Müller, B.; Kaminsky, W.; Kahr, B.; Jin, L.-W. *Mol. Cryst. Liq. Cryst.* **2002**, *389*, 1.
(290) Kaminsky, W.; Gunn, E.; Sours, R.; Kahr, B. *J. Microscopy* **2007**, *228*, 153.
(291) Kaminsky, W.; Jin, L.-W.; Powell, S.; Maezawa, I.; Claborn, K.; Branham, C.; Kahr, B. *Micron* **2006**, *37*, 324.
(292) Kirkpatrick, R. J. *Am. Mineral.* **1975**, *60*, 798.
(293) Muncill, G. E.; Lasaga, A. C. *Am. Mineral.* **1988**, *73*, 982.
(294) Chang, I.; Fujara, F.; Geil, B.; Heuberger, G.; Mangel, T.; Sillescu, H. *J. Non-Cryst. Solids* **1994**, *172*−*174*, 248.
(295) Ediger, M. D.; Angell, C. A.; Nagel, S. R. *J. Phys. Chem.* **1996**, *100*, 13200.
(296) Ngai, K. L.; Magill, J. H.; Plazek, D. J. *J. Chem. Phys.* **2000**, *112*, 1887.
(297) Gránásy, L.; Pusztai, T.; Börzsönyi, T.; Warren, J. A.; Douglas, J. F. *Nat. Mater.* **2004**, *3*, 645.
(298) Gránásy, L.; Pusztai, T.; Warren, J. A. *J. Phys.: Condens. Matter* **2004**, *16*, R1205.
(299) Gránásy, L.; Pusztai, T.; Börzsönyi, T. *Handbook of Theoretical and Computational Nanotechnology*; American Scientific Publisher: Stevenson Ranch, CA, 2006, Vol. 9; p 525.
(300) Gránásy, L.; Pusztai, T.; Börzsönyi, T.; Tóth, G. I.; Tegze, G.; Warren, J. A.; Douglas, J. F. *Phil. Mag.* **2006**, *86*, 3757.
(301) Urakawa, O.; Swallen, S. F.; Ediger, M. D.; von Meerwall, E. D. *Macromolecules* **2004**, *37*, 1558.
(302) Magill, J. H.; Plazek, D. J. *J. Chem. Phys.* **1967**, *46*, 3757.
(303) Gan, Z.; Abe, H.; Doi, Y. *Biomacromol* **2001**, *2*, 313.
(304) Cheng, S. Z. D.; Chen, J. *J. Polym. Sci., Part B* **1991**, *29*, 311.
(305) Hong, P.-D.; Chung, W.-T.; Hsu, C.-F. *Polymer* **2002**, *43*, 3335.
(306) Xu, J.; Guo, B.-H.; Zhou, J.-J.; Li, L.; Wu, J.; Kowalczuk, M. *Polymer* **2005**, *46*, 9176.
(307) Degen, M. M.; Costanzino, N.; Bechhoefer, J. *J. Cryst. Growth* **2000**, *209*, 953.
(308) Keith, H. D.; Padden, F. J. *Macromolecules* **1996**, *29*, 7776.
(309) Maillard, D.; Prud'homme, R. E. *Macromolecules* **2008**, *41*, 1705.
(310) Armistead, J. P.; Hoffman, J. D. *Macromolecules* **2002**, *35*, 3895.
(311) Keith, H. D.; Padden, F. J. *J. Appl. Phys.* **1964**, *35*, 1286.
(312) Kahr, B.; McBride, J. M. *Angew. Chem., Int. Ed. Engl.* **1992**, *31*, 1.
(313) Park, S.-W.; Choi, J.-M.; Lee, K. H.; Yeom, H. W.; Im, S.; Lee, Y. K. *J. Phys. Chem. B* **2010**, *114*, 5661.
(314) Putnis, A.; Prieto, M.; Fernández-Díaz, L. *Geol. Mag.* **1995**, *132*, 1.
(315) Fernández-Díaz, L.; Astilleros, J. M.; Pina, C. M. *Chem. Geol.* **2006**, *225*, 314.
(316) Wang, G.; Li, L.; Lan, J.; Chen, L.; You, J. *J. Mater. Chem.* **2008**, *18*, 2789.
(317) Ulčinas, A.; Butler, M. F.; Heppenstall-Butler, M.; Singleton, S.; Miles, M. J. *J. Cryst. Growth* **2007**, *307*, 378.
(318) Heijna, M. C. R.; Theelen, M. J.; van Enckevort, W. J. P.; Vlieg, E. *J. Phys. Chem. B* **2007**, *111*, 1567.
(319) Oaki, Y.; Imai, H. *Cryst. Growth Des.* **2003**, *3*, 711.
(320) Kohri, K.; Garside, J.; Blacklock, N. J. *Br. J. Urol.* **1988**, *61*, 107.
(321) Chernov, A. A. *J. Cryst. Growth* **1997**, *174*, 354.
(322) Kalischewski, F.; Lubashevsky, I.; Heuer, A. *Phys. Rev. E* **2007**, *75*, 021601.
(323) Li, W.; Sun, S.; Yu, Q.; Wu, P. *Cryst. Growth Des.* **2010**, *10*, 2685.
(324) Jongen, N.; Bowen, P.; Lemaître, J.; Valmalette, J.-Ch; Hofmann, H. *J. Colloid Interface Sci.* **2000**, *226*, 189.
(325) Sen Guptha, S.; Kar, T.; Sen Guptha, S. P. *Mater. Chem. Phys.* **1999**, *58*, 227.
(326) Shenoy, P.; Bangera, K. V.; Shivakumar, G. K. *Cryst. Res. Technol.* **2010**, *45*, 825.
(327) Bechhoefer, J. *Int. J. Nanotech.* **2008**, *5*, 1121.
(328) Punin, Yu. O. In *Growth of Crystals*; Consultants Bureau: New York, 1983; Vol. 14, p 121.
(329) Ulianova, T. P.; Punin, Yu. O.; Petrov, T. G. In *Crystal Growth*; Yerevan University Press: Yerevan, USSR, 1977; p 133 (in Russian).
(330) Smolsky, I. L.; Voloshin, A. E.; Zaitseva, N. P.; Rudneva, E. B.; Klapper, H. *Proc. XII Int. Conf. Cryst. Growth Isr.* **1998**, 76.
(331) Smolsky, I. L.; Zaitzeva, N. P.; Klapper, H.; Hägele, E.; Shtukenberg, A. *Jahrestagung der Deutschen Gesellschaft für Kristallwachstum und Kristallzüchtung* **1998**, *28*, V7.
(332) Vorobiev, A. S.; Punin, Yu. O.; Ulianova, T. P. *Uchenie Zapisky Leningradskogo Universiteta, N378; Series of Geological Sciences, N 15; Crystallography and Crystal Chemistry*, N3; Leningrad University Press: Leningrad: USSR, 1974; p 188 (in Russian).
(333) Chernov, A. A. *J. Cryst. Growth* **1999**, *196*, 524.
(334) Kennunen, D. S.; Punin, Yu. O.; Franke, V. D.; Smetannikova, O. G. *Vestnik of St.-Petersburg State University, Series 7* **2002**, *N 4*, 25 (in Russian).
(335) Kosevich, V. M.; Sokol, A. A.; Bortnik, B. I.; Melnikov, P. C. *Sov. Phys.: Crystallogr.* **1980**, *25*, 599.Sokol, A. A.; Kosevich, V. M. In *Growth of Crystals*; Consultants Bureau: New York, 1983; Vol. 14, p 62.
(336) Kosevich, V. M.; Sokol, A. A.; Bagmut, A. G. *Sov. Phys.: Crystallogr* **1979**, *24*, 80.
(337) Punin, Yu. O.; Kuz'mina, M. A.; Il'inskaya, T. G. In *Physics of Crystallization*; Kalinin University Press: Kalinin, USSR, 1986; p 53 (in Russian).
(338) Vladimirov, V. I.; Kuz'mina, I. P.; Loshmanov, A. A.; Regel', V. R.; Sizova, N. L.; Chernysheva, M. A.; Kostyukova, E. P.; Smirnov, I. S.; Shaldin, Yu. V. *Cryst. Res. Technol.* **1986**, *21*, 1055.

(339) Regel, V. R.; Vladimirov, V. I.; Sizova, N. L.; Chernysheva, M. A.; Kuz'mina, I. P.; Lazarevskaya, O. A. *Sov. Phys.: Crystallogr.* **1984**, *29*, 713.
(340) Kuz'mina, M. A.; Moshkin, S. V.; Vlasov, M. Yu.; Zhogoleva, V. Yu.; Nesterov, A. R.; Efimova, E. F. In *Physics of Crystallization*; Tver University Press: Tver, Russia, 1991; p 65 (in Russian).
(341) Blattner, A.; Ortiz, C. *Appl. Phys. Lett.* **1993**, *63*, 2896–2898.
(342) Jiang, Y.; Yan, D.-D.; Gao, X.; Han, C. C.; Jin, X.-G.; Li, L.; Wang, Y.; Chan, C.-M. *Macromol* **2003**, *36*, 3652.
(343) Beck, R.; Malthe-Sørenssen, D.; Andreassen, J.-P. *J. Cryst. Growth* **2009**, *311*, 320.
(344) Beck, R.; Flaten, E.; Andreassen, J.-P. *Chem. Eng. Technol.* **2011**, *34*, 631.
(345) Bardsley, W.; Boulton, J. S.; Hurle, D. T. J. *Solid-State Electron.* **1962**, *5*, 395.
(346) Grabmaier, J. G.; Plättner, R. D.; Schieber, M. *J. Cryst. Growth* **1973**, *20*, 82.
(347) Zeng, H. C.; Chong, T. C.; Lim, L. C.; Kumagai, H.; Hirano, M. *J. Cryst. Growth* **1994**, *140*, 148.
(348) Goldenfeld, N. *J. Cryst. Growth* **1987**, *84*, 601.
(349) Mullins, W. W.; Sekerka, R. F. *J. Appl. Phys.* **1963**, *34*, 323.
(350) Tiller, W. A. *The Science of Crystallization: Macroscopic Phenomena and Defect Generation*; Cambridge University Press: Cambridge, UK, 1991.
(351) Caroli, B.; Caroli, C.; Roulet, B.; Faivre, G. *J. Cryst. Growth* **1989**, *94*, 253.
(352) Bassett, D. C.; Hodge, A. M. *Proc. R. Soc. London A* **1981**, *377*, 25.
(353) Bassett, D. C.; Hodge, A. M.; Olley, R. H. *Proc. R. Soc. London A* **1981**, *377*, 39.
(354) Bassett, D. C.; Hodge, A. M. *Proc. R. Soc. London A* **1981**, *377*, 61.
(355) Abo el Maaty, M. I.; Bassett, D. C.; Olley, R. H.; Jääskeläinen, P. *Macromolecules* **1998**, *31*, 7800.
(356) van Veenendaal, E.; van Hoof, P. J. C. M.; van Suchtelen, J.; van Enckevort, W. J. P.; Bennema, P. *J. Cryst. Growth* **1999**, *198−199*, 22.
(357) Kniep, R.; Busch, S. *Angew. Chem., Int. Ed. Engl.* **1996**, *35*, 2624.
(358) Simon, P.; Zahn, D.; Lichte, H.; Kniep, R. *Angew. Chem., Int. Ed.* **2006**, *45*, 1911.
(359) Simon, P.; Rosseeva, E.; Buder, J.; Carrillo-Cabrera, W.; Kniep, R. *Adv. Funct. Mater.* **2009**, *19*, 3596.
(360) Paparcone, R.; Kniep, R.; Brickmann, J. *Phys. Chem. Chem. Phys.* **2009**, *11*, 2186.
(361) Cölfen, H.; Qi, L. *Prog. Colloid Polym. Sci.* **2001**, *117*, 200.
(362) Yu, S. H.; Cölfen, H.; Antonietti, M. *J. Phys. Chem. B* **2003**, *107*, 7396.
(363) Yu, S. H.; Cölfen, H.; Xu, A.-W.; Dong, W. *Cryst. Growth Des.* **2004**, *4*, 33.
(364) Henisch, H. K. *Crystals in Gels and Liesegang Rings*; Cambridge University Press: Cambridge, 1988.
(365) Kawska, A.; Hochrein, O.; Brickmann, J.; Kniep, R.; Zahn, D. *Angew. Chem., Int. Ed.* **2008**, *47*, 4982.
(366) Kniep, R.; Simon, P. *Angew. Chem., Int. Ed.* **2008**, *47*, 1405.
(367) Lei, Y.-G.; Chan, C.-M.; Li, J.-X.; Ng, K.-M.; Wang, Y.; Jiang, Y.; Li, L. *Macromolecules* **2002**, *35*, 6751.
(368) Wang, Y.; Chan, C.-M.; Ng, K.-M.; Jiang, Y.; Li, L. *Langmuir* **2004**, *20*, 8220.
(369) Bassett, D. C. *Phil. Trans. Roy. Soc. London A* **1994**, *348*, 29.
(370) Davies, C. K. L.; Long, O. E. *J. Mater. Sci.* **1977**, *12*, 2165.
(371) Punin, Yu. O. *J. Struct. Chem* **1994**, *35*, 616.
(372) Gorskaya, M. G.; Punin, Yu. O.; Sokolov, P. B.; Kretzer, Yu. L. *Mineral. Z.* **1992**, *14*, 3 (in Russian).
(373) Ulianova, T. P.; Punin, Yu. O.; Petrov, T. G. In *Crystallography and Crystal Chemistry*; Leningrad University Press: Leningrad, USSR, 1973; p 101 (in Russian).
(374) Punin, Yu. O.; Ivanova, T. Ya. In *Crystallography and Crystal Chemistry*; Leningrad University Press: Leningrad, USSR, 1982; p 164 (in Russian).
(375) Punin, Yu. O.; Ulianova, T. P.; Il'inskaya, T. G. *Zap. Vseross. Mineral. O-va.* **1977**, *106*, 274 (in Russian).
(376) Kuz'mina, M. A.; Punin, Yu. O.; Moshkin, S. V.; Boldyreva, O. M. In *Physics of Crystallization*; Tver University Press: Tver, Russia, 1992; p 57 (in Russian).
(377) Kuz'mina, M. A.; Punin, Yu. O.; Moshkin, S. V.; Karyakina, T. A. *Zap. Vseross. Mineral. O-va.* **1997**, *126*, 30 (in Russian).
(378) Punin, Yu. O. *Zap. Vseross. Mineral. O-va.* **2000**, *129*, 1 (in Russian).
(379) Punin, Yu. O. In *Crystallography and Crystal Chemistry*; Leningrad University Press: Leningrad, USSR, 1982, p 143 (in Russian).
(380) Punin, Yu. O.; Ivanova, T. Ya *Zap. Vseross. Mineral. O-va.* **1993**, *122*, 99in Russian.
(381) Punin, Yu. O.; Ivanova, T. Ya.; Artamonova, O. I. *Vestnik of St.-Petersburg State University, Series 7* **1996**, *N3*, 61 (in Russian).
(382) Miyazaki, N. *J. Cryst. Growth* **2002**, *236*, 455. Miyazaki, N.; Uchida, H.; Tsukada, T.; Fukuda, T. *J. Cryst. Growth* **1996**, *162*, 83.
(383) Dupret, F.; Nicodème, P.; Ryckmans, Y. *J. Cryst. Growth* **1989**, *97*, 162.
(384) Shtukenberg, A. G.; Punin, Yu. O. *Optically Anomalous Crystals*; Kahr, B., Ed.; Springer: Dordrecht, 2007.
(385) Denisov, A. V.; Punin, Yu. O.; Gabrielyan, V. T.; Grunsky, O. S.; Shtukenberg, A. G. *Crystallogr. Rep.* **2006**, *51*, 128.
(386) Tsukada, T.; Kakinoki, K.; Hozawa, M.; Imaishi, N.; Shimamura, K.; Fukuda, T. *J. Cryst. Growth* **1997**, *180*, 543.
(387) Bolotov, I. E.; Novikova, L. P. *Sov. Phys.: Crystallogr* **1976**, *21*, 85.
(388) Shtukenberg, A. G.; Punin, Yu. O.; Haegele, E.; Klapper, H. *Phys. Chem. Miner.* **2001**, *28*, 665.
(389) Shtukenberg, A. G.; Punin, Yu. O.; Frank-Kamenetskaya, O. V.; Kovalev, O. G.; Sokolov, P. B. *Mineral. Mag.* **2001**, *65*, 445.
(390) Shtukenberg, A. G.; Punin, Yu. O. *Mineral. Mag.* **2011**, *75*, 169.
(391) Klapper, H. *Mater. Sci. Forum* **1998**, *276−277*, 291.
(392) Klapper, H. In *Characterization of Crystal Growth Defects by X-ray Methods*; Plenum Press: NY, 1980; p 133.
(393) Hollingsworth, M. D.; Peterson, M. L.; Rush, J. R.; Brown, M. E.; Abel, M. J.; Black, A. A.; Dudley, M.; Raghothamachar, B.; Werner-Zwanziger, U.; Still, E. J.; Vanecko, J. A. *Cryst. Growth Des.* **2005**, *5*, 2100.
(394) Khaimov-Mal'kov, V. Y. In *Growth of Crystals*; Consultants Bureau: New York, 1959; Vol. 2, p 3.
(395) Franke, V. D.; Punin, Yu. O.; P'yankova, L. A. *Crystallogr. Rep.* **2007**, *52*, 365.
(396) Shuvalov, L. A. *Modern Crystallography IV. Physical Properties of Crystals*; Springer-Verlag: Berlin, 1988.
(397) Hurle, D. T. J.; Cockayne, B. In *Characterization of Crystal Growth Defects by X-ray Methods*; Plenum Press: New York, 1980; p 46.
(398) Honeycombe, R. W. K. *The Plastic Deformation of Metals*, 2nd ed.; Edward Arnold: London, 1984.
(399) Poirier, J. P. *Creep of Crystals: High Temperature Deformation Processes in Metals, Ceramics and Minerals*; Cambridge University Press: Cambridge, UK, 1985.
(400) Frost, H. J.; Ashby, M. F. *Deformation-Mechanism Maps: The Plasticity and Creep of Metals and Ceramics*; Pergamon Press: Oxford, UK, 1982.
(401) Indenbom, V. L.; Osvenskii, V. B. In *Growth of Crystals*; Consultants Bureau: New York, 1980; Vol. 13, p 279.
(402) Shternberg, A. A. *Sov. Phys.: Crystallogr.* **1962**, *7*, 92.
(403) Vladimirov, V. I.; Romanov, A. E. *Disclinations in Crystals*; Nauka: Leningrad, USSR, 1986 (in Russian).
(404) Romanov, A. E.; Vladimirov, V. I. In *Dislocations in Crystals*; Elsevier: Amsterdam, 1992; Vol. 9, p 191.
(405) Friedel, J. *Dislocations*; Pergamon: Oxford, 1964.
(406) Humphreys, F. J.; Hatherly, M. *Recrystallization and Related Annealing Phenomena*, 2nd ed.; Elsevier: Oxford, 2004.
(407) Zaiser, M. In *Crystal Growth - from Fundamentals to Technology*; Elsevier: Amsterdam, 2004; p 215.
(408) Hirth, J. P.; Lothe, J. *Theory of Dislocations*, 2nd ed.; Wiley: New York, 1982.

(409) Ulianova, T. P.; Punin, Yu. O.; Petrov, T. G. In *Crystallography and Crystal Chemistry*; Leningrad University Press: Leningrad, USSR, 1974; p 193 (in Russian).
(410) Van Bueren, H. G. *Imperfections in Crystals*; North-Holland, Amsterdam; Interscience: New York, 1960.
(411) Dodson, B. W.; Tsao, J. Y. *Appl. Phys. Lett.* **1987**, *51*, 1325.
(412) Houghton, D. C. *J. Appl. Phys.* **1991**, *70*, 2136.
(413) Fox, B. A.; Jesser, W. A. *J. Appl. Phys.* **1990**, *68*, 2801.
(414) Moshkin, S. V.; Russo, G. V.; Nardov, A. V.; Petrov, T. G. In *Crystallography and Crystal Chemistry*; Leningrad University Press: Leningrad, USSR, 1982; p 179 (in Russian).
(415) Meggie, M.; Jones, R. *Phil. Mag. A* **1986**, *53*, L65.
(416) Laemmlein, G. G. *Dokl. Akad. Nauk SSSR* **1945**, *48*, 168.
(417) Gray, N. H. *Math. Geol.* **1984**, *16*, 91.
(418) Gross, R.; Möller, H. *Z. Phys* **1923**, *19* (5/6), 375.
(419) Hartshorne, N. H. *Nature* **1961**, *190*, 1191.
(420) Kozlovskii, M. I. *Sov. Phys.: Crystallogr.* **1965**, *10*, 101.
(421) Lehmann, O. *Z. Krystallogr* **1890**, *18*, 459.
(422) Shubnikov, A. V. *Trudy Lomonosov Inst. Geokhim. Krist. Mineral* **1936**, *8*, 5 (in Russian).
(423) Shubnikov, A. V. *Sov. Phys.: Crystallogr.* **1957**, *2*, 578.
(424) Shubnikov, A. V. *Sov. Phys.: Crystallogr.* **1956**, *1*, 295.
(425) Bons, P. D.; Koehn, D.; Jessell, M. W., Eds. *Microdynamics Simulation*; Springer: Berlin, 2008.
(426) Mattozzi, A.; Serralunga, P.; Hedenqvist, M. S.; Gedde, U. W. *Polymer* **2006**, *47*, 5588.
(427) Raabe, D. *Acta Mater.* **2004**, *52*, 2653.
(428) Kupferman, R.; Shochet, O.; Ben Jacob, E. *Phys. Rev. E* **1994**, *50*, 1005.
(429) Xu, H.; Chiu, H.-W.; Okabe, Y.; Kyu, T. *Phys. Rev. E* **2006**, *74*, 011801.
(430) Takaki, T.; Asanishi, M.; Yamanaka, A.; Tomita, Y. *Key Eng. Mater* **2007**, *345*−*346*, 939.
(431) Kurbatova, L. A.; Gordeev, A. P.; Tarabanchuk, V. P. In *Physics of Crystallization*; Kalinin University Press: Kalinin, USSR, 1988; p 97 (in Russian).
(432) Komarov, I. A.; Kurbatova, L. A.; Smirnov, Yu. M.; Khomullo, G. V. In *Physics of Crystallization*; Tver University Press: Tver, Russia, 1994; p 88 (in Russian).
(433) http://bevshots.com/all.html?limit=all
(434) Artsis, M. I.; Bonartsev, A. P.; Iordanskii, A. L.; Bonartseva, G. A.; Zaikov, G. E. *Mol. Cryst. Liq. Cryst.* **2010**, *523*, 21–49.
(435) Akhtar, S.; Pouton, C. W.; Notarianni, L. *J. Polymer* **1992**, *33*, 117.
(436) Akhtar, S.; Pouton, C. W.; Notarianni, L. *J. Controlled Release* **1991**, *17*, 225.
(437) Ma, U. V. L; Floros, J. D.; Ziegler, G. R. *Carbohyd. Polym.* **2011**, *83*, 1869.
(438) Jiang, Y. B.; Shi, K.; Xia, D. N.; Wang, S. O.; Song, T.; Cui, F. D. *J. Pharm. Sci.* **2011**, *100*, 1913.
(439) Benedict, J. B.; Freudenthal, J.; Hollis, E.; Kahr, B. *J. Am. Chem. Soc.* **2008**, *130*, 10714–10719.
(440) Lloyd, M. T.; Mayer, A. C.; Subramanian, S.; Mourey, D. A.; Herman, D. J.; Bapat, A. V.; Anthony, J. E.; Malliaras, G. G. *J. Am. Chem. Soc.* **2007**, *129*, 9144.
(441) Li, J. L.; Yuan, B.; Liu, X. Y.; Xu, X. Y. *Cryst. Growth Des.* **2010**, *10*, 2699.
(442) Brodin, B. V. In *The Genesis of Mineral Individuals and Aggregates*; Nauka: Moscow, 1966; p 51 (in Russian).
(443) Dowlatshahi, K. P. *Drawing with Light: The Pencil of Nature*, Ph.D. Dissertation, University of Gloucestershire, 2004.
(444) Hang, C.; Simonov, M. A.; Belov, N. V. *Sov. Phys.: Crystallogr.* **1970**, *15*, 387.
(445) Rudkovskaya, N. V.; Mikhailenko, N. Yu *Glass Ceram.* **2001**, *58*, 387.
(446) Norton, F. H. *J. Am. Ceram. Soc.* **1937**, *20*, 217.
(447) Kraner, H. M. *J. Am. Ceram. Soc.* **1924**, *7*, 868.
(448) Sun, C.; Kuan, C.; Kao, F. J.; Wang, Y. M.; Chen, J. C.; Chang, C. C.; Shien, P. *Mater. Sci. Eng., A* **2004**, *379*, 327.
(449) Hargittai, I.; Vainshtein, B. K., Eds. *Crystal Symmetries*; Oxford: Pergamon Press, 1988.
(450) Talbot, H. F. *C. R. Hebd. Seances Acad. Sci.* **1836**, *2*, 472.